TECHNICAL REPORT S-78-16

EFFECT OF SHEAR STRESS ON DYNAMIC BULK MODULUS OF SAND

by

John H. Schmertmann

Professor of Civil Engineering
University of Florida
Gainesville, Florida 32611

October 1978
Final Report

Approved For Public Release; Distribution Unlimited

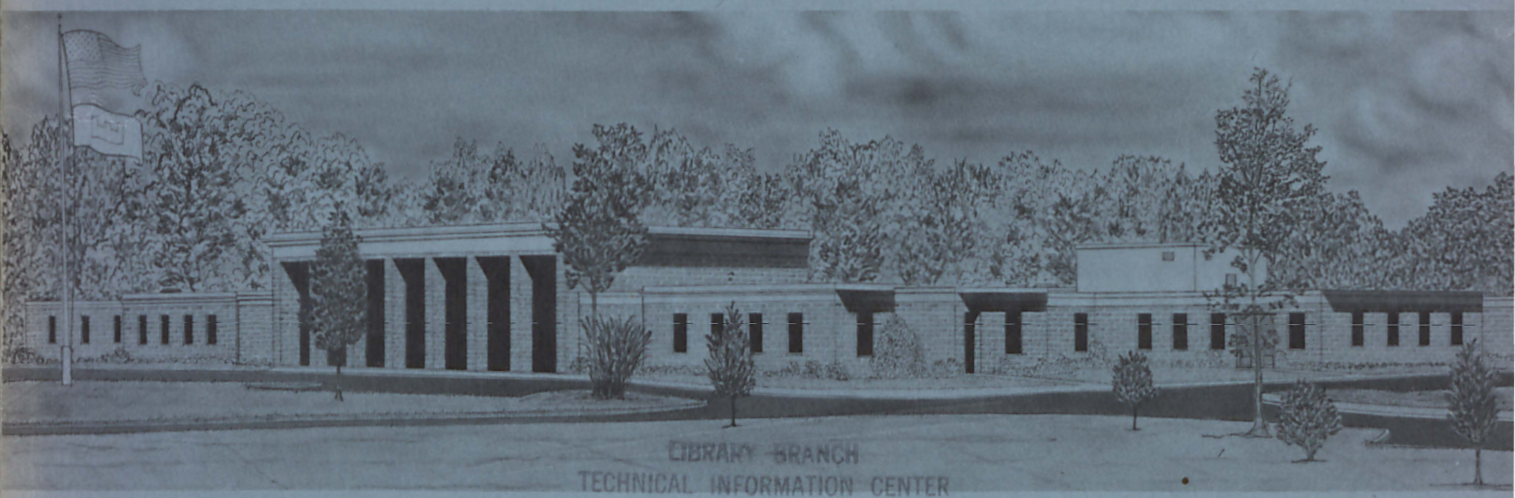

Prepared for Office, Chief of Engineers, U. S. Army
Washington, D. C. 20314

Under Contract No. DACW39-76-M-6676

Monitored by Geotechnical Laboratory
U. S. Army Engineer Waterways Experiment Station
P. O. Box 631, Vicksburg, Miss. 39180

REPORT DOCUMENTATION PAGE

READ INSTRUCTIONS BEFORE COMPLETING FORM

1. REPORT NUMBER: Technical Report S-78-16
2. GOVT ACCESSION NO.:
3. RECIPIENT'S CATALOG NUMBER:

4. TITLE (and Subtitle): EFFECT OF SHEAR STRESS ON DYNAMIC BULK MODULUS OF SAND

5. TYPE OF REPORT & PERIOD COVERED: Final report

6. PERFORMING ORG. REPORT NUMBER:

7. AUTHOR(s): John H. Schmertmann

8. CONTRACT OR GRANT NUMBER(s): Contract No. DACW39-76-M-6676

9. PERFORMING ORGANIZATION NAME AND ADDRESS
John H. Schmertmann, Ph. D., P. E., Consultant
Department of Civil Engineering,
University of Florida
Gainesville, Florida 32611

10. PROGRAM ELEMENT, PROJECT, TASK AREA & WORK UNIT NUMBERS: CWIS 31144

11. CONTROLLING OFFICE NAME AND ADDRESS
Office, Chief of Engineers, U. S. Army
Washington, D. C. 20314

12. REPORT DATE: October 1978

13. NUMBER OF PAGES: 92

14. MONITORING AGENCY NAME & ADDRESS (if different from Controlling Office)
U. S. Army Engineer Waterways Experiment Station
Geotechnical Laboratory
P. O. Box 631, Vicksburg, Miss. 39180

15. SECURITY CLASS. (of this report): Unclassified

15a. DECLASSIFICATION/DOWNGRADING SCHEDULE:

16. DISTRIBUTION STATEMENT (of this Report)

Approved for public release; distribution unlimited.

17. DISTRIBUTION STATEMENT (of the abstract entered in Block 20, if different from Report)

18. SUPPLEMENTARY NOTES

19. KEY WORDS (Continue on reverse side if necessary and identify by block number)
Bulk modulus
Compression waves
Shear stress
Shear waves
Sands

20. ABSTRACT (Continue on reverse side if necessary and identify by block number)

The effect of shear stress on the magnitude and directional variation of the dynamic bulk modulus of sand was investigated by means of a program of laboratory measurements of P-wave and S-wave velocities under varied stress conditions. The sand used was air-dry Reid-Bedford Model sand and was tested at relative densities of about 25% and 80%. Test specimens were 4 ft high by 4 ft in diameter, formed by pluviation in air in a cylindrical pressure chamber. At each relative density, tests were done with values

(Continued)

20. ABSTRACT (Continued).

of octahedral normal stress of 5, 10, and 20 psi, and with σ_3/σ_1 ratios of 1 and 1/3. Measurements of P-wave and S-wave velocities were made in three or four directions with accelerometers buried in the test specimens.

The test results indicate that compression and shear wave velocities vary with direction in an isotropic stress field due to inherent anisotropy of the sand structure, but that this phenomenon has only a modest (0-20%) effect in producing anisotropy in the bulk modulus. The work tends to confirm, within $\pm$10%, that the shear wave velocity depends only on the level of octahedral normal effective stress and not on stress anisotropy. In contrast with the shear wave velocity, the compression wave velocity increases significantly in the direction of the major principal stress and depends primarily on the effective stress on the plane normal to wave travel. Values of bulk modulus, computed from the wave velocities under the assumption of elastic isotropy, show a variation with direction, which contradicts the assumption of isotropy.

Appendix A contains photographs of typical oscilloscope waveforms from each replicate series of five impacts, and Appendix B presents tables of corrected V_p and V_s, the push wave and shear wave velocities, respectively, from each test.

THE CONTENTS OF THIS REPORT ARE NOT TO BE USED FOR ADVERTISING, PUBLICATION, OR PROMOTIONAL PURPOSES. CITATION OF TRADE NAMES DOES NOT CONSTITUTE AN OFFICIAL ENDORSEMENT OR APPROVAL OF THE USE OF SUCH COMMERCIAL PRODUCTS.

PREFACE

This report was prepared by Professor John H. Schmertmann of the University of Florida under Contract No. DACW39-76-M-6676, as a part of the research effort under CWIS Work Unit 31144, "Earthquake Resistance of Earth and Rockfill Dams," which is monitored for Office, Chief of Engineers, by Mr. Ralph Beene. The study was monitored for the Waterways Experiment Station (WES) by Dr. A. G. Franklin. General guidance was provided by Dr. Francis G. McLean, Chief, Earthquake Engineering and Vibrations Division, Geotechnical Laboratory (GL), fomerly Soils and Pavements Laboratory, Mr. Stanley J. Johnson, Special Assistant (retired), GL, and Mr. James P. Sale, Chief, GL.

Dr. R. D. Woods, Professor of Civil Engineering at the University of Michigan, helped significantly with the planning and execution of this research. Mr. Hristo Margas, University of Florida graduate student in civil engineering, worked extensively on this research under his research assistantship assignment and for his master's thesis. Mr. William Whitehead, Assistant Instructor in Civil Engineering at the University of Florida, supervised the student assistant crew that performed the chamber fillings and instrument placement and operation. Besides Mr. Margas, this crew had the following undergraduate assistants: Messrs. William Goodloe, Raymond Melee, Julio Palacios, and John Sexton.

Directors of WES during this study and the preparation of the report were COL G. H. Hilt, CE, and COL J. L. Cannon, CE. The Technical Director was Mr. F. R. Brown.

CONTENTS

CONVERSION FACTORS, U. S. CUSTOMARY TO METRIC (SI) UNITS OF MEASUREMENT

U. S. customary units of measurement used in this report can be converted to metric (SI) units as follows:

Multiply	By	To Obtain
cubic feet	0.02831685	cubic metres
degrees (angle)	0.1745329	radians
feet	0.3048	metres
feet per second	0.3048	metres per second
inches	25.4	millimetres
pounds (force) per square inch	6894.757	pascals
pounds (mass)	0.4535924	kilograms
pounds (mass) per cubic foot	16.01846	kilograms per cubic metre

1. INTRODUCTION

1.1 Purpose

The bulk modulus, B, represents one of the most important soil properties that determine the possible liquefaction behavior of a cohesionless soil. The greater the value of B, the lower the magnitude of pore pressure response to cyclic loading and the less likely is liquefaction.

In accord with the theory of elasticity in a homogeneous, isotropic medium, most if not all investigators have assumed B is an isotropic property independent of the direction of the travel of the disturbing stress waves that might induce liquefaction. The new theoretical analysis proposals by F. E. Richart, Jr., and co-workers at the University of Michigan have caused new questions to arise about the validity of the assumption of isotropic B. Accordingly, the U. S. Army Engineer Waterways Experiment Station (WES), CE, initiated research to make at least a preliminary assessment of the degree of validity of the isotropic B assumption.

In an isotropic, homogeneous, elastic medium:

$$B = \rho\left(V_p^2 - \frac{4}{3} V_s^2\right) \tag{1}$$

Thus, we need only determine the push (compression) wave and shear wave velocities, V_p and V_s, respectively, together with the mass density of the sand, ρ, to determine its bulk modulus when subjected to stress wave loadings. We know that sands behave as particulate systems and that many of their properties depend on the level of ambient effective stress. Previous research (Hardin and Black, 1966) showed that the shear wave velocity depended only, within about $\pm 5\%$, on the magnitude of octahedral effective stress in a soil element and not on the ratio of the principal stresses and therefore the shear stress magnitudes.

This investigation had the primary purpose of determining if B also depended only on the magnitude of octahedral stress and to check its independence from the direction of wave propagation when in an anisotropic stress field.

1.2 Scope

The scope of this work includes a single sand, tested air-dry, following pluvial deposition to two relative densities, about 25% and 80%, corresponding to dry density, γ_d, of 93 and 103 pcf.* Four sensitive accelerometers, buried in the sand during the casting of each of ten separate specimens, permitted determination of the V_p and V_s velocities in three or four directions within a 4-ft-diam, 4-ft-high sand specimen in a test chamber. At each relative density condition, we performed a test with $K = \sigma_3/\sigma_1 = 1$ and $K = 1/3$ to evaluate the importance of nonequal principal stresses on the behavior of V_p, V_s, and B for the different directions of wave travel. For each test and for each direction of wave travel, we made out measurements at three levels of constant octahedral stress σ'_o--5, 10, and 20 psi. Furthermore, we performed either two or three replicate tests at each of the relative density and K conditions.

In sum, we made over five hundred separate determinations of each V_p and V_s. Our summarized results show a minor, perhaps negligible, dependence of B on wave propagation direction under isotropic (K = 1) stress conditions, but a strong dependence of B on direction when subjected to an anisotropic (K = 1/3) stress condition.

2. EQUIPMENT

2.1 Test Chamber

The key piece of equipment that made this research possible was

---

* A table of factors for converting U. S. customary units of measurement to metric (SI) units is given on page 5.

the 4-ft-diam, 4-ft-high, triaxial chamber specimen within which we placed accelerometers during the pluvial deposition used to cast the specimens. This University of Florida calibration chamber permits independent control of the radial and vertical boundary stresses on the specimen. The pluvial deposition permits the casting and testing of approximately duplicate specimens. The sand falls from a traveling hopper, through shutter plates, through two layers of coarse screen, and then into the chamber. By varying the size of the holes in the shutter plate, we can achieve different relative densities. Figure 1 presents a schematic cross section through this test chamber. Please refer to other references (Schmertmann, 1978: Veismanis, 1974: Laier et al., 1975) for more detailed descriptions of the design and operation of this chamber.

The work of Caillemer (1975) and others has shown that a given shutter plate hole size produces repeatable average chamber densities within ±1 pcf, and that dry unit weight variations, both vertically and radially within the 50-ft^3 test specimen, vary randomly within ±1.5 pcf from the whole specimen average. Caillemer tested with samples having a volume of 492 cm^3, or 0.035% of the total specimen, and took 20 samples per specimen.

2.2 Sand

For all tests in this research we used only one sand, the Reid-Bedford Model sand. We obtained this sand from WES in 1976. Multiple use of the sand through our pluvial deposition equipment and subsequent crop-type dryer equipment in those cases in previous research where we wetted the sand has resulted in our losing most of the minus 200 sieve fines. Figure 2 shows the results of several recent sieve analyses on the sand we used.

2.3 Accelerometers and Oscilloscope

In each of the chamber test samples, we buried four accelerometers, all Piezotronics model No. 308A02, with a sensitivity of

100 mv/g. Each of these accelerometers had its own battery-operated signal conditioning unit supplied by the manufacturer. In general, the accelerometers appeared to work well for all tests. We did have some trouble with the conditioning units, which in the final few tests required the switching of accelerometers A1 and A2 (numbering discussed subsequently) into the conditioning units for A3 and A4. While this affected the calibration for acceleration magnitude, it did not influence the more important time intervals between wave arrivals.

By the use of an appropriate triggering system, we displayed the response from each pair of accelerometers on a dual, chopped-beam, storage oscilloscope. We used an HP 181A scope with a 1807A dual channel vertical amplifier and a 1821A time base generator. We used only the 0.2, 0.5, and 1.0 msec/division (ms/d) sweep rates for the key determinations of the differences in the times of first arrival for the push and shear waves at each accelerometer. After the research, we calibrated these sweep rates and corrected the velocity data for the small (about 0.5 percent) errors involved.

Figure 3, photo (a), shows the transducers we used. Photo (b) shows the oscilloscope. Photo (c) shows two of the accelerometers, Nos. 2 and 3, being carefully laid at their positions for Tests 6 through 13 during the filling of the sand in the chamber. Photo (d) shows the operators monitoring the oscilloscope during the performance of the test.

2.4 Impact Equipment

For Tests 3 and 4, we used a hand-held and swung ball peen hammer for our wave-producing impact system. It soon became evident that we could improve operations significantly by introducing a mechanical impact system to make our impacts and resulting waveforms less operator-dependent and therefore more reproducible. The photos in Figure 4 show the mechanical system we used for Tests 7 through 13. (Test 5 was aborted when the need for a better impact system became evident.)

The mechanical impact system consisted of either dropping or

swinging a steel ball weighing 176 grams. When we wanted to produce waves relatively rich in compression energy, we dropped the ball from 2 to 6 in. onto the center of a steel plate capping the vertical steel rod extending from aluminum plates buried at two positions, each 3 cm below the top of the sand specimen. When we wanted to produce waves relatively rich in shear energy, we swung the weight as a pendulum and struck a horizontal bar attached to a horizontally braced (with plastic pipe) vertical steel rod from the buried plate. Both types of impact involved kinetic energies at impacts of about 1.0 kg-cm, $\pm$50%.

3. METHODS

3.1 Placement of Accelerometers

As noted above, and also illustrated in Figure 3(c), we placed the accelerometers in the chamber during appropriate interruptions in the pluvial filling process. We placed all accelerometers in a single, vertical plane passing through the chamber axis. When the sand filling reached an appropriate depth, we put each accelerometer in its planned location with an estimated precision of better than $\pm$1/4 cm in both depth and radial position. After some initial experimentation with alternate orientations of the axes of the accelerometers, I decided to place all accelerometers with their axes horizontal and perpendicular to plane in which we placed all the accelerometers. All the accelerometers had their wires coming out of the same side, giving all the same polarity.

Figure 5 shows my initial choice for the position of the four accelerometers along a vertical plane cutting through the chamber diameter and through the center of the two impact access holes in the top of the chamber. The accelerometer positions shown in Figure 5 are the ones we used for Tests 3 and 4. These positions had certain advantages, such as providing three wave speed measurement directions at the same average magnitude of octahedral stress. However, we found serious interference at accelerometers A3 and A4 due to their position near the chamber

boundaries and the consequent first arrival of the waves traveling through the boundary steel and water. To help correct this, I changed to a new pattern for the accelerometers, shown in Figure 6, which we used for Tests 6 through 13. This pattern moved the outermost accelerometers farther away from the walls of the chamber and provided for velocity measurements in four directions with the horizontal, 90° (A2-A4), 60° (A3-A4), 30° (A1-A2), a 0° (A3-A2). The Figure 6 pattern proved reasonably successful, although we did not completely eliminate chamber boundary wave interference effects at the furthermost accelerometer in each paired direction.

We placed each accelerometer in position with a minimum of bedding disturbance to the surrounding, pluvially placed sand, with the wires going directly to the side of the chamber away from the plane of the velocity testing. These wires eventually came out through the central hole in the chamber, but we kept them as far as possible from the plane of the testing. We placed each accelerometer with its protective rubber cap as recommended by the manufacturer. Figure 3(e) shows a photo of one of these accelerometers with the cap removed.

3.2 Applying the Chamber Pressure

For each test, we controlled the chamber pressure by means of two pressure regulators, one controlling vertical pressure and one controlling radial pressure. The entire bottom of the specimen rested on a hydraulic load cell, constructed as a water-filled, neoprene-covered, disc-shaped recess in the top of the vertical piston. This piston acted at the bottom of the chamber and specimen. Attached to this load cell on top of the piston was a Heise Bourdon gauge with 0.2-psi divisions and a readability of $\pm$0.05 psi, and connected to the water around the circumference of the specimen was a similar Heise Bourdon gauge to monitor the water pressure in this circumferential water.

During the application of the sample confining pressure, the operator used air pressure regulators and the Heise gauges to increase both radial and vertical pressures in small increments, according to a

set constant-K path that depended on whether the test called for K = 1 or K = 1/3 conditions. Except for an initial adjustment, he maintained the proper K loading path until reaching the specified test levels of 5.0-, 10.0-, and 20.0-psi average octahedral stress midheight between accelerometers A2-A4 and A3-A4.

We applied chamber pressure only in the direction of increasing stress. None of the samples had ever been subjected to higher levels of effective stress than they had at the time of testing.

3.3 Production of the Impact Waves

For this purpose we used the impact equipment described in section 2.4. With the mechanical system, the ball impacted against steel, and the resulting stress wave traveled down the vertical, standard pipe rod of 1/2-in. diameter. This steel rod was, in turn, rigidly attached to a horizontal aluminum plate or disc of 3-in. diameter and 1/4-in. thickness. We buried this plate with its bottom approximately 3 cm below the top of the specimen. We had two such plates, one below the center access hole and one below the side access hole. The bottom of each plate had rough sandpaper glued to it to assure good frictional contact between soil and plate. The vertical rods coming up from the plate were also braced with concentric plastic pipe. This pipe had the dual purpose of electrically isolating the vertical rod from the chamber and thus preventing early triggering of the scope impact sweep and also of providing a reaction against the rocking component of the impact generated by the horizontal, pendulum ball impact.

With the system we used, the operator would clear the storage scope, set it for the next sweep, and then call for the impact device operator to either drop or allow the ball to swing and make the impact. The contact of the ball with the vertical rod system would then complete the triggering circuit and start the sweep of the scope beams at approximately the same instant as the stress wave started in the rods, through the plate, and then through the sand to the accelerometers. We used a separate 5-v system to actuate the triggering for all tests.

For Tests 9 through 13, we also measured V_p along the horizontal direction between accelerometers A3-A2 (see Figure 6). To do this, we used the mechanical ball system, but hand-held the ball and struck it against the steel outside of the tank at the point where the projection from A2-A3 intersects the side of the tank. Despite attempts, we could not interpret the resulting waveforms for V_s.

3.4 Interpreting and Recording the Impact Waveforms

Following the impact, the oscilloscope displayed the waveform record as sensed by each pair of accelerometers, displaying this by use of the chopped mode. The operator at the scope (usually the writer) would call for a succession of impacts until, by manipulation of the gain and sweep rate controls, he obtained a reproducible and informative waveform. First he called for vertical (dropped ball) impacts to get the first arrival times of the push (compression) waves at any two of the matched accelerometer locations. The actual arrival times at each were only of concern with respect to the reasonableness of the waveform interpretation for first push wave arrival. Of greatest concern was an accurate measure of the time interval between the first arrival at the two accelerometers. To obtain this difference, the operator made an estimate, directly from the stored scope waveform record, of the time of first arrival to ± 0.05 major time divisions on the face of the scope. To achieve better accuracy in the final wave velocity computation, we repeated the above-mentioned impacts until we obtained five waveforms that we could interpret for time differences in the first arrival. These five were called out to a recorder (usually a graduate student). We then averaged these five for the time difference used to calculate V_p (and V_s).

The scope operator then repeated the above-mentioned procedure with the swinging ball for an interpretation of the first arrival times of the shear wave. This usually involved a more difficult interpretation because the arrival of the shear wave was always superposed on the now already present push wave. Unfortunately, with our impact system we

were not able to obtain a reversal in the polarity of the shear wave without a simultaneous reversal in the polarity in the accompanying push waves. Thus, reversal did not aid interpretation. Our oscilloscope did not have an enhancement capability. However, we doubt that this would have improved the ease of interpretation because we had virtually no random background noise with which to contend.

3.5 Photographing the Impact Waveforms

During each series of the five scope displays of waveforms for which we interpreted first arrival times at each accelerometer, the operator chose a typical set of waveforms and photographed them, using a suitable Polaroid camera. The recorder noted the particular set of readings for which a photograph was taken. The operator then immediately noted on the photograph its sequence number, and such other information as test number, test time, test pressures, and scope gain and sweep settings, and most important--his assumption for the push and/or shear wave arrival times for that waveform. Except for a few readings in Test 3, all the series of five waveforms have at least one photograph documenting a typical waveform and our interpretation.

Appendix A presents annotated copies of all the waveform photographs we took to document this research. At the time of taking the photograph each was given the next successive acquisition number. The photographs are presented in order of acquisition number, given in the upper right corner of each.

3.6 Measured Average Dry Unit Weight

We weighed all the sand removed from the chamber after completion of each test. We knew the volume of the specimen at the beginning of each test because we knew the initial volume of the chamber (50.3 ft^3) and the volume changes measured during the application of pressures before each test. Thus, we could easily compute the average air-dry unit weight of the sand for each test. Considering the accuracy of our spring-scale weighing system (readability ± 5 lb) and the number of

weighings to complete weighing all the sand (about 5), we believe we obtained the total weight of the sand within ±25 lb. In terms of unit weight, this represents about ±0.5 pcf. In two tests (3 and 8), we had a greater error because some of the sand got wet due to membrane leakage prior to completion of the wave velocity testing.

3.7 Time Sequence

Table 1 presents a chronological listing of the major operations involved in one of our tests, with the purpose of giving the reader a better concept of the sequence of events in a test and the various typical times required.

From Table 1 the reader can see that we could perform between one and two tests per week and that each test required approximately 45 man-hours of work to complete, independent of any subsequent plotting and analyses of data.

4. ANALYSES OF DATA

4.1 Correction of Raw Data

As explained in the previous sections, the basic data from this research consist of differences in the arrival times for the push and shear waves, which permit the calculation of V_p and V_s. Some of the associated measurement errors are random, and some systematic. In turn, some of these systematic errors can be estimated and corrected. We have included such corrections. The following explains what we did.

4.1.1 Different Levels of Octahedral Effective Stress Between Accelerometers. We do not have uniform effective stress conditions in a test chamber sample because of the effect of the unit weight of the sample itself. The higher the point in the sample, the lower both the horizontal and vertical effective stresses. Reference to Figure 6 will show that the average effective stresses between accelerometers A1-A2 and A3-A2 must be less than between A2-A4 and A3-A4. Because both push and shear wave velocities increase with effective stress, we corrected

the velocity data between A1-A2 and A3-A2 (angles 30° and 0°) to make them conform to the same 5.0-, 10.0-, or 20.0-psi octahedral stress magnitude between accelerometers A2-A4 and A3-A4 (the 90° and 60° directions).

The formula by Hardin and Drnevich (1972) indicates the shear wave velocity will vary with the 1/4 power of the octahedral stress. A recent unpublished Japanese reference indicates that the shear wave velocity varies with a little less than the 1/5 power. Plotting some of our results on log-log paper indicates that both V_p and V_s vary with about the 1/5 power. We used the 1/5 power as our basis for increasing the wave velocities measured between accelerometers A1-A2 and A3-A2 to have these velocities conform to the stated octahedral stress level of either 5, 10, or 20 psi. Doing this introduced a maximum correction of +3% at the 5-psi level, reducing to a maximum of +0.07% at the 20-psi level.

4.1.2 Compression of Sample Under Pressure. With the application of pressure to the various octahedral stress levels for the test, the sample usually changed both vertical and radial dimensions. Because we measured volume changes in both directions, we could compute the average vertical and radial strains. By assuming these strains occur uniformly throughout the sample, we corrected the original as-placed distances between accelerometers to slightly modified distances after the sample compressed to reach each successive octahedral stress level. Because the distances shorten, this correction reduces the velocities calculated by use of the as-placed distances. We also applied this correction, which had a typical value of about -1/2% and a maximum of -1%. The angles changed a negligible amount, and we disregarded this effect.

4.1.3 Unit Weight Variations. For the purposes of comparing the V_p and V_s determinations within each group of low and high relative density tests, we also corrected for the probable differences in dry density between each individual test and the average for the entire group. We based this correction on the measured changes in V_p and V_s over the much larger increment in unit weight between the high and low

density tests. Over this increment we found an average increase in velocity of 1.0% for each 1.0-pcf increase. We then used this as a basis to further correct the wave velocity results to have each group conform to the average dry unit weight for that group (as determined by the weighing method described in section 3.6).

4.1.4 Scope Sweep Calibration. Several days after completion of Test 13, we took the oscilloscope used in this research to the University of Florida Instrument Standards Laboratory and calibrated the sweep rates with a Tektronix type-184 signal generator. We only used the 0.2, 0.5, and 1.0 ms/d sweep rates in this research. In all cases we found the sweep rate in error by less than 1%.

As a result of this calibration, we used the following factors by which to multiply V_p and V_s to correct for instrument sweep rate error: 0.994 for the 0.2 scale, and 0.996 for both the 0.5 and 1.0 ms/d scales.

4.2 Graphs and Tables of Corrected Velocities

Figures 7 through 12 present polar coordinate, graphical summaries of the above-corrected V_p and V_s data obtained in this research. Figures 7 through 9 present the variation of these velocities with the direction of wave speed measurement, θ. These figures consider only the tests at low density, with figures for each of the octahedral stress levels of 5, 10, and 20 psi. Figures 10 through 12 present the same sequence of data, but consider only the tests at high relative density.

Appendix B presents the same information as in Figures 7 through 12, but in the form of tables. This appendix includes a separate table for each test, presented in order of test number. These tables include the composite correction factor resulting from the corrections described in sections 4.1.1 through 4.1.4, as well as the resulting corrected velocity. These tables also include the reference number of the matching photo in Appendix A that documents the waveform.

4.3 Least-Squares Curve Fitting

I first attempted to fit straight lines and parabolas through Cartesian coordinate plots of each of the various groups of data in Figures 7 through 12. While both fit about equally well, it soon became obvious that each would produce a discontinuity in V versus θ when θ passed through either 0° or 90°. This is not compatible with the physical situation. I then went to the more suitable polar coordinate system and sought another form of curve.

A number of engineers have used the following form of equation, adapted to the present problem, to express anisotropic behavior of soils:

$$V_\theta = V_{90} + (V_0 - V_{90}) \cos^2\theta \qquad (2)$$

where numerical subscripts represent degrees. Casagrande and Carrillo (1944) first intuitively proposed an equation of this type to express soil strength anisotropy. They also noted that such an equation expresses the strain in any direction in terms of the principal strains in an elastic material. Schmertmann (1964) presented the same equation, in a different form, to express the induced variation in effective stress on any plane in an anisotropic stress field. Lo (1965) also used this form of equation to express his measured undrained strength anisotropy in various clays and included it in his analytical correction procedure for anisotropic strength effects. It seems well established that this form of equation can be used to express anisotropic soil behavior, both inherent due to soil structure and induced due to anisotropic stress. I therefore used Equation 2. I found the standard error, Equation 3, about the same as when I tried Cartesian lines or parabolas--thus further confirming the suitability of Equation 2.

Each best-fit curve is graphed in Figures 7 through 12. Table 2 presents the results in terms of the best-fit values of V_{90} and V_0 and the standard error of the estimate, S_y, given by:

$$S_y = \left[\frac{(V_{\theta meas.} - V_{\theta eqn.})^2}{(\text{no. data pts})}\right]^{1/2} \qquad (3)$$

In almost all cases we used all the data points available to us to determine the best-fit Equation 2. This number of points varied from 5 to 11. However, within Tests 3 and 10 we discarded a few points as being nonrepresentative of the remainder of the data.

The results of the aforementioned curve fitting also provide a basis for describing the degree of anisotropic behavior of the sand with respect to V_p and V_s. Consider the ratio V_0/V_{90} for such a purpose, for both the push and shear waves. Table 3 presents the individual and averaged V_0/V_{90} ratios as taken from Table 2.

4.4 Determinations of Bulk Moduli, B

One can now use the best-fit curves illustrated in Figures 7 through 12, and summarized in Table 2, to determine the variations in B with θ. Putting Equation 2 for both V_p and V_s into Equation 1 yields an equation for B as a function of θ in terms of V_0 and V_{90}. Use of the various V_0 and V_{90} values in Table 2 then permits solving for B versus θ for each density, K, and octahedral stress condition.

For more efficient presentation, the writer chose to transform the various V_0 and V_{90} values at σ_o' = 5 and 20 psi to equivalent values at 10 psi and then average these with the real values at 10 psi to obtain an overall average at 10 psi. For this transformation the writer assumed $V \sim \sigma_o^{0.2}$, as described in section 4.1.1. Table 4 lists these overall average best-fit velocities at 10 psi. Use of the Table 4 values for V_0 and V_{90} in the equation for B produced the results graphed in Figure 13. This figure presents one of the final products of this research and illustrates the inherent sand structure and the stress induced anisotropy of B. The values of B plotted in Figure 13 result from Equation 1 and involve the prior assumption of elastic isotropy. The resulting anisotropy of B indicates that the assumption of isotropy is not valid in our sand, especially when subjected to an anisotropic stress system.

5. DISCUSSION OF RESULTS

5.1 Anisotropy of Sand Structure

The heavy lines in Figures 7 through 12 indicate the best-fit Equation 2 curves expressing the variation in either V_p or V_s with the direction of wave velocity measurement, θ. These figures and Table 4 clearly show that these velocities do not remain constant with direction, even in the K = 1 isotropic stress field. There seems to exist a perhaps slight, but definite, trend for velocities to increase as the wave travel direction changes from the vertical ($\theta = 90°$) to the horizontal ($\theta = 0°$). Table 3 shows V_0/V_{90} averages of 1.067 for V_p and 1.133 for V_s at low density, and 1.120 and 1.134 at high density. This probably reflects an inherent anisotropy in the sand structure itself at all densities, resulting from its raining deposition in a gravity field.

The falling and then striking and bouncing sand grains probably arrange themselves with a statistical preference for their long and intermediate axes to lie on the horizontal plane, which would represent the position of minimum potential energy. Thus, waves propagating in the horizontal direction would statistically have fewer grain-grain gaps/contacts to jump across. Because such jumps presumably slow the wave, it follows that with such axis preference the waves would travel faster in the horizontal direction. Hence, at K = 1.0 we found both V_p and V_s greater at $\theta = 0°$ for all γ_d and σ'_o.

Reference to Equation 1 shows that the difference between V_p and V_s controls B. B would not necessarily change with θ if both V_p and V_s change in the same direction. Table 3 shows they do so change. The K = 1 curves in Figure 13 show that when considering the overall average results from this research, one can say that B is approximately isotropic in an isotropic stress situation in our pluvially deposited sand. The calculations used to plot Figure 13 show that at low density $B_0/B_{90} = 1.01$ and at high density $B_0/B_{90} = 1.21$.

5.2 Effect of an Anisotropic Stress Condition

It seems apparent from Figures 7 through 12 and Tables 3 and 4 that the shear wave velocity is not strongly influenced by an isotropic stress condition if we make comparisons at the same level of octahedral stress. The Table 4 average V_{s0} at K = 1 equals 1026 ft/sec and 1059 ft/sec at K = 1/3. The similar comparison for V_{s90} is 916 and 933 ft/sec. The differences fall within experimental error. An isotropic V_s agrees with the conclusion of Hardin and Black (1966) and also stated in Richart, Hall, and Woods (1970) that the shear modulus and shear velocity at a point depend only on the magnitude of octahedral effective stress and not on the principal stress ratio at that point.

Contrary to the above, our data show that V_p is measurably anisotropic in an anisotropic stress situation. The data from the K = 1/3 tests seem to show clearly that V_p decreases as θ decreases. The Table 4 average V_{p90} equals 1701 while V_{p0} equals 1460 ft/sec, a difference well outside experimental error. This means we get the greatest compression wave velocity with waves traveling in the same direction as the major principal stress (vertical) and the least velocity when traveling in the direction of a minor principal stress (horizontal).

To further confirm the above, I also performed a supplemental Test 13a in which we reversed the direction of principal stresses and performed a few check velocity measurements with K = 2.2. We performed these tests after releasing the stresses from Test 13, which produced some local slumping of the sample around its top perimeter. We then let the sample sit over the weekend. Nevertheless, after reapplying anisotropic stresses to bring the sample to σ_o' = 5.0 psi, but with K = 2.2, we now found maximum V_p = 1513 ft/sec in the horizontal direction and minimum V_p = 985 in the vertical. Note that this gives a V_0/V_{90} ratio of 1.54 compared with an average of 0.87 when K = 1/3. Figure 7(b) includes the V_{p0} and V_{p90} points (solid triangles) from Test 13a. These points differ markedly from the K = 1/3 data. It seems well confirmed that V_p behaves anisotropically in an anisotropic stress field.

The stress-anisotropic behavior of V_p has an exaggerated effect on B because of the nature of Equation 1, which involves the subtraction of two large numbers to give relatively small differences. Figure 13 shows clearly the stress-induced anisotropic behavior of B. B_0/B_{90} has now decreased to 0.32 at low density and 0.42 at high density, compared with the corresponding K = 1 values of 1.01 and 1.21.

Note that the ratios 0.32/1.01 = 0.32 and 0.42/1.21 = 0.35 seem remarkably close to the stress ratio K = 0.33. This suggests that B depends in an important way on the effective stress acting on the plane normal to the direction of wave travel.

5.3 Dr. Woods, Consultant

As planned, Dr. R. D. Woods, Professor of Civil Engineering at the University of Michigan and an acknowledged expert in the field of soil dynamics, served as an active consultant to this project. While at the University of Florida as a Fugro Fellow, he helped with the initial planning of this project. He then followed the progress of the work by means of letter reports from the writer. He also came to the University of Florida April 14-16 and spent two and a half days working with us on the project. Before this visit he reviewed many of our first-arrival interpretations by studying the then-available typical waveform photos, presented here in Appendix A. During this visit he reviewed in detail all our interpretations for V_p and V_s from Tests 10, 11, and 12. In all this review he found no consistent and major differences between his and our interpretations. He did find minor differences and an occasional major difference. But, even the acceptance of his interpretations would not change significantly the best-fit equations given herein.

On April 15, Dr. Woods participated through the entire Test 13. He did most of the first-arrival interpretations. His first-arrival interpretations resulted in velocities that fit in well with our interpretations in previous replicate Tests 3 and 9.

Dr. Woods has also reviewed this report and agrees in general with

the results and conclusions presented herein.

5.4 Errors and Accuracy

Table 5 presents a list of all of the known possible sources of error in this work, together with some comments concerning the randomness of the error, its possible or likely magnitude, and the possible importance of the error. Note that in section 4.1 four of these sources of error (Nos. 6 through 9) were discussed, and we applied appropriate corrections to the raw data for these sources before plotting V_p and V_s in Figures 7 through 12.

By far the most important uncorrected source of error comes from the difficulty in interpreting the first arrivals. This proved only an occasional problem with the compression waves, due mostly to prearrival of the wave in the second transducer as a result of short-circuiting around the chamber steel-water-rubber perimeter. More serious was the more common problem of detecting the first arrival of the shear wave. Appendix A presents a typical set of waveform data for each V_p or V_s determination and the reader can judge for himself or herself about the interpretation. As noted in section 5.3, Dr. Woods agreed with the interpretations he checked.

Note that our values are too high compared with predictions from the well-known empirical equations from Hardin and Drnevich (1972), also found in Richart, Hall, and Woods (1970), p. 154), as well as the more recent ones from Kuribayashi et al. (1975, unpublished). Our shear velocities are approximately 30% higher than predicted using the Hardin-Black equation and about 20% higher when using the newer Kuribayashi equation. This may indicate an error in our results or that the equations do not apply to our sand and/or our chamber test. Both of these equations result from interpretations of laboratory data using only resonant column testing.

The writer looked into the possibility that different magnitudes of shear strain might account for the above differences in shear

velocity. Using equation 5 for shear strain, γ, suggested by Dr. Woods, and the second form of it that results from assuming simple harmonic motion,

$$\gamma \simeq \frac{A_{pp}}{V_s T_s} \simeq \frac{1.63\left(\frac{a_{max}}{g}\right)}{fV_s} \qquad (5)$$

where

A_{pp} = maximum peak to peak amplitude
V_s = velocity of the shear wave, ft/sec
T_s = period of shear wave = 1/f sec
a_{max} = maximum acceleration ft/sec^2
g = gravitational constant = 32.2 ft/sec^2
f = frequency, Hz

the writer obtained a shear strain range of about 0.05 to 0.5 $\times 10^{-3}$% at the first arrival of the shear wave for a representative group of 10 determinations during this research. These strain magnitudes fall below the 10^{-3}% noted by Hardin and Drnevich as below those for maximum shear modulus, G_{max}, and therefore fall in the range for which they report their equation applicable. Dr. Woods reported the data from Kuribayashi et al. involved strains of 10^{-4}%. Differing strain levels do not appear to explain the differences in V_s.

In addition to the shear wave velocities, the ratio of V_p/V_s measured in this research in the K = 1 tests varied from about 1.4 to 1.6, suggesting a Poisson's ratio of about 0.0 to 0.2. This seems too low compared with the values of 0.25 to 0.4 usually suggested for sand. However, the 0.0-0.2 range results from computations assuming an isotropic, elastic half-space, which we found did not exist even with the K = 1 stress condition.

5.5 Supplemental Test 14 for V_s

Because of a nagging uncertainty in the accuracy of our V_s interpretations, we decided to perform a check test using a more accurate

method for detecting the first arrival of the shear wave. Adapting the work of Anderson and Woods (1975), we made a miniature scissors-type wave generator which we then used to produce inverted polarized shear waves (Figure 14). This device expands out and slides down when struck downwards, and again expands out but slides up when struck upwards. This produces the same compression wave but a different polarization of the shear wave when alternately struck up and down. The point of divergence in overlaid successive waveforms gives the point of shear wave arrival. We used this technique successfully in supplemental Test 14.

Test 14 repeated the previous Tests 3, 9, and 13 with the same dry sand at the low density condition and the boundary stresses at K = 1. However, because we had sent two accelerometers away for service, we had only two available for Test 14. We placed these at the A1 and A2 locations, giving $\theta = 30°$, and introduced the waves at the side access hole (see Figure 6). After some experimentation with the scissors device, we were able to get reproducible divergent waveforms to clearly define the first arrival of the shear wave. The final photos in Appendix A (Nos. 218 through 220) document the typical sets of superposed waveforms we obtained in supplemental Test 14, and our interpretations for V_s (and V_p) first-arrival times. Appendix B also includes a table for the correction factors and the resulting final average V_s and V_p values we obtained from Test 14.

The open triangles in Figures 7(a), 8(a), and 9(a) show the Test 14 results for V_s together with the previous values from our other methods of interpretation. The solid triangles in these figures show our Test 14 values for V_p. The reader will see that these additional values for V_s fit well with our previous determinations at the 10- and 20-psi stress levels and appear superior to our previous determinations at $\theta = 30°$ at 5 psi, which we had already discounted as anomalous and likely in error. Test 14 further confirmed the overall validity of our previous V_s interpretations wherein we did not have the advantage of inverted shear waveforms.

6. CONCLUSIONS

6.1 - The scope and accuracy of the present research appears adequate to answer the research question concerning the possible anisotropy of the bulk modulus in an isotropic stress field.

6.2 - The compression and shear wave velocities vary with direction in an isotropic stress field due to inherent anisotropy in the sand structure. While observable, these trends seem to have only a modest (0-20%) effect on producing an inherent anisotropy in B.

6.3 - This work tends to confirm, within $\pm$10 percent, that the shear wave velocity depends only on the level of octahedral effective stress and not on stress anisotropy.

6.4 - In contrast with V_s, the compression wave velocity, V_p, increases significantly in the direction of the major principal stress. V_p depends primarily on the effective stress on the plane normal to wave travel.

6.5 - The values of B determined, listed, and plotted in this report result from the use of Equation 1 and involve the prior assumption of elastic isotropy. The resulting anisotropy of B shows that this assumption and, therefore, Equation 1 are not correct. A correct equation would require the use of at least two values each of an elastic modulus and Poisson's ratio to express a minimum degree of elastic anisotropy.

SELECTED BIBLIOGRAPHY

Anderson, D. B. and Woods, R. D. (1975), "Comparison of Field and Laboratory Shear Modulus," Proceedings, Specialty Conference on In Situ Measurement of Soil Properties, American Society of Civil Engineers, Vol I, pp 69-92.

Caillemer, B. M. (1975), An Experimental Study in the UF Static Cone Test Calibration Chamber; Part 1, Density of Distribution of Pluvially Placed Sand, M.S. Thesis, Department of Civil Engineering, University of Florida, Gainesville, Fla., August.

Casagrande, A. and Carrillo, N. (1944), "Shear Failure of Anisotropic Materials," Journal of the Boston Society of Civil Engineers, Contribution to Soil Mechanics 1941-53, Equation 6, p 127.

Hardin, B. O. and Black, W. L. (1966), "Sand Stiffness Under Various Triaxial Stresses," Journal, Soil Mechanics and Foundations Division, American Society of Civil Engineers, Vol 92, No. SM2, March.

Hardin, B. O. and Drnevich, V. P. (1972), "Shear Modulus and Damping in Soils: Design Equations and Curves," Journal, Soil Mechanics and Foundations Division, American Society of Civil Engineers, Vol 98, No. SM7, pp 670-671, July.

Laier, J. E., Schmertmann, J. H., and Schaub, J. H. (1975), "Effect of Finite Pressuremeter Length in Dry Sand," Proceedings, Specialty Conference on In Situ Measurement of Soil Properties, American Society of Civil Engineers, Vol I, pp 241-259.

Lo, K. Y. (1965), "Stability of Slopes in Anisotropic Soils," Journal, Soil Mechanics and Foundations Division, American Society of Civil Engineers, Vol 91, No. SM4, Equations 2 and 3.

Richart, F. E., Jr., Hall, J. R., Jr., and Woods, R. D. (1970), Vibrations of Soils and Foundations, Prentice-Hall, Englewood Cliffs, N. J.

Schmertmann, J. H. (1964), Discussion, Journal, Soil Mechanics and Foundations Division, American Society of Civil Engineers, Vol 90, No. SM4, Equation 31, p 184.

Schmertmann, J. H. (1978), "Study of Feasibility of Using Wissa-Type Piezometer Probe to Identify Liquefaction Potential of Saturated Fine Sands," Technical Report S-78-2, U. S. Army Engineer Waterways Experiment Station, CE, Vicksburg, Miss., February.

Veismanis, A. (1974), "Laboratory Investigations of Electrical Friction-Cone Penetrometers in Sands," Proceedings, European Symposium on Penetration Testing, Stockholm, Vol 2.2, pp 407-420.

TABLE 1 - CHRONOLOGY OF TEST OPERATIONS FOR A TYPICAL TEST 3 TO 13

Day	Operation	Time Required	Men Required
1	Empty chamber from previous test, weigh sand as removed, put into dryer if needed	3 hr	2
	Set up chamber for next pluvial deposition	3	2
2	Rain sand to form specimen and place four accelerometers at proper positions	3 (low) γ_d 7 (high) γ_d	1 or 2
	Seal chamber and complete test setup	3	1
3	Apply K = 1 or K = 1/3 chamber pressures to 5-psi test level	1/4	1
	Hold pressure for 15 min	1/4	
	Alternately get V_p and V_s from each pair of accelerometers, do five times, get a typical scope waveform photo	1-1/2	
	Repeat above for other two pressure levels	4	
	Release pressures, close down chamber	1	2
	Average total hours = 21 Average total man-hour = 45		

TABLE 2 - RESULTS OF THE LEAST-SQUARES FITTING OF EQUATION 2 THROUGH CORRECTED DATA

γ_d (pcf)	σ'_o (psi)	K	V_p or V_s	$V_\theta = V_{90} + (V_0 - V_{90}) \cos^2 \theta$.....(Eqn. 2) No. Pts	V_{90} (ft/sec)	V_0 (ft/sec)	V_0/V_{90} (ft/sec)	S_y (ft/sec)	Fig.
93	5	1.0	V_p	11	1106	1269	1.147	62	7a
			V_s	6	806	578	0.717	40	
		1/3	V_p	6	1422	1272	0.895	67	7b
			V_s	5	888	978	1.101	37	
	10	1.0	V_p	11	1325	1375	1.038	111	8a
			V_s	9	853	975	1.143	43	
		1/3	V_p	6	1619	1369	0.846	35	8b
			V_s	6	878	1144	1.303	28	
	20	1.0	V_p	11	1513	1538	1.017	127	9a
			V_s	9	1000	1122	1.122	67	
		1/3	V_p	6	1794	1556	0.867	71	9b
			V_s	6	978	1069	1.093	27	
103	5	1.0	V_p	7	1253	1438	1.148	50	10a
			V_s	6	825	866	1.050	42	
		1/3	V_p	9	1606	1328	0.827	97	10b
			V_s	7	897	928	1.035	103	
	10	1.0	V_p	7	1453	1609	1.107	50	11a
			V_s	6	947	1106	1.168	57	
		1/3	V_p	9	1791	1503	0.839	52	11b
			V_s	7	997	1000	1.003	114	
	20	1.0	V_p	7	1666	1841	1.105	60	12a
			V_s	6	1091	1291	1.183	44	
		1/3	V_p	9	2013	1775	0.882	62	12b
			V_s	7	1116	1353	1.212	139	

TABLE 3 - SUMMARY OF BEST-FIT EQUATION 2 ANISOTROPIC (V_0/V_{90}) RATIOS

γ_d	K	σ_o', psi	Ratio for V_p	Ratio for V_s
93	1.0	5	1.147	Not used
		10	1.038	1.143
		20	1.017	1.122
		Avg	1.067	1.133
	1/3	5	0.895	1.101
		10	0.846	1.303
		20	0.867	1.093
		Avg	0.869	1.166
103	1.0	5	1.148	1.050
		10	1.107	1.168
		20	1.105	1.183
		Avg	1.120	1.134
	1/3	5	0.827	1.035
		10	0.839	1.003
		20	0.882	1.212
		Avg	0.849	1.083

TABLE 4 - AVERAGE BEST-FIT V_p AND V_s (FT/SEC) AT σ_o' = 10 PSI

γ_d	K	V_{p0}	V_{p90}	V_{s0}	V_{s90}
93	1	1391	1304	976	883
	1/3	1395	1605	1037	865
103	1	1621	1447	1075	948
	1/3	1524	1796	1081	1000

TABLE 5 - POSSIBLE SOURCES OF ERROR IN V AND B DETERMINATIONS

No.	Type Error	Estimated Maximum % Effect on V_p	Estimated Maximum % Effect on V_s	Estimated Maximum % Effect on Both	Random	Comments
1	First arrival interpretation	5	25		No	Some independent checks by Dr. Woods
2	Accelerometer vibrations not fixed in surrounding sand	Unknown, but probably small			No	Accelerometer 4 cm long, 2 cm ϕ, test wave-lengths 5 to 15 cm, c-c spacing 35 to 69 cm
3	Estimated times on scope			4	Yes	Reduces to 2% when average 5
4	Inaccurate accelerometer placement			2	Yes	Placed to $\pm$1/4 cm
5	Nonuniform stress condition at top chamber due to rigid top platen	Unknown			No	Affects only $\theta = 0°$ and 30° tests, tend to increase V_p at K = 1/3, tend to reduce anisotropy of B
6	Varying levels of average σ'_o between accelerometers			3	No	Corrected (see 4.1)
7	Scope sweep rate			0.5	No	Calibrated and corrected
8	Sand compression under chamber stress			1	No	Measured and corrected
9	Varying average whole-chamber γ_d between tests in a density group			1	Yes	Measured and corrected
10	Relatively loose/dense layers between accelerometers			1/2	Yes	Minor due to replicate tests and averaging
11	Loosening dense sand and densifying loose sand around accelerometer during placement			1/4	No	
12	Different levels of shear strain during V_p and V_s determinations	Probably small			No	Approximately 50% of push impact energy used in shear impacts, both strain less than 10-3%

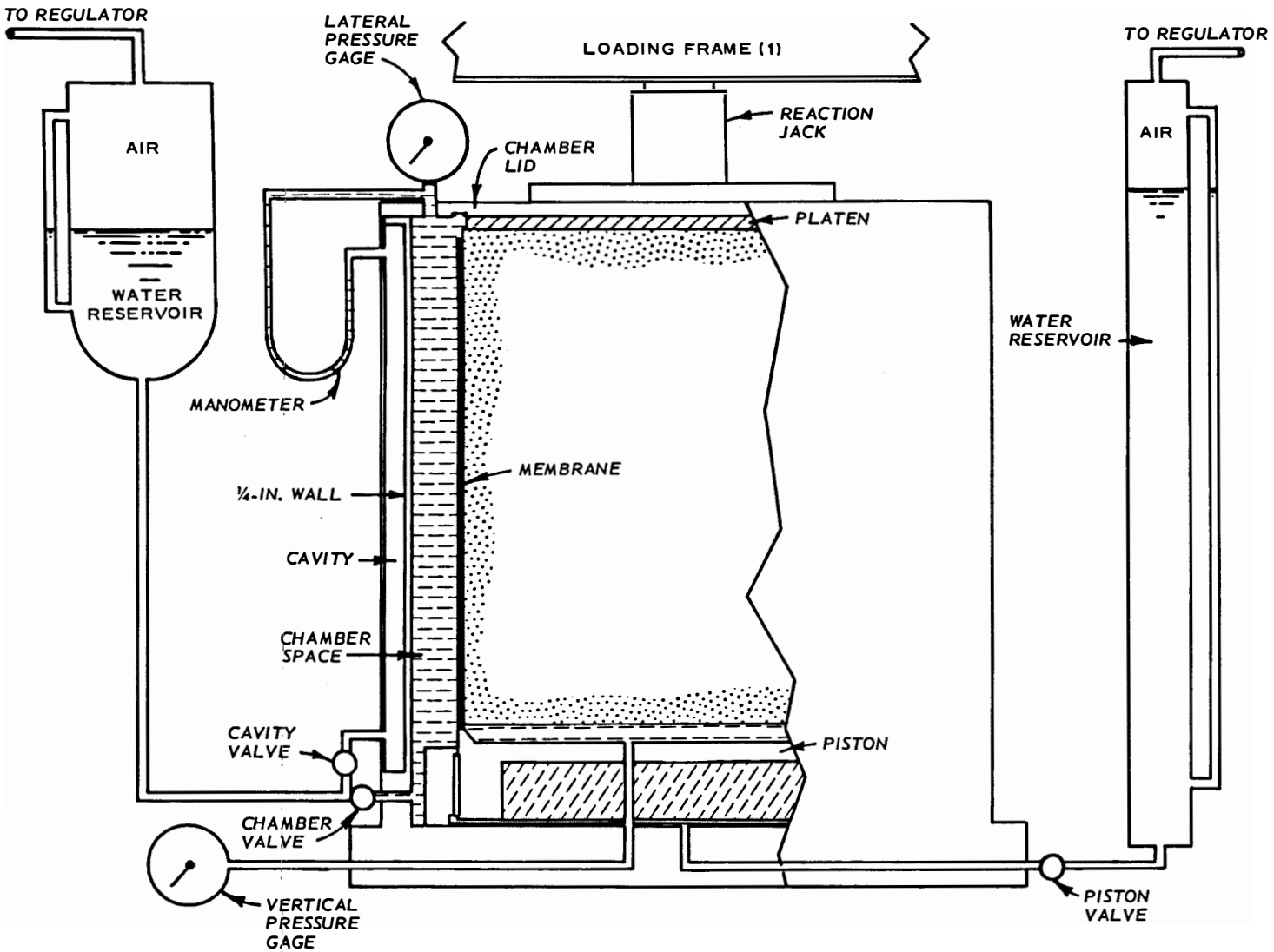

FIGURE 1 - SCHEMATIC OF UNIVERSITY OF FLORIDA CALIBRATION CHAMBER AND LOADING SYSTEM

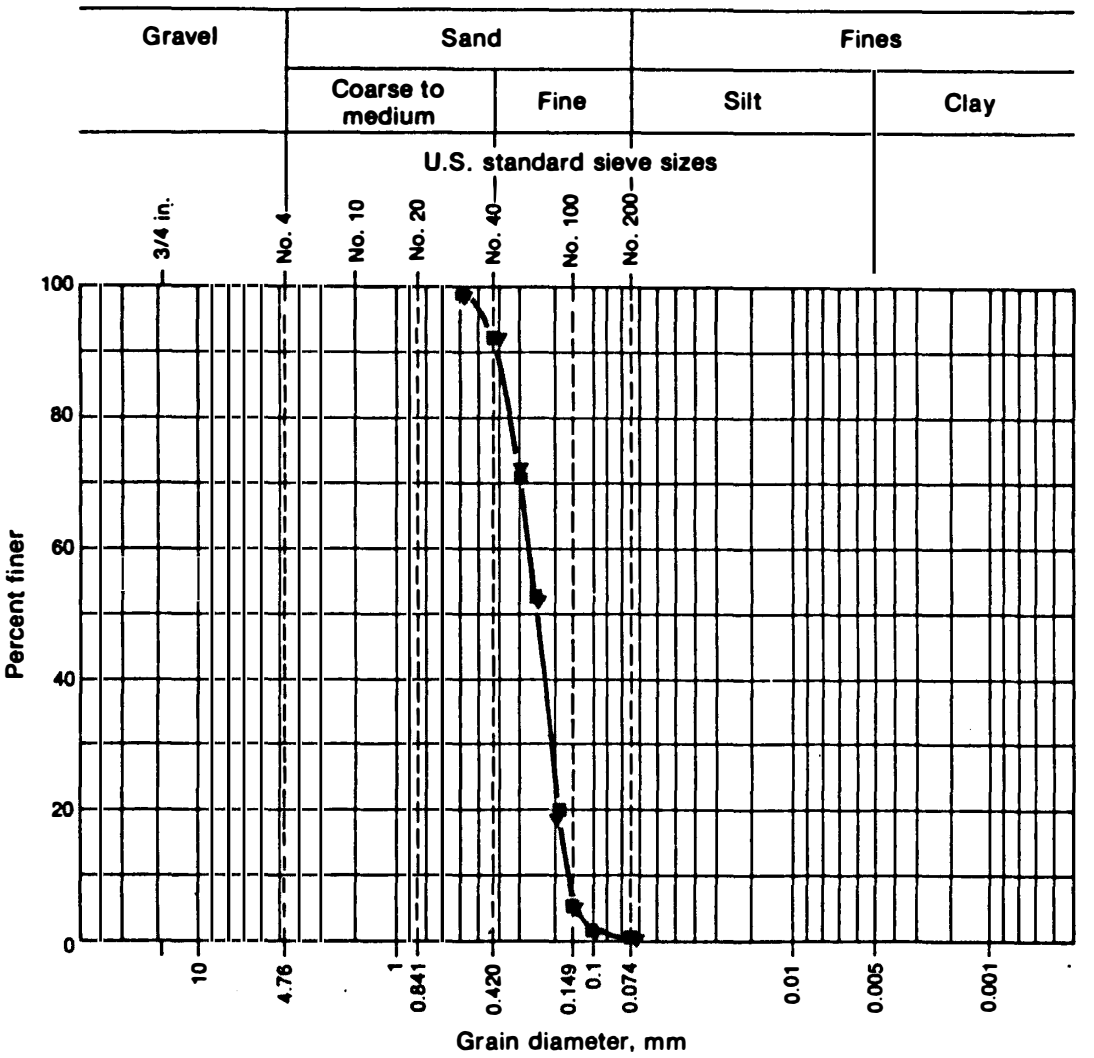

FIGURE 2 - SIEVE ANALYSES OF THE REID-BEDFORD MODEL SAND USED IN THIS RESEARCH

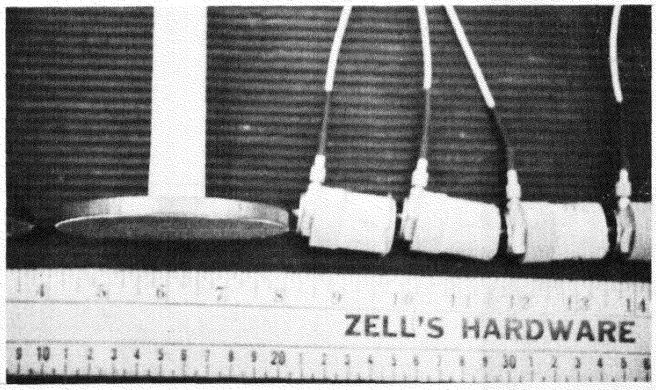

(a) Plates and accelerometers

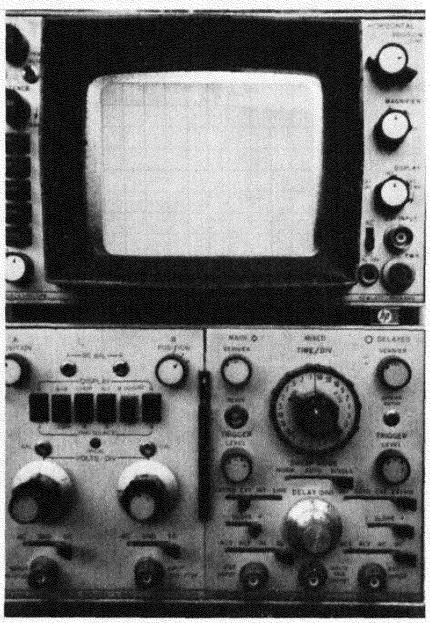

(b) HP oscilloscope

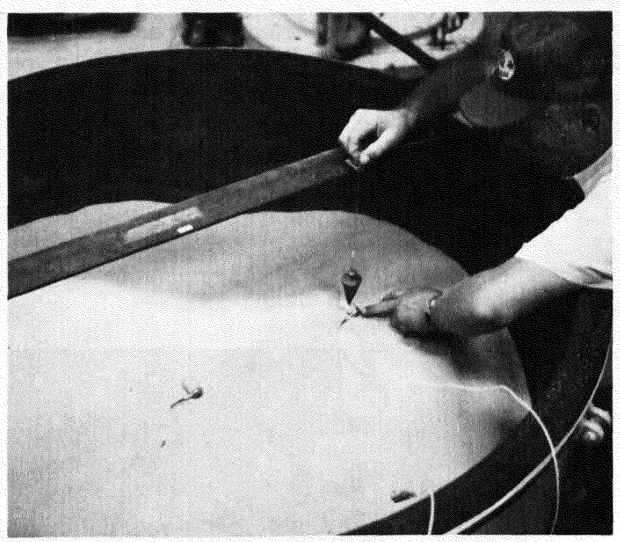

(c) W. Whitehead positioning A3

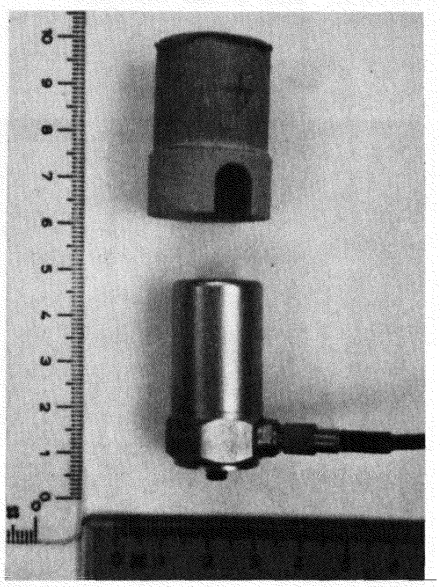

(e) Accelerometer and cap

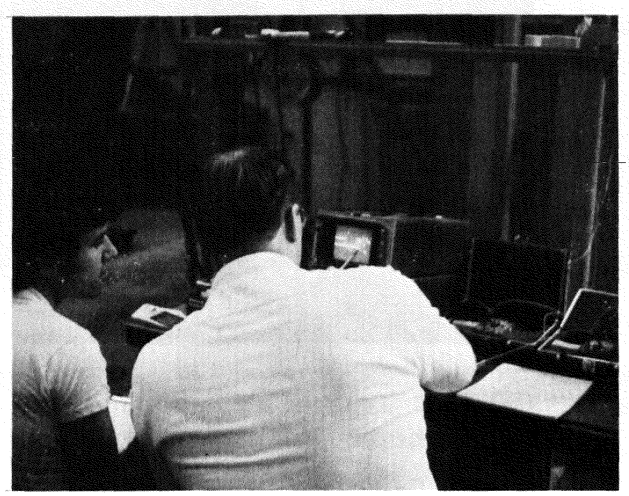

(d) H. Margas (L) and Dr. Woods (R) interpreting waveforms during Test 13

FIGURE 3 - RESEARCH EQUIPMENT AND METHODS

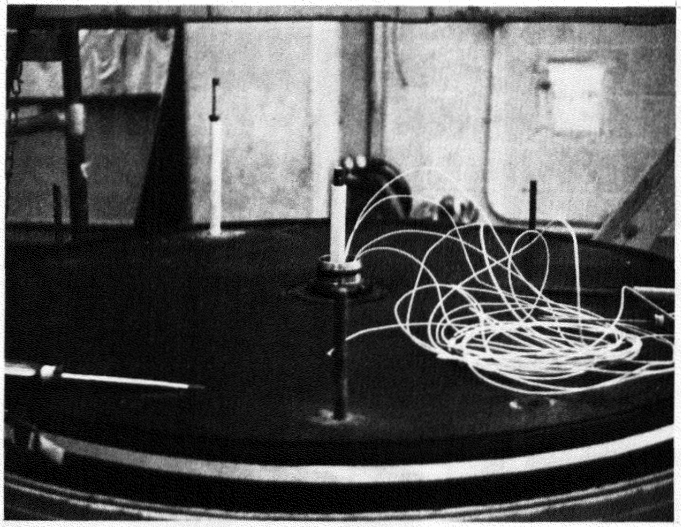

(a) Photo shows the vertical rods, attached to the 3-in. diameter, rough-bottomed plates buried 3 cm below sand surface, passing through the two holes in the top platen. They are encased in an insulating plastic pipe to prevent shorting of the signal trigger system. The cables from the four buried accelerometers come out through the larger center hole. All accelerometer cables were carried as far as possible away from wave paths between accelerometers within the sand sample

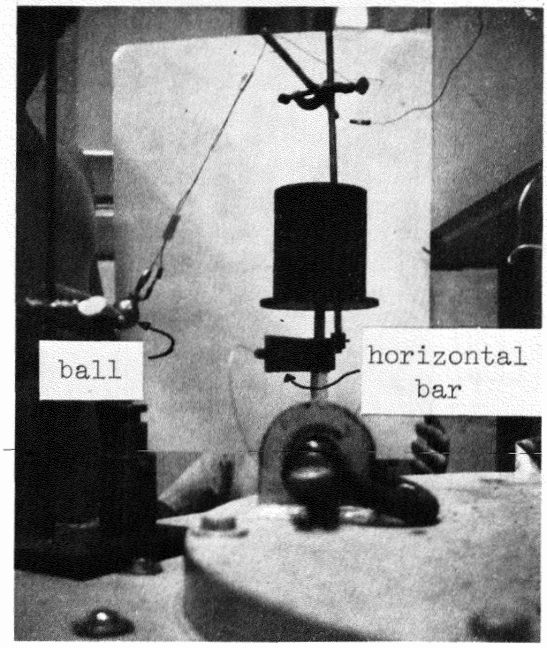

(b) Ball pulled back to reference bar, then let go to swing and strike horizontal bar clamped to vertical rod. Weight was added to insure no plate slip during impact

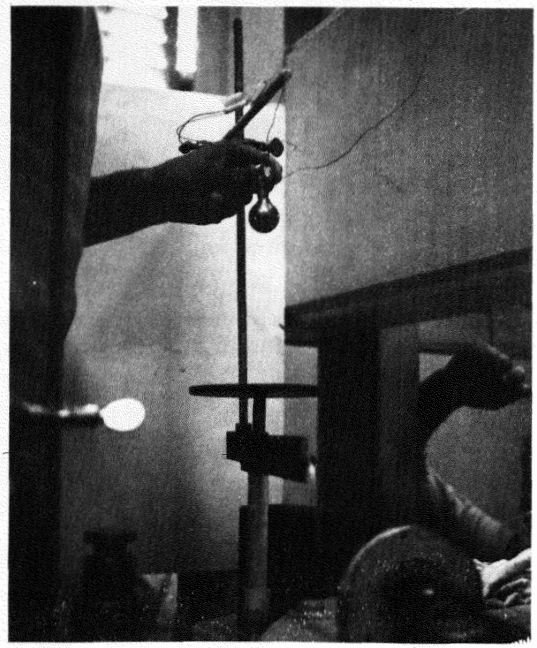

(c) Ball dropped from reference bar height to strike center of plate

FIGURE 4 - THE MECHANICAL SWINGING AND DROPPING BALL IMPACT SYSTEM USED IN TESTS 7 THROUGH 13a

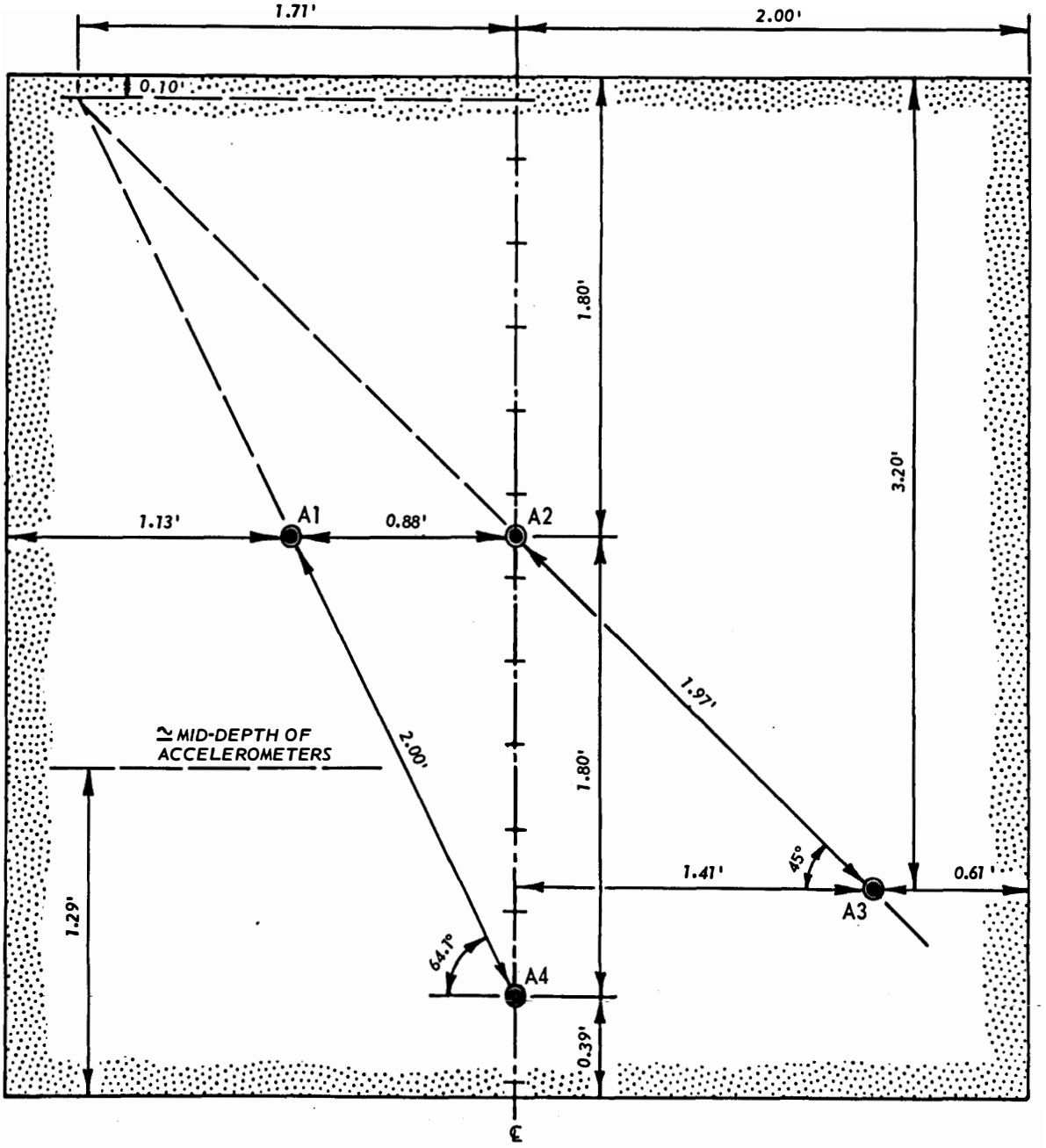

FIGURE 5 - ACCELEROMETER PATTERN IN PLANE THROUGH AXIS OF CHAMBER, USED FOR TESTS 3 AND 4

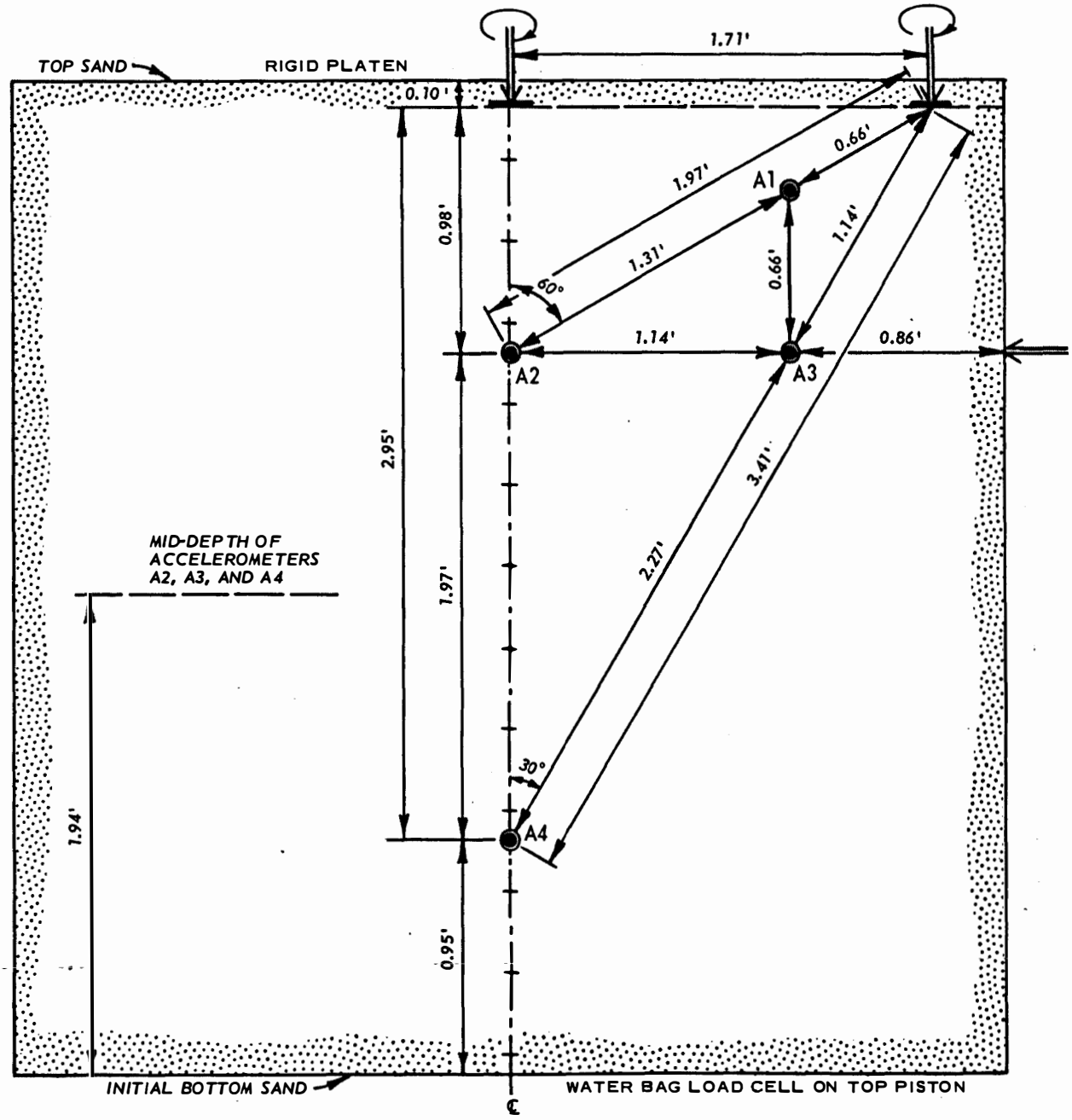

FIGURE 6 - ACCELEROMETER PATTERN IN PLANE THROUGH AXIS OF CHAMBER, USED FOR TESTS 6 THROUGH 13

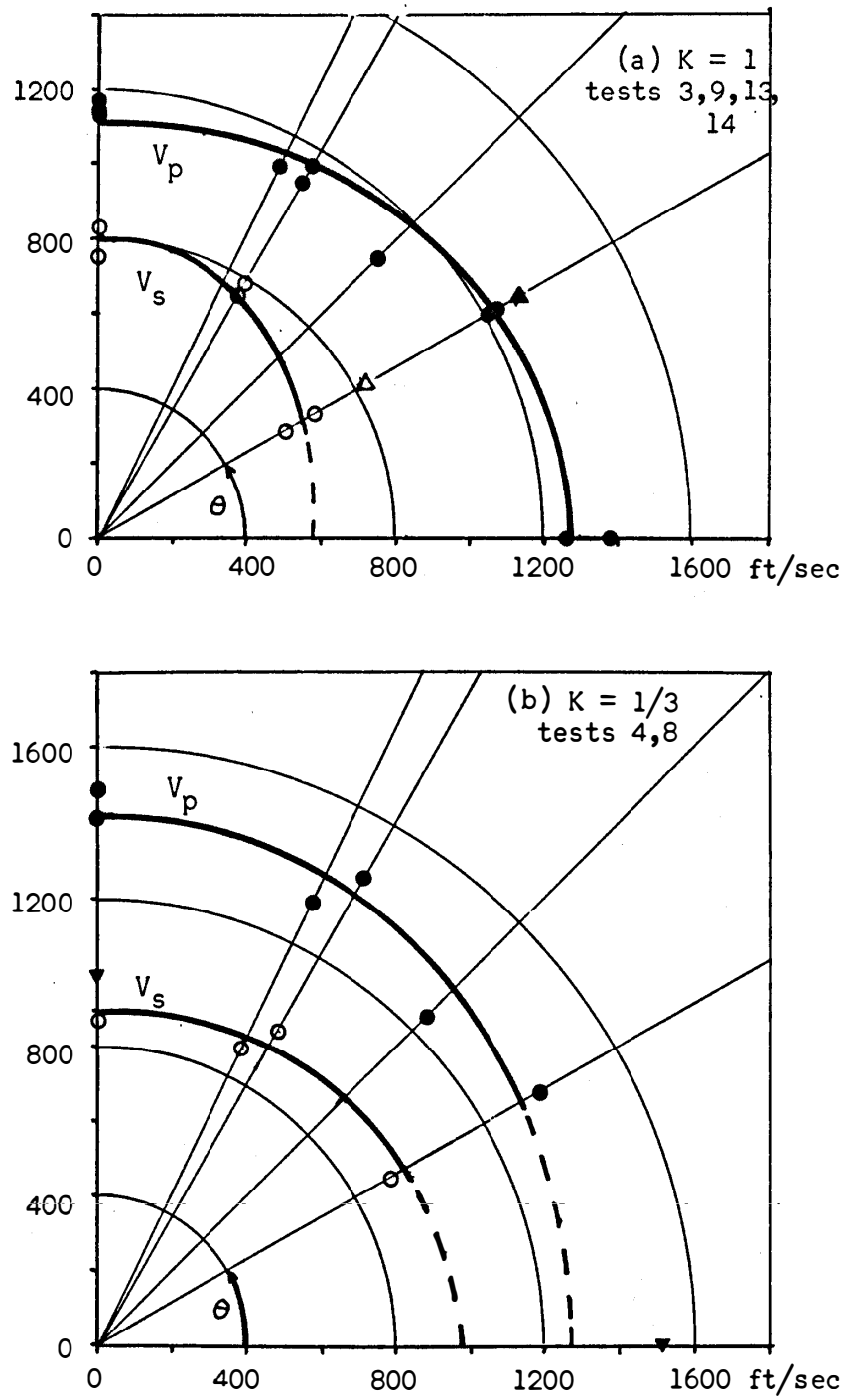

FIGURE 7 - BEST-FIT EQUATION 2 CURVES THROUGH V_p AND V_s DATA AT LOW DENSITY, OCTAHEDRAL STRESS = 5.0 PSI

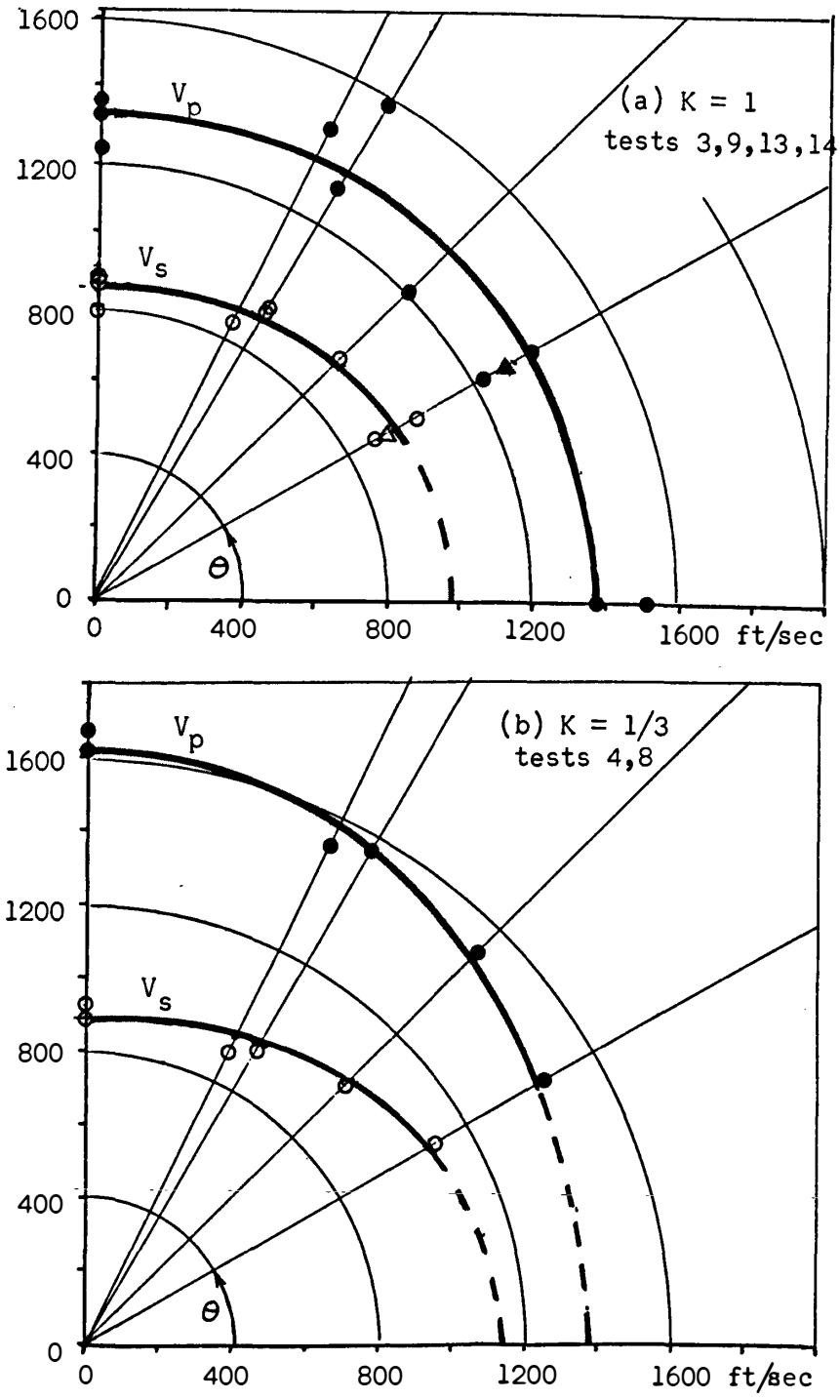

FIGURE 8 - BEST-FIT EQUATION 2 CURVES THROUGH V_p AND V_s DATA AT LOW DENSITY, OCTAHEDRAL STRESS = 10.0 PSI

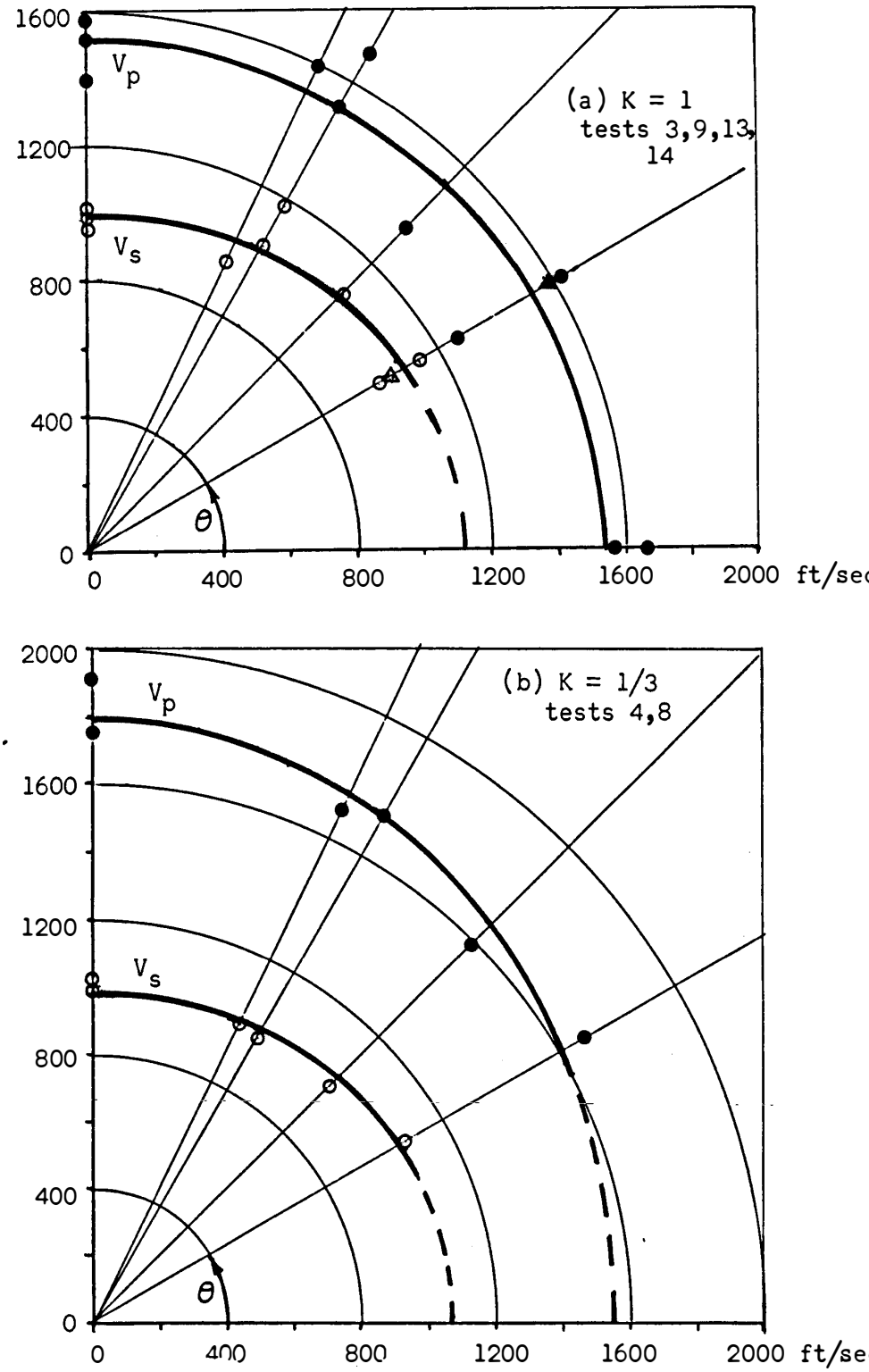

FIGURE 9 - BEST-FIT EQUATION 2 CURVES THROUGH V_p AND V_s DATA AT LOW DENSITY, OCTAHEDRAL STRESS = 20.0 PSI

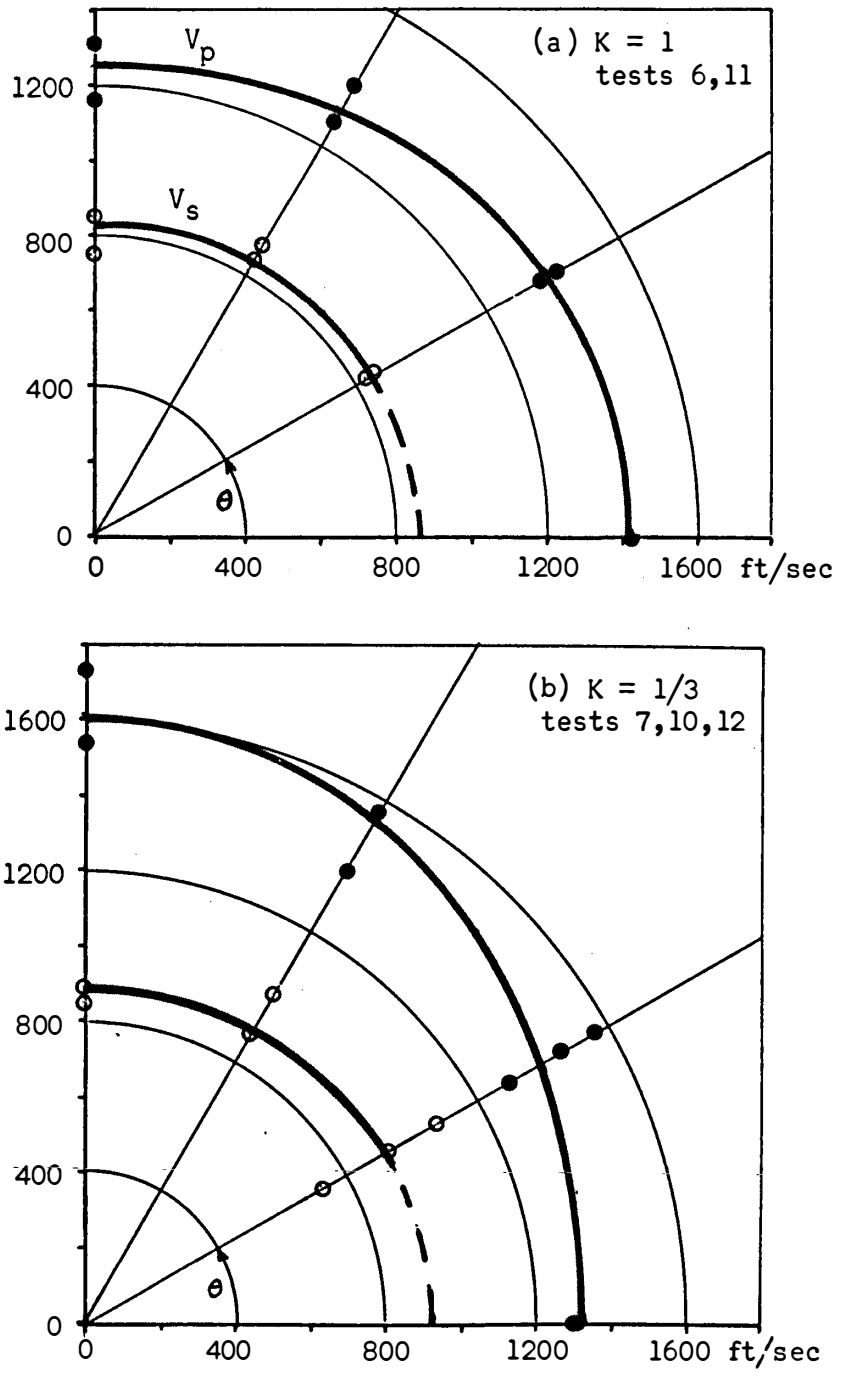

FIGURE 10 - BEST-FIT EQUATION 2 CURVES THROUGH V_p AND V_s DATA AT HIGH DENSITY, OCTAHEDRAL STRESS = 5.0 PSI

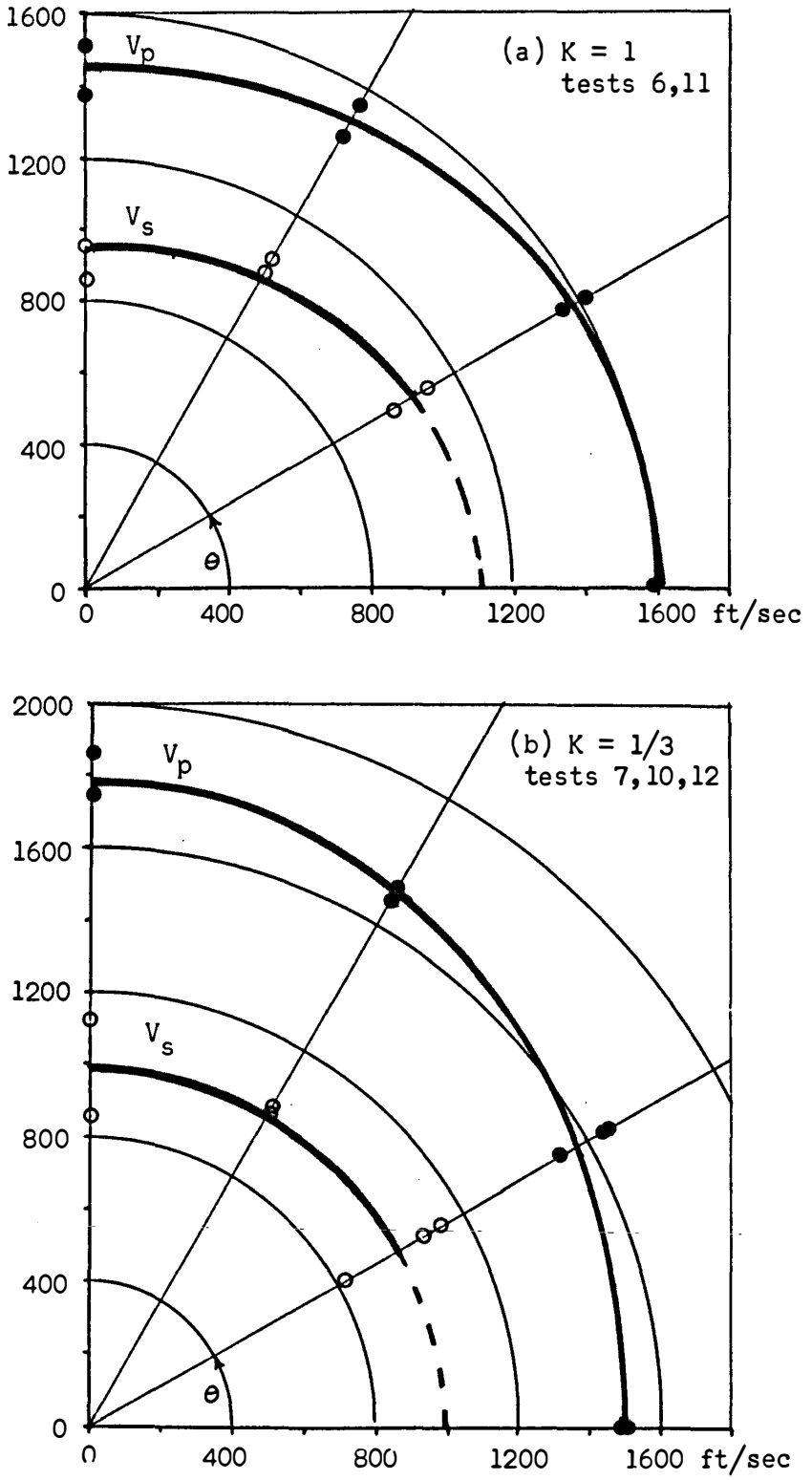

FIGURE 11 - BEST-FIT EQUATION 2 CURVES THROUGH V_p AND V_s DATA AT HIGH DENSITY, OCTAHEDRAL STRESS = 10.0 PSI

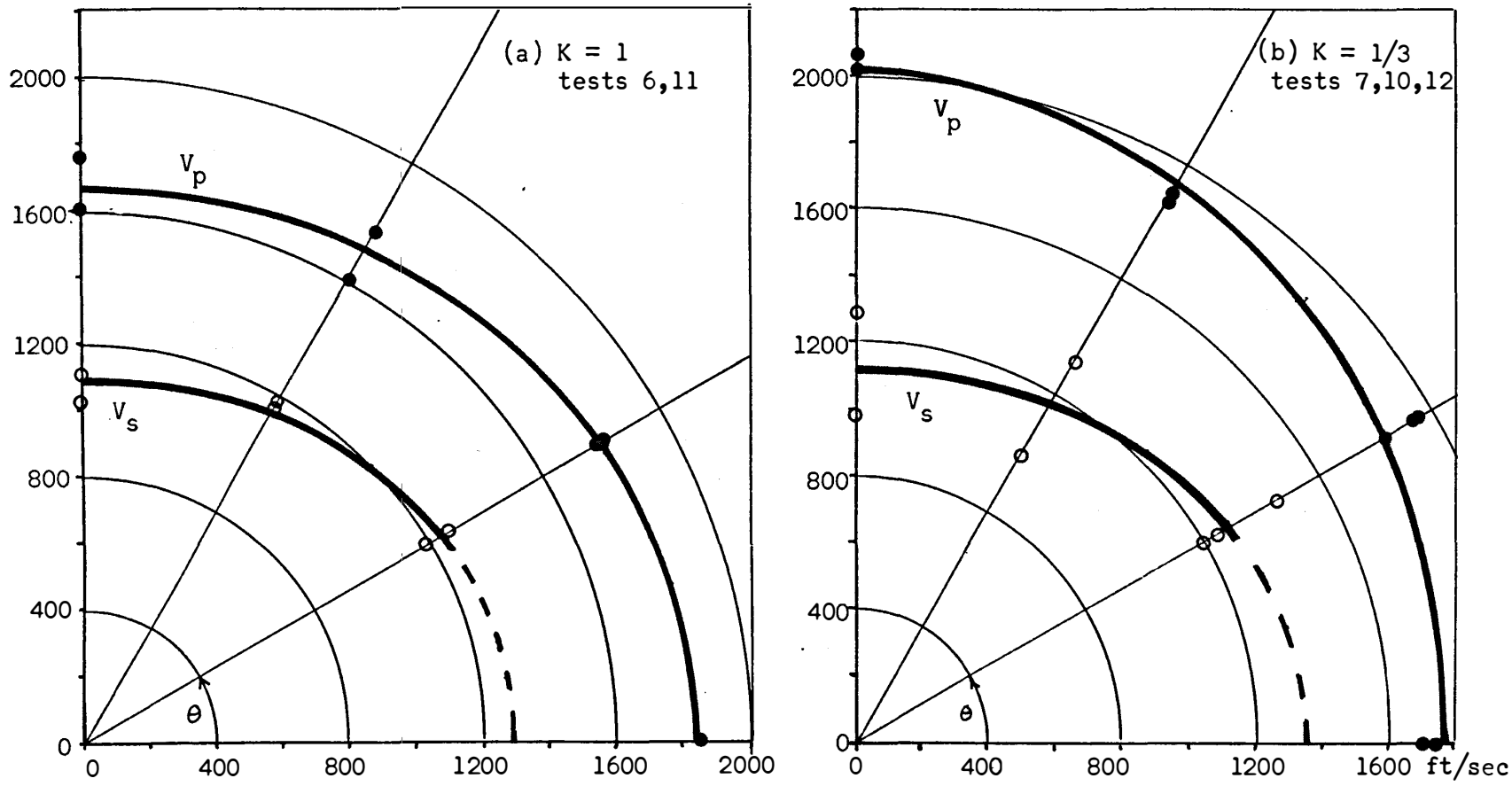

FIGURE 12 - BEST-FIT EQUATION 2 CURVES THROUGH V_p AND V_s DATA AT HIGH DENSITY, OCTAHEDRAL STRESS = 20.0 PSI

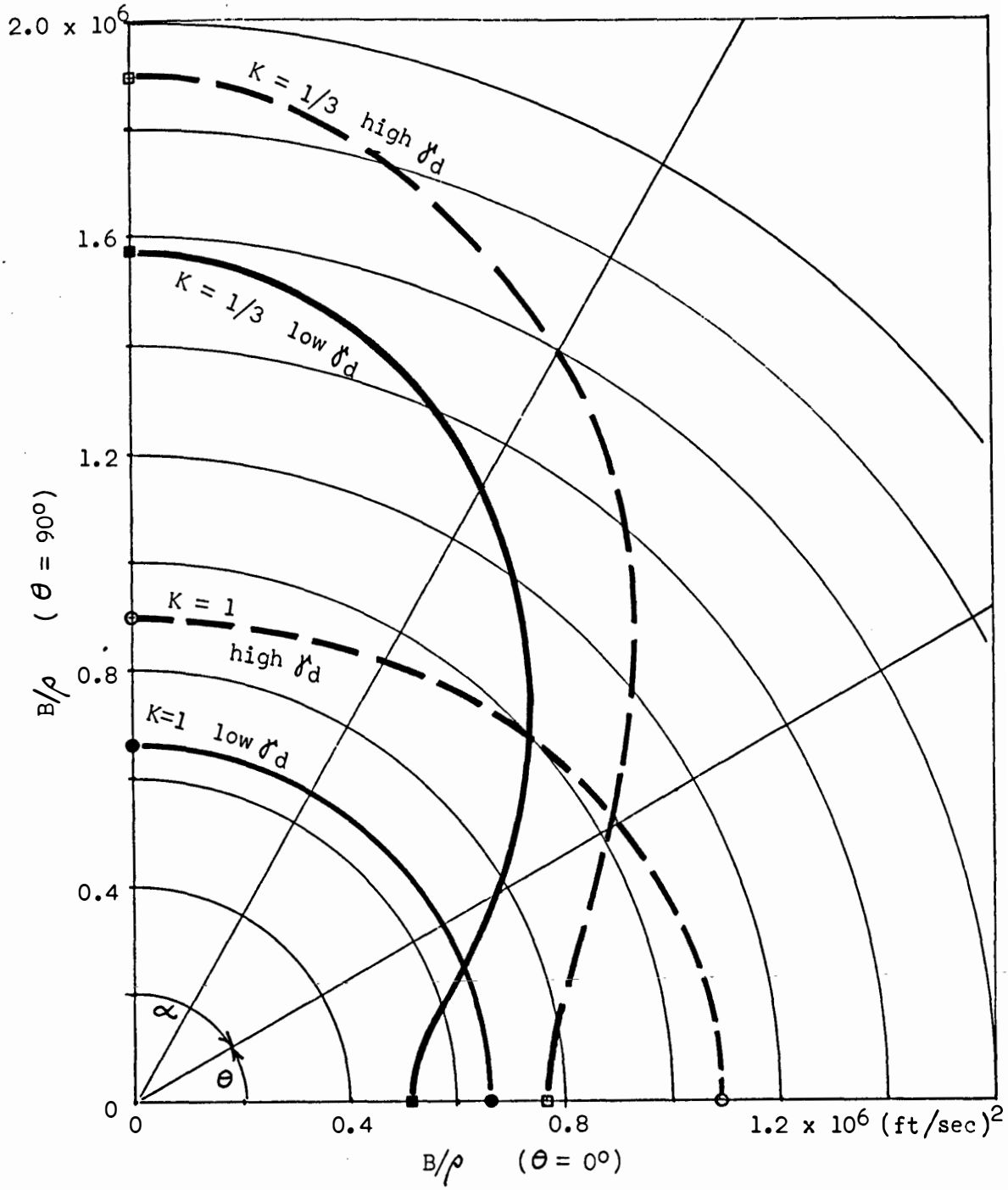

FIGURE 13 - ANISOTROPIC CHARACTER OF DYNAMIC BULK MODULUS FROM TABLE 4, EQUATION 2, WITH σ_o' = 10.0 PSI

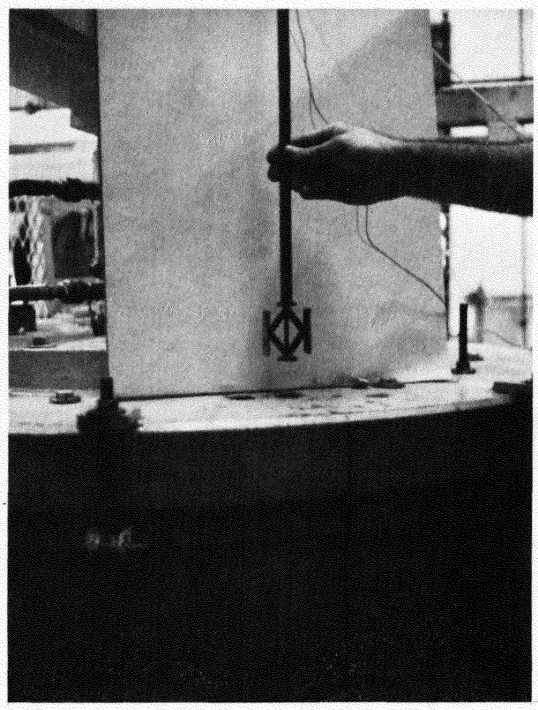

(a) Down-hole scissor--source of reversible shear wave

(b) Impact, trigger and counterweight system

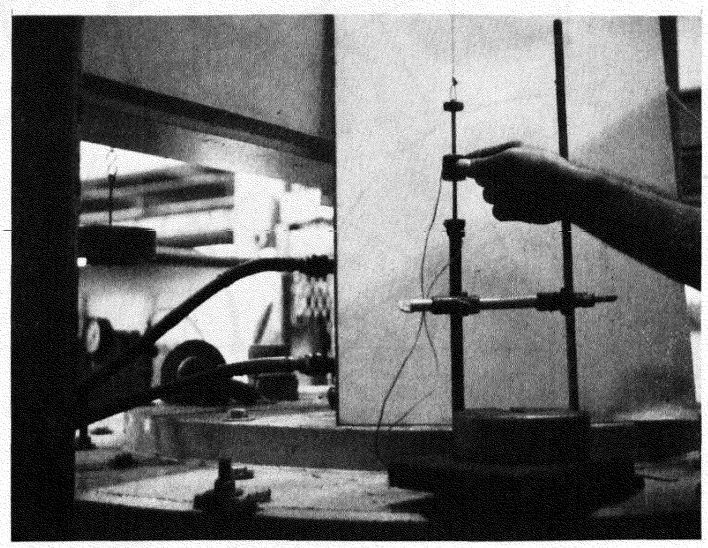

FIGURE 14 - SCISSOR-TYPE EQUIPMENT USED IN TEST 14

APPENDIX A

POLAROID PHOTOGRAPHS OF TYPICAL OSCILLOSCOPE WAVEFORMS FROM EACH REPLICATE SERIES OF FIVE IMPACTS IN ORDER OF ACQUISITION NUMBER .

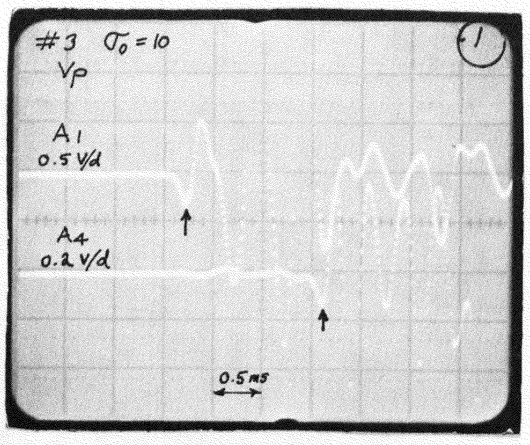
#3 $\sigma_0 = 10$
Vp
1
A1
0.5 V/d
A4
0.2 V/d
0.5 ms

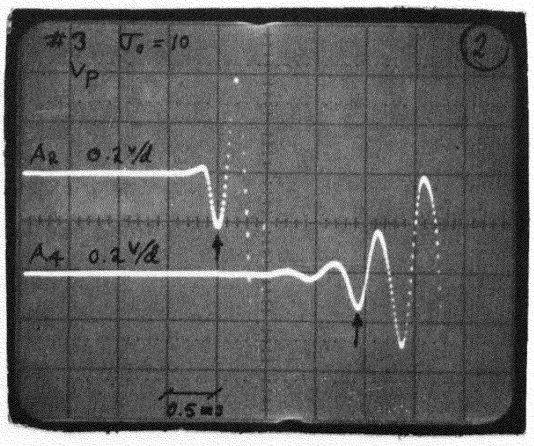
#3 $\sigma_0 = 10$
Vp
2
A2 0.2 V/d
A4 0.2 V/d
0.5 ms

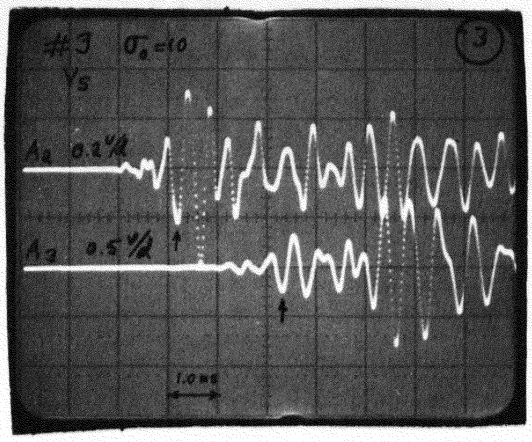
#3 $\sigma_0 = 10$
Vs
3
A2 0.2 V/d
A3 0.5 V/d
1.0 ms

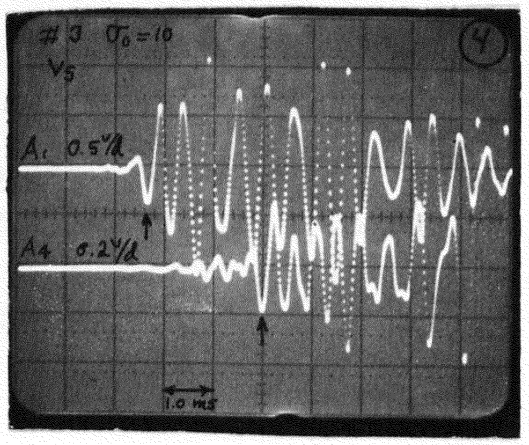
#3 $\sigma_0 = 10$
Vs
4
A1 0.5 V/d
A4 0.2 V/d
1.0 ms

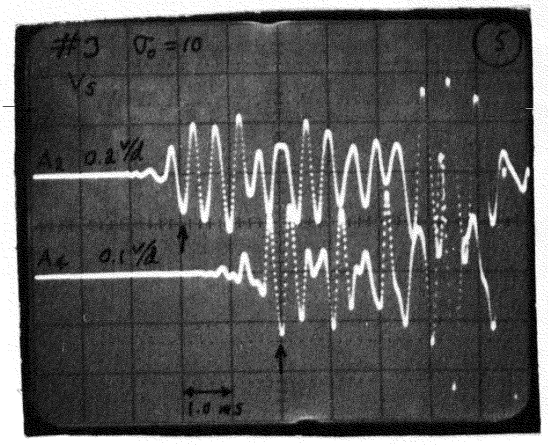
#3 $\sigma_0 = 10$
Vs
5
A2 0.2 V/d
A4 0.1 V/d
1.0 ms

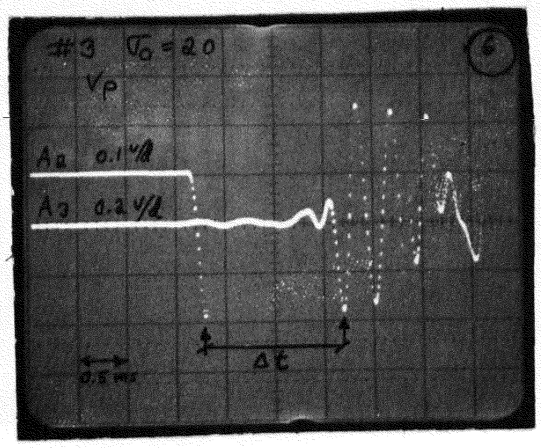
#3 $\sigma_0 = 20$
Vp
6
A2 0.1 V/d
A3 0.2 V/d
Δt
0.5 ms

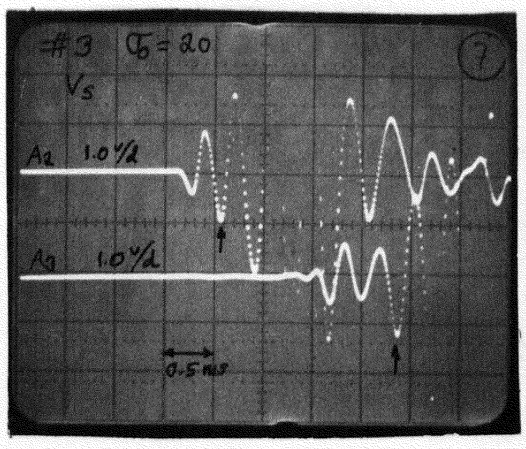
#3 $\sigma_0 = 20$
7
V_S
A_2 1.0 v/d
A_3 1.0 v/d
0.5 ms

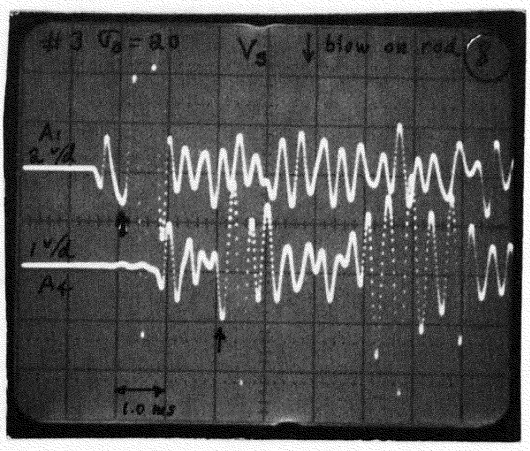
#3 $\sigma_0 = 20$
V_S
↓ blow on rod
8
A_1
2 v/d
1 v/d
A_4
1.0 ms

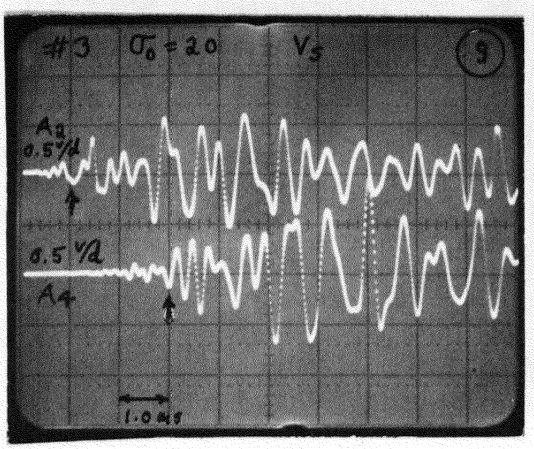
#3 $\sigma_0 = 20$
V_S
9
A_3
0.5 v/d
0.5 v/d
A_4
1.0 ms

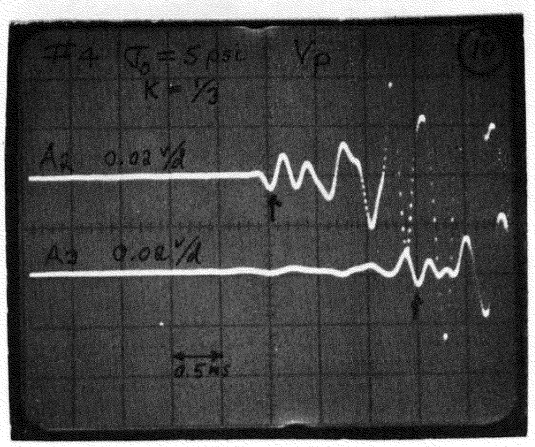
#4 $\sigma_0 = 5$ psi
$K = 1/3$
V_P
10
A_2 0.02 v/d
A_3 0.02 v/d
0.5 ms

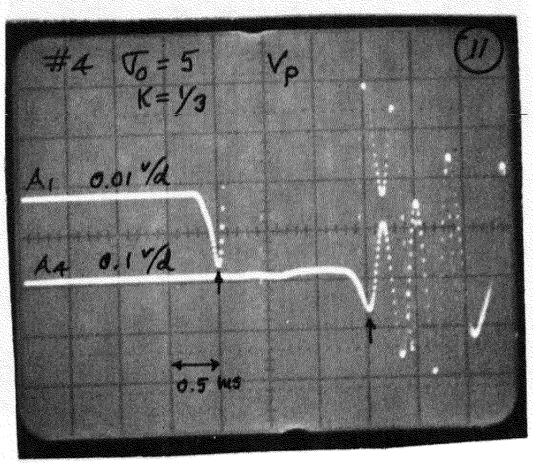
#4 $\sigma_0 = 5$
$K = 1/3$
V_P
11
A_1 0.01 v/d
A_4 0.1 v/d
0.5 ms

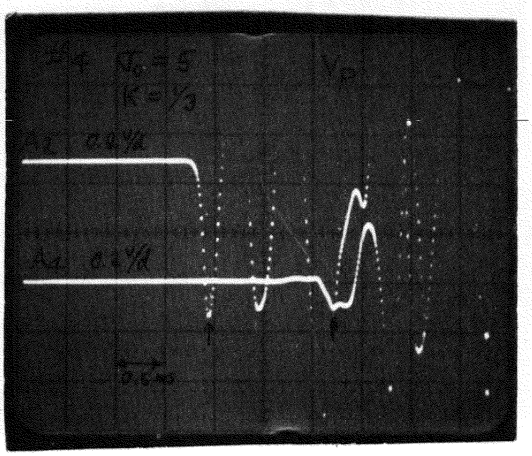
#4 $\sigma_0 = 5$
$K = 1/3$
V_P
A_1 0.4 v/d
A_4 0.4 v/d
0.5 ms

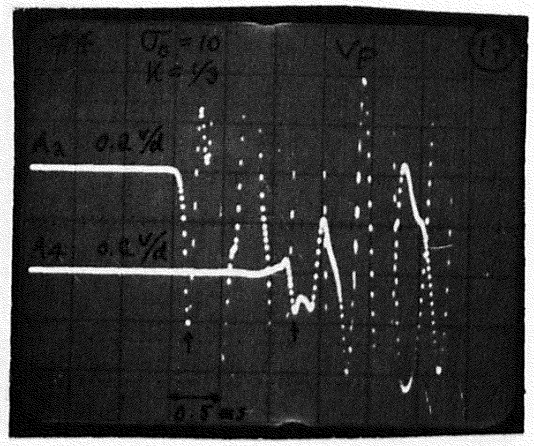
#4 $\sigma_0 = 10$
$K = 1/3$
V_p
(13)
A_2 0.2 V/d
A_4 0.2 V/d
0.5 ms

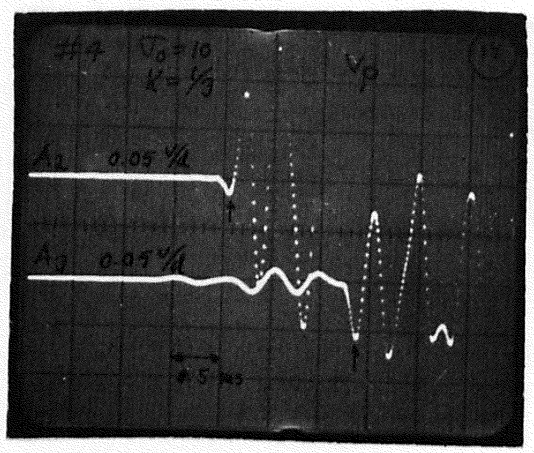
#4 $\sigma_0 = 10$
$K = 1/3$
V_p
(14)
A_2 0.05 V/d
A_3 0.05 V/d
0.5 ms

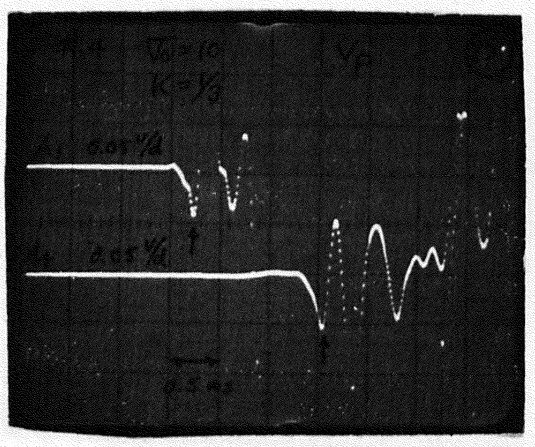
#4 $\sigma_0 = 10$
$K = 1/3$
V_p
(15)
A_1 0.05 V/d
A_2 0.05 V/d
0.5 ms

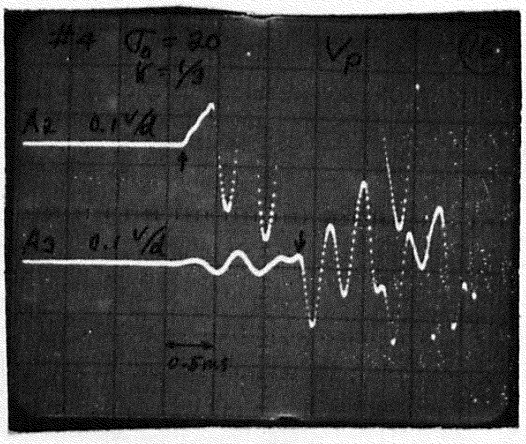
#4 $\sigma_0 = 20$
$K = 1/3$
V_p
(16)
A_2 0.1 V/d
A_3 0.1 V/d
0.5 ms

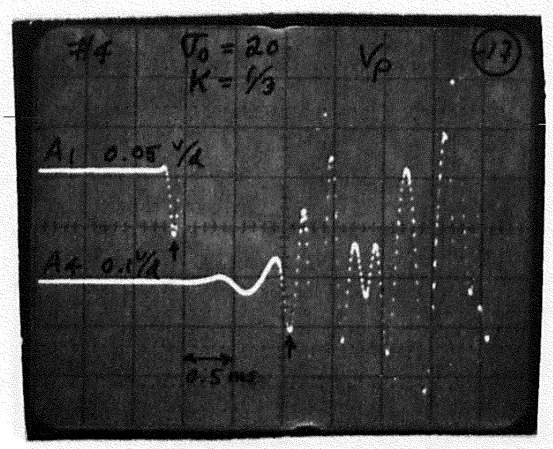
#4 $\sigma_0 = 20$
$K = 1/3$
V_p
(17)
A_1 0.05 V/d
A_4 0.1 V/d
0.5 ms

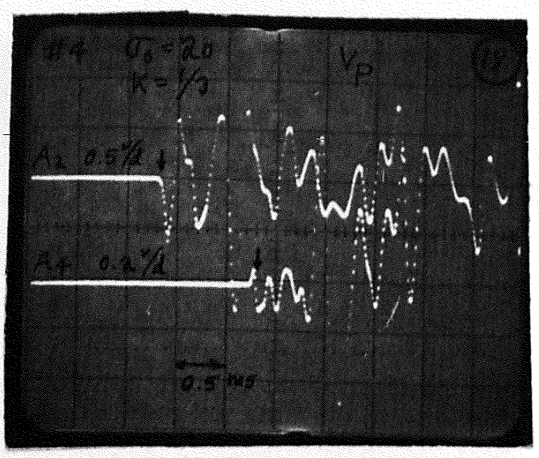
#4 $\sigma_0 = 20$
$K = 1/3$
V_p
(18)
A_2 0.5 V/d
A_4 0.2 V/d
0.5 ms

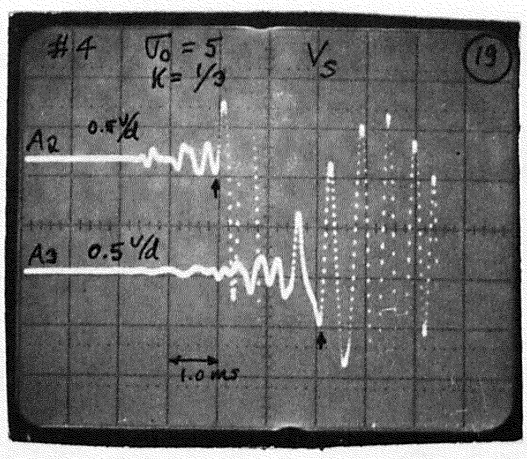
#4 $\sigma_0 = 5$ $K = 1/3$ V_S (19)
A_2 0.5 V/d
A_3 0.5 V/d
1.0 MS

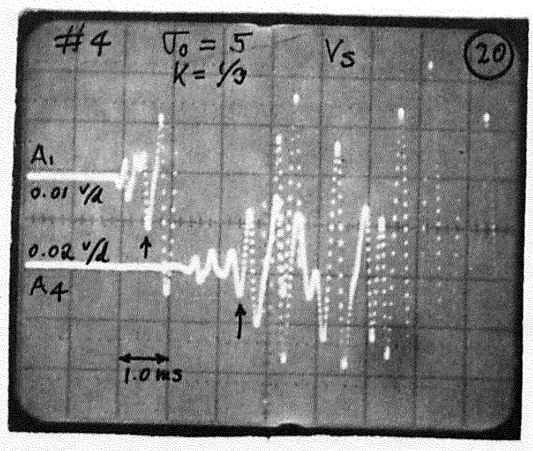
#4 $\sigma_0 = 5$ $K = 1/3$ V_S (20)
A_1
0.01 V/d
0.02 V/d
A_4
1.0 MS

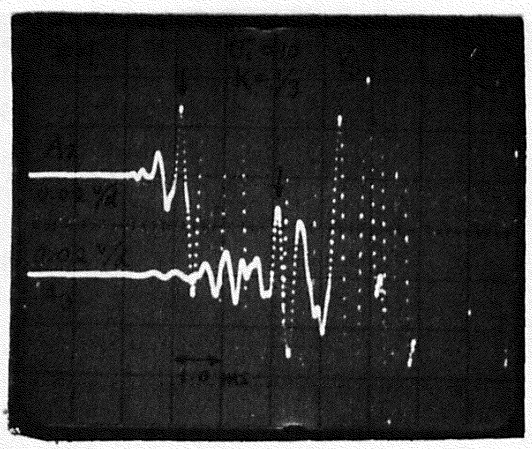

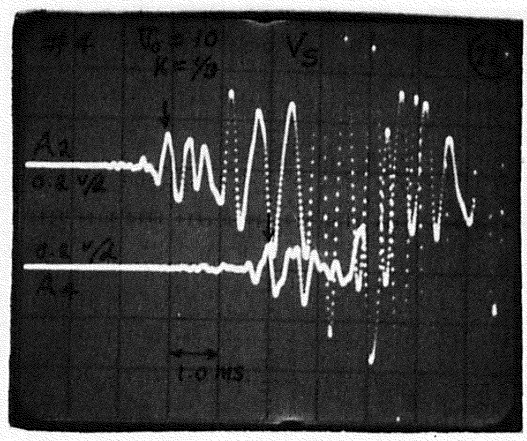
#4 $\sigma_0 = 10$ $K = 1/3$ V_S
A_3
0.2 V/d
0.2 V/d
A_4
1.0 MS

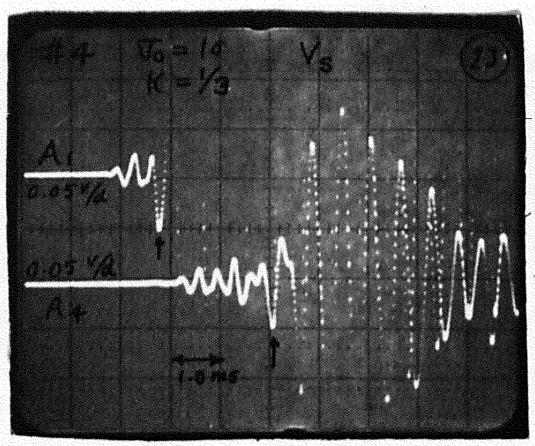
#4 $\sigma_0 = 14$ $K = 1/3$ V_S (13)
A_1
0.05 V/d
0.05 V/d
A_4
1.0 MS

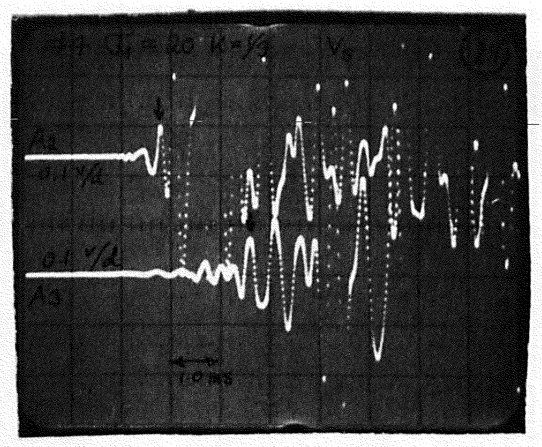
#4 $\sigma_0 = 20$ $K = 1/3$ V_S
A_3
0.1 V/d
0.1 V/d
A_3
1.0 MS

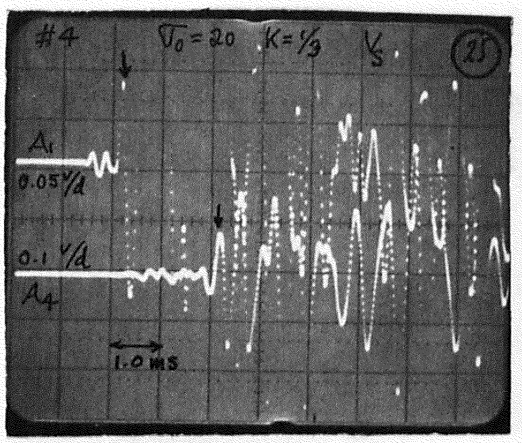
#4
$\sigma_0 = 20$
K = 1/3
V_S
25
A_1
0.05 v/d
0.1 v/d
A_4
1.0 ms

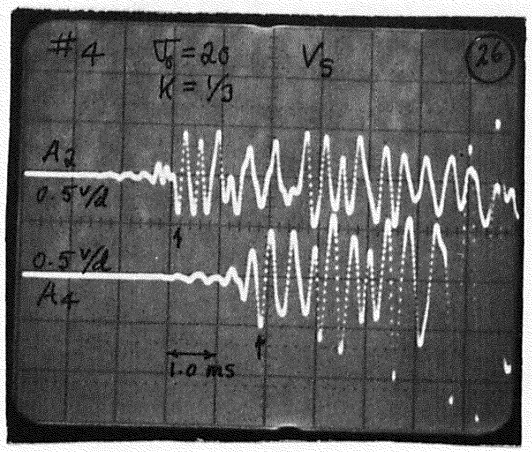
#4
$\sigma_0 = 20$
K = 1/3
V_S
26
A_2
0.5 v/d
0.5 v/d
A_4
1.0 ms

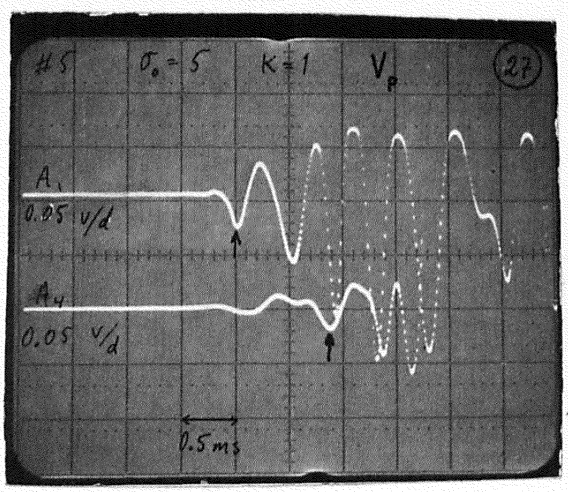
#5
$\sigma_0 = 5$
K = 1
V_P
27
A_1
0.05 v/d
A_4
0.05 v/d
0.5 ms

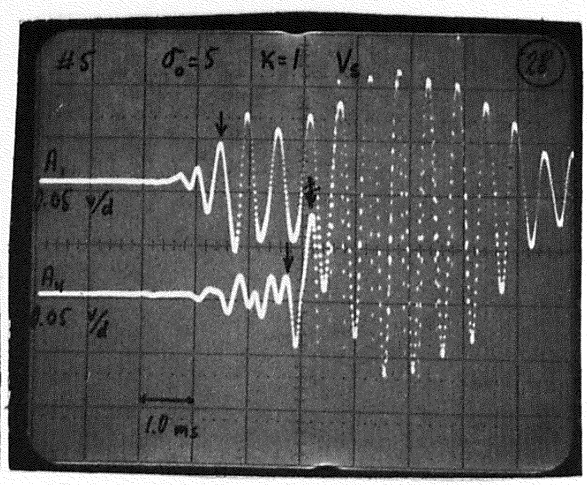
#5
$\sigma_0 = 5$
K = 1
V_S
28
A_1
0.05 v/d
A_4
0.05 v/d
1.0 ms

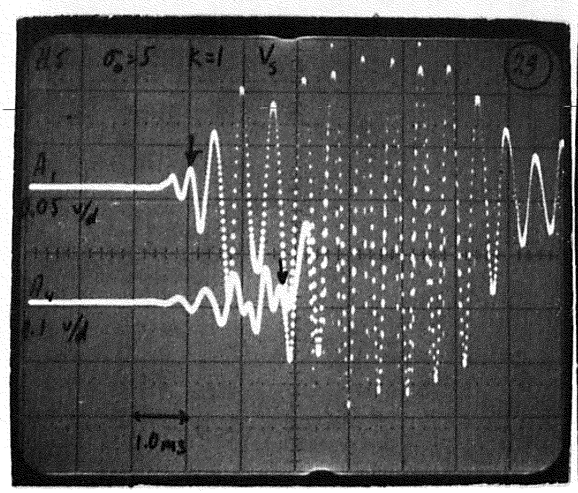
#5
$\sigma_0 = 5$
K = 1
V_S
29
A_1
0.05 v/d
A_4
0.1 v/d
1.0 ms

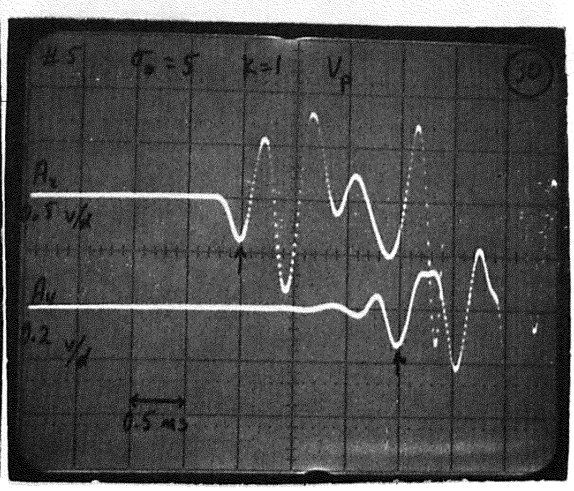
#5
$\sigma_0 = 5$
K = 1
V_P
30
A_1
0.5 v/d
A_4
0.2 v/d
0.5 ms

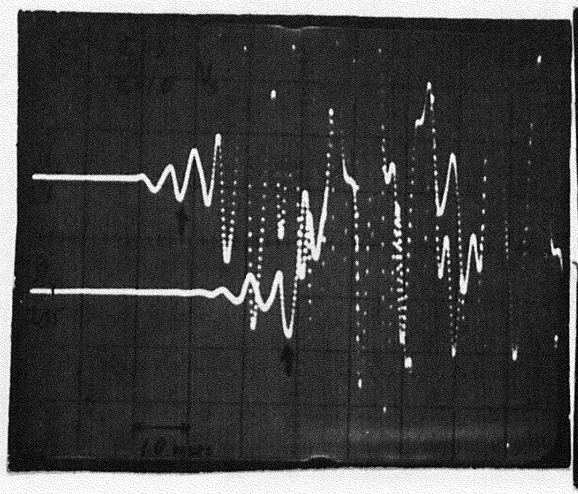

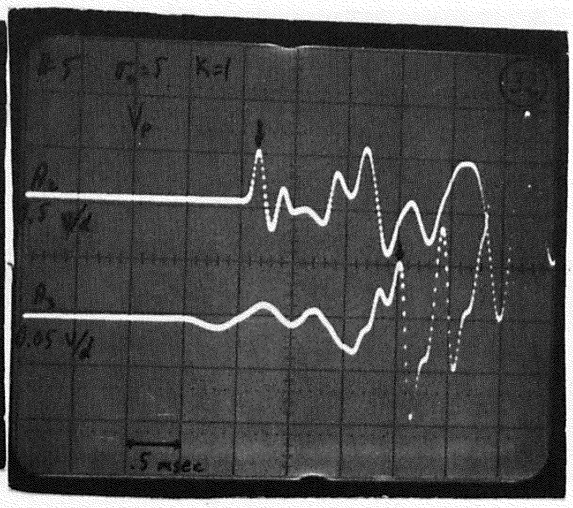
#5 σ_0=5 K=1
V_P
A_2
1.5 v/d
A_1
0.05 v/d
.5 msec

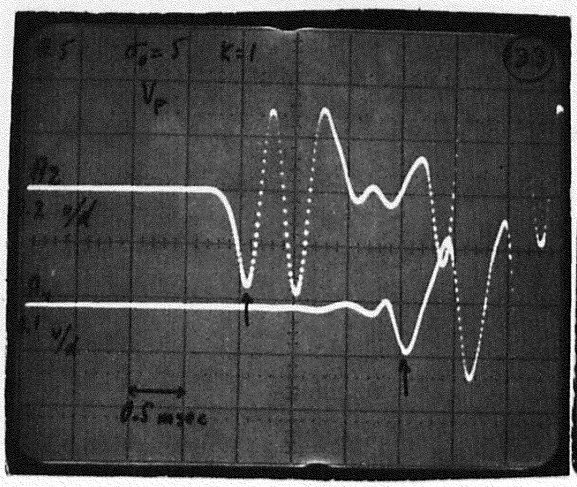
#5 σ_0=5 K=1
V_P
A_2
0.2 v/d
A_1
0.1 v/d
0.5 msec

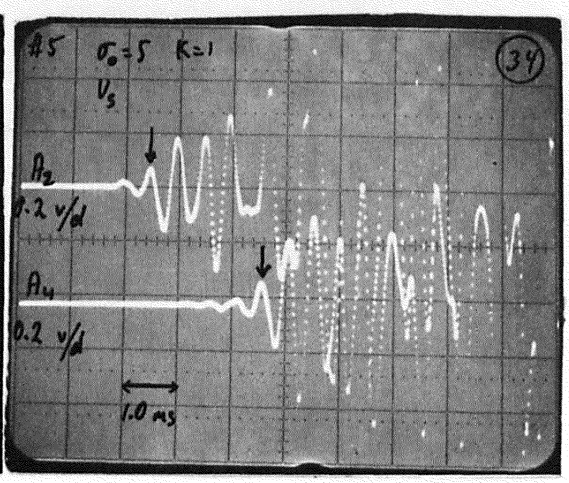
#5 σ_0=5 K=1
V_S
A_2
0.2 v/d
A_1
0.2 v/d
1.0 ms

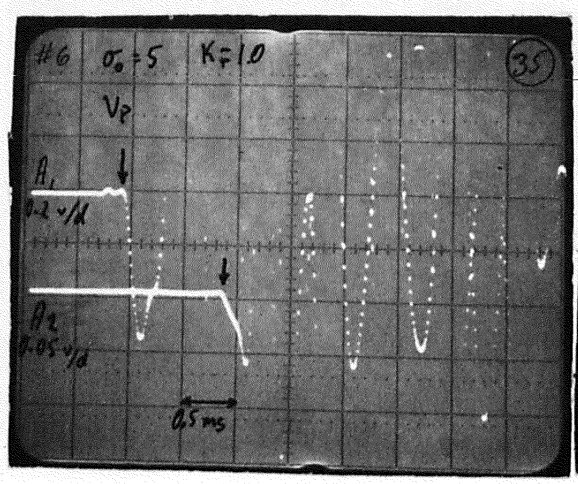
#6 σ_0=5 K=1.0
V_P
A_1
0.2 v/d
A_2
0.05 v/d
0.5 ms

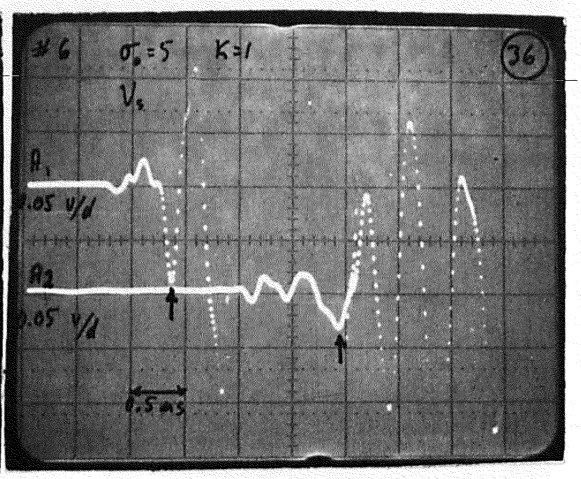
#6 σ_0=5 K=1
V_S
A_1
0.05 v/d
A_2
0.05 v/d
0.5 ms

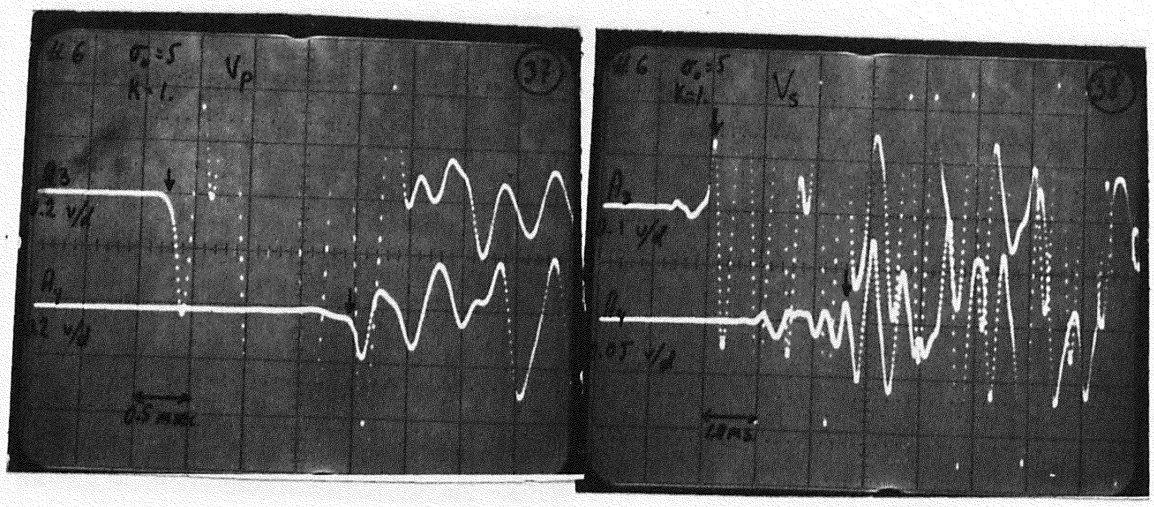
σ₀=5
K=1
Vp
37
A3
0.2 v/d
A4
0.2 v/d
0.5 msec
σ₀=5
K=1
Vs
38
A3
0.1 v/d
A4
0.05 v/d
2.0 ms

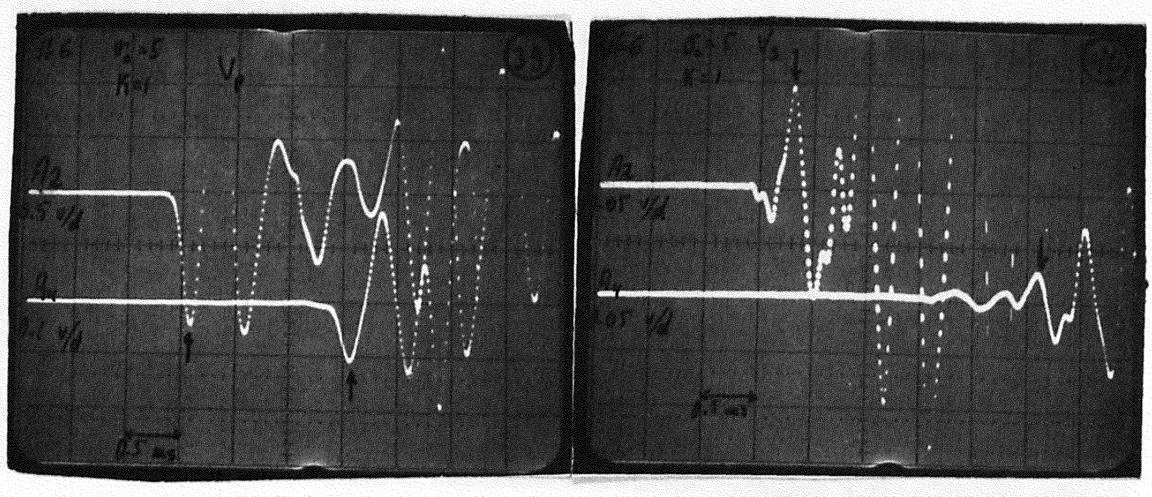
σ₀=5
K=1
Vp
39
A2
0.5 v/d
A4
0.1 v/d
0.5 ms
σ₀=5
K=1
Vs
40
A2
0.05 v/d
A4
0.05 v/d
0.5 ms

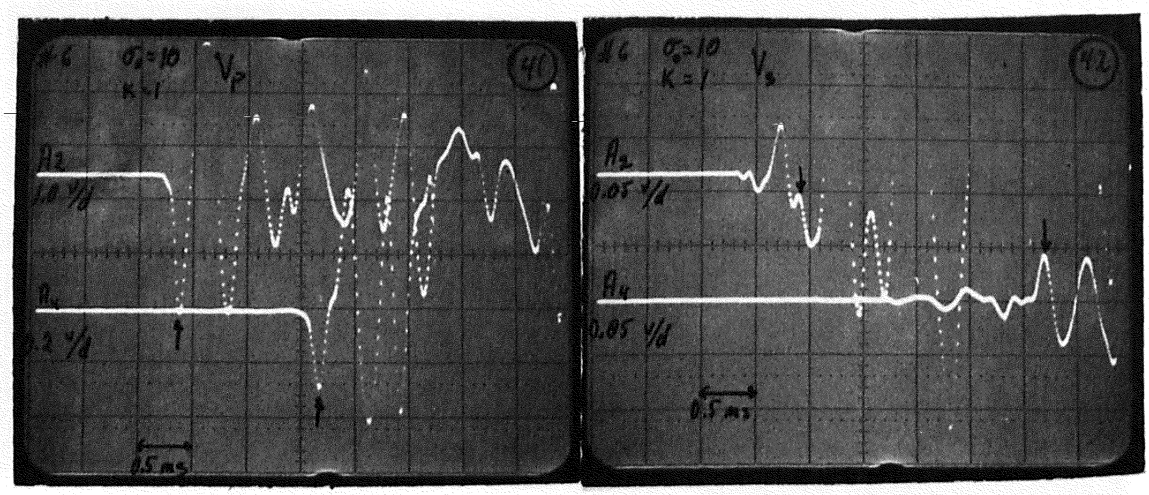
σ₀=10
K=1
Vp
41
A3
1.0 v/d
A4
0.2 v/d
0.5 ms
σ₀=10
K=1
Vs
42
A2
0.05 v/d
A4
0.05 v/d
0.5 ms

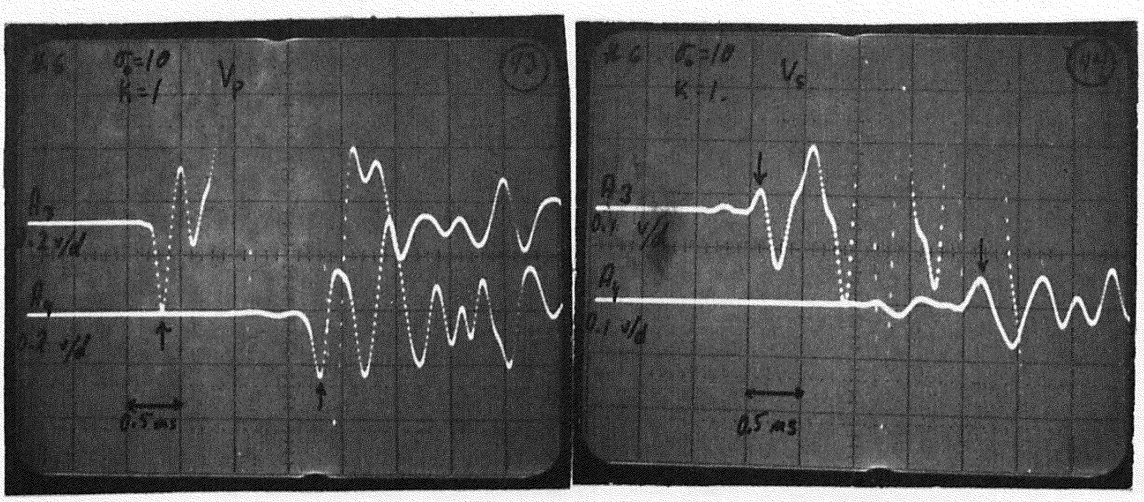
#6 σ_0=10 K=1 V_p (43)
A_3 0.2 v/d
A_1 0.2 v/d
0.5 ms
#6 σ_0=10 K=1 V_s (44)
A_3 0.1 v/d
A_1 0.1 v/d
0.5 ms

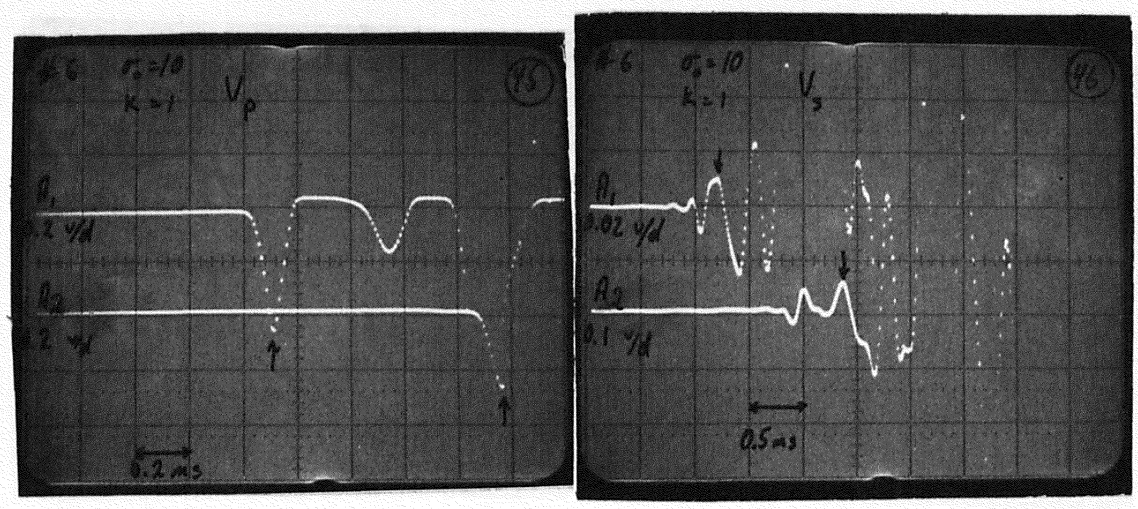
#6 σ_0=10 K=1 V_p (45)
A_1 0.2 v/d
A_2 0.2 v/d
0.2 ms
#6 σ_0=10 K=1 V_s (46)
A_1 0.02 v/d
A_2 0.1 v/d
0.5 ms

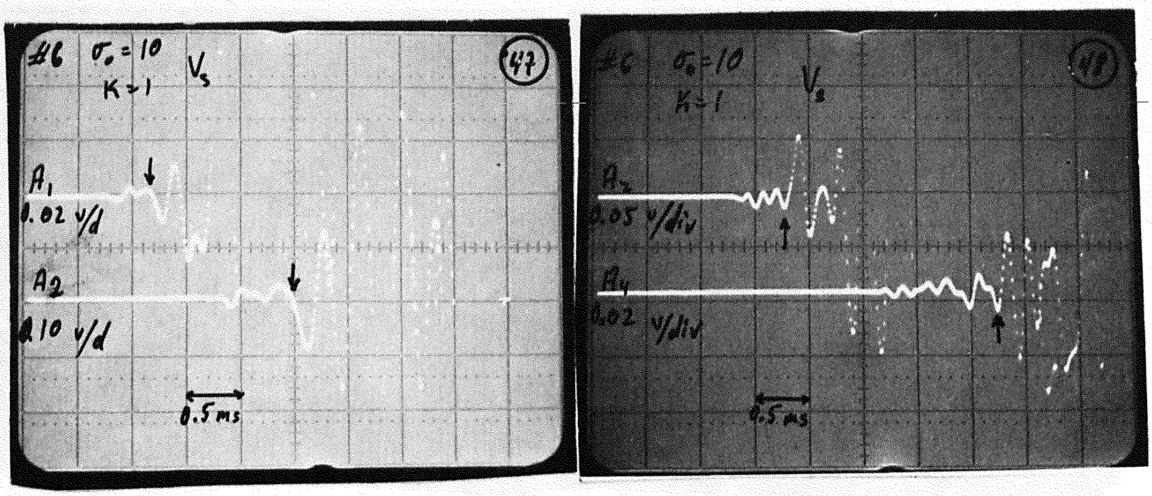
#6 σ_0=10 K=1 V_s (47)
A_1 0.02 v/d
A_2 0.10 v/d
0.5 ms
#6 σ_0=10 K=1 V_s (48)
A_3 0.05 v/div
A_1 0.02 v/div
0.5 ms

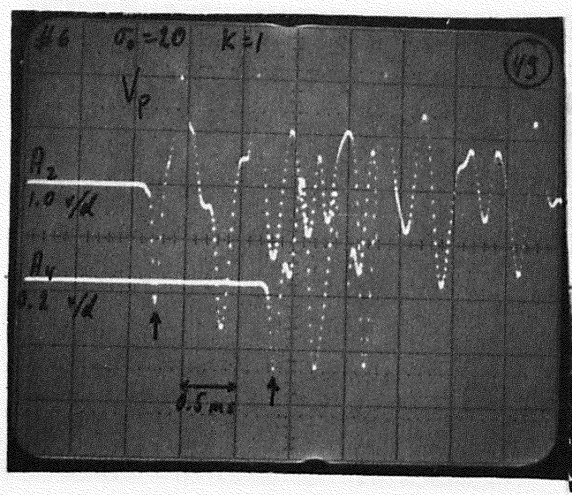
#6 σ_0=20 K=1
V3
V_P
A_2
1.0 v/d
A_4
0.2 v/d
0.5 ms

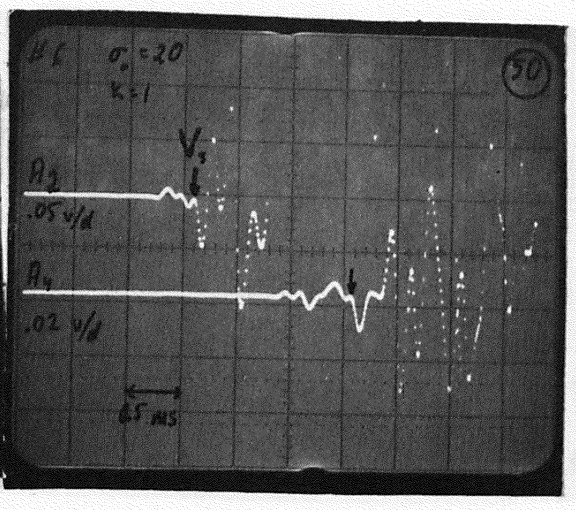
#6 σ_0=20
K=1
50
V_S
A_3
.05 v/d
A_4
.02 v/d
0.5 ms

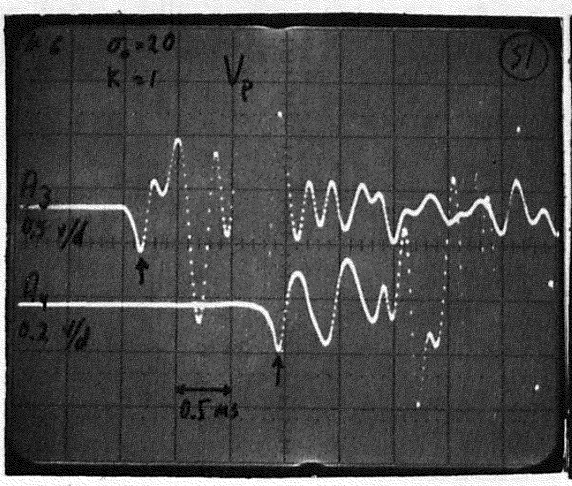
#6 σ_0=20
K=1
V_P
51
A_3
0.5 v/d
A_4
0.2 v/d
0.5 ms

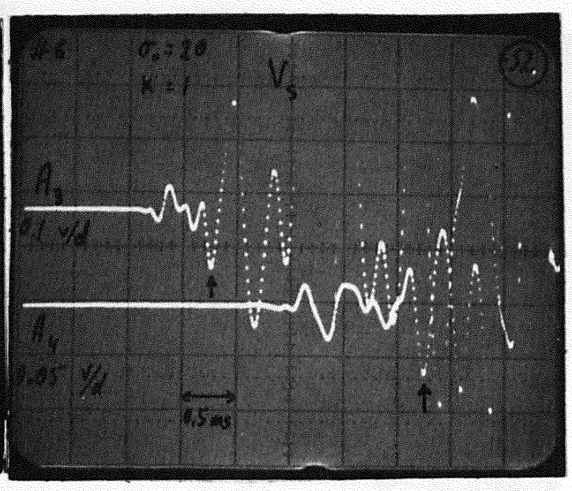
#6 σ_0=20
K=1
V_S
52
A_3
0.1 v/d
A_4
0.05 v/d
0.5 ms

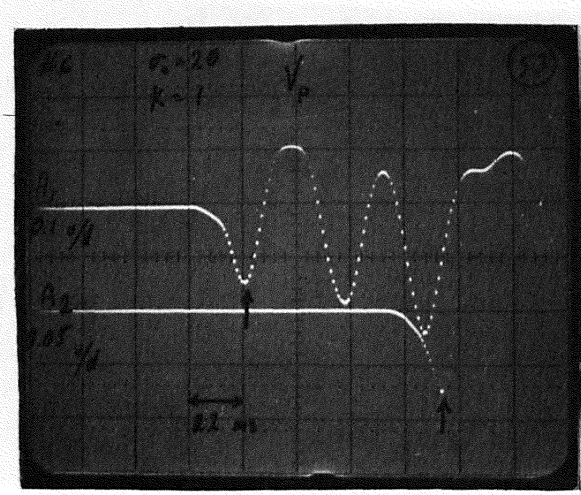
#6 σ_0=20
K=1
V_P
53
A_1
0.1 v/d
A_2
0.05 v/d
0.2 ms

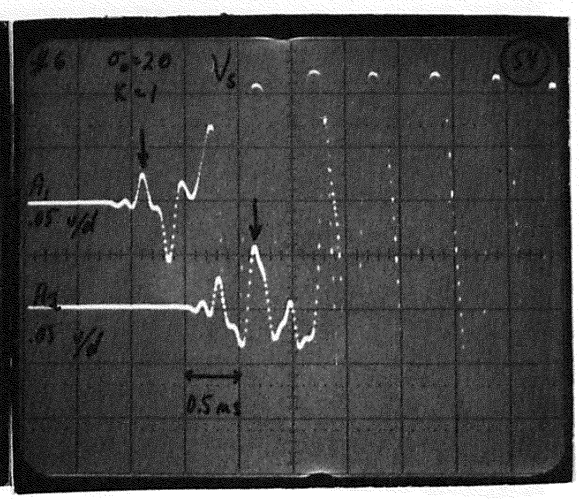
#6 σ_0=20
K=1
V_S
54
A_1
.05 v/d
A_2
.03 v/d
0.5 ms

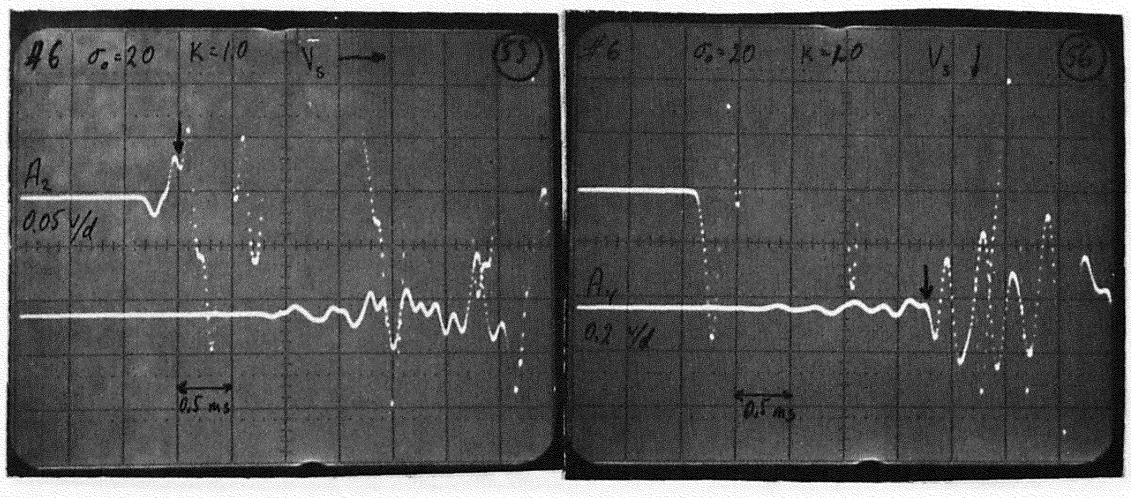
#6 σ_0=20 K=1.0 V_s 55
A_2
0.05 v/d
0.5 ms
#6 σ_0=20 K=1.0 V_s 56
A_4
0.2 v/d
0.5 ms

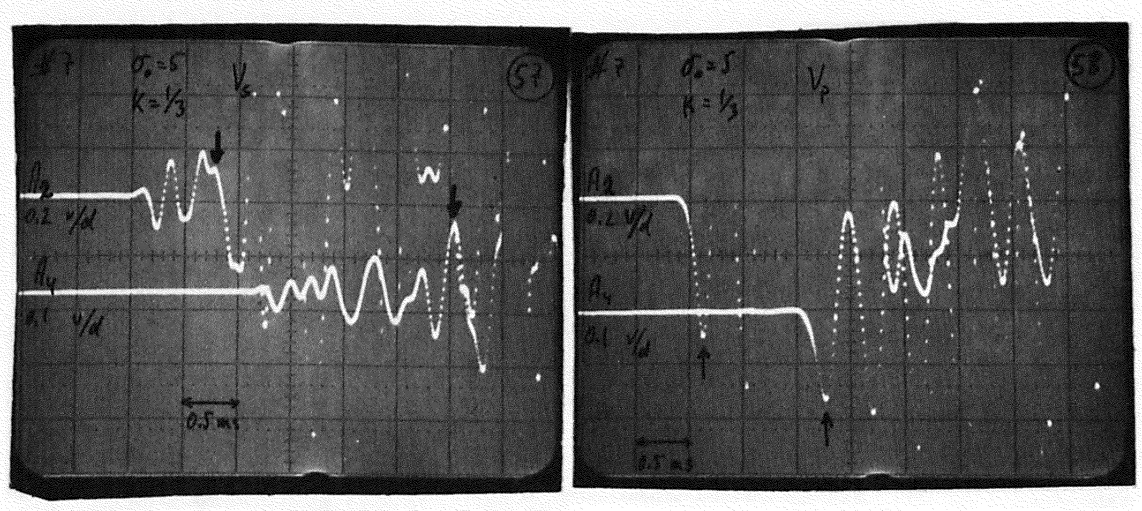
#7 σ_0=5 K=1/3 V_s 57
A_2
0.2 v/d
A_4
0.1 v/d
0.5 ms
#7 σ_0=5 K=1/3 V_p 58
A_2
0.2 v/d
A_4
0.1 v/d
0.5 ms

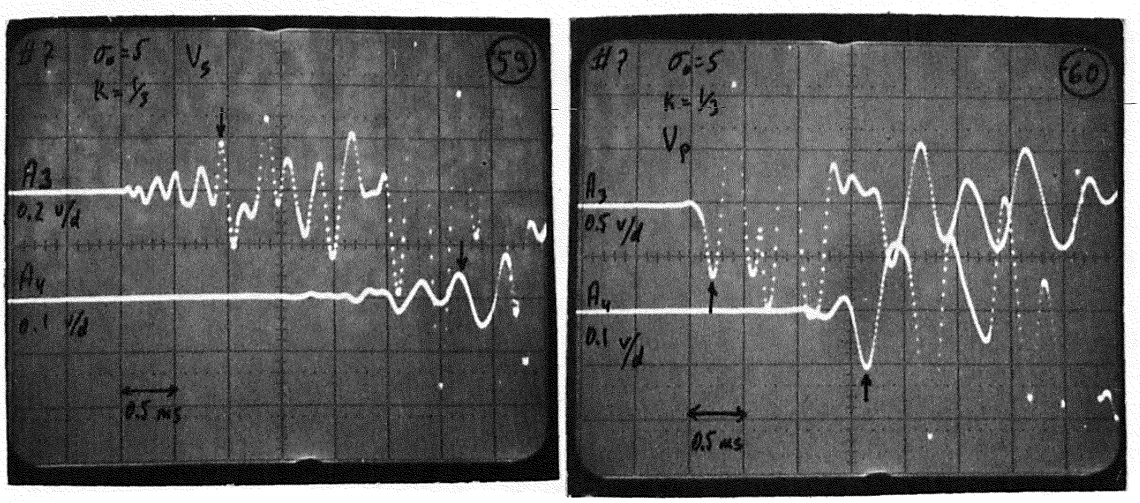
#7 σ_0=5 K=1/3 V_s 59
A_3
0.2 v/d
A_4
0.1 v/d
0.5 ms
#7 σ_0=5 K=1/3 V_p 60
A_3
0.5 v/d
A_4
0.1 v/d
0.5 ms

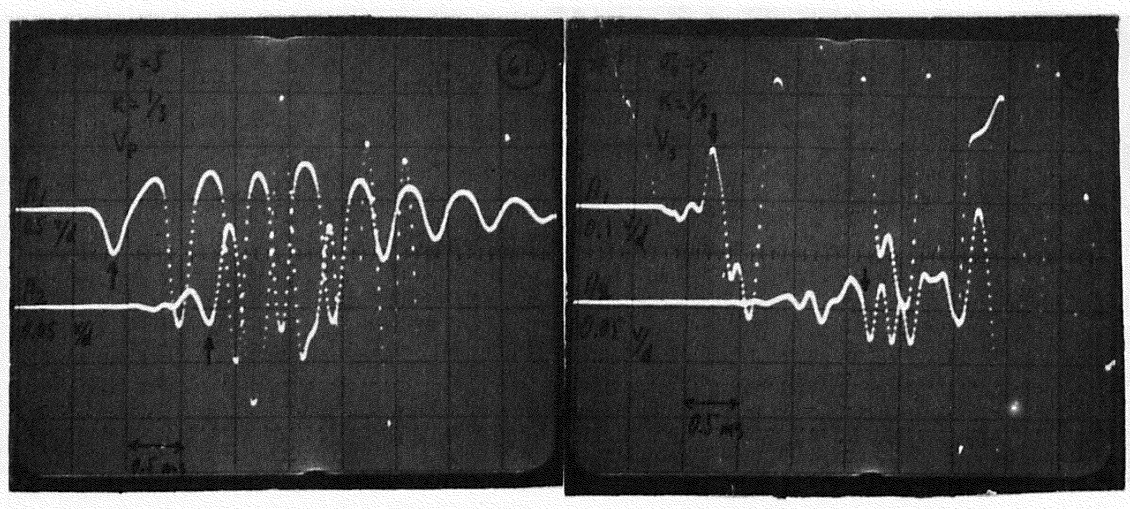
0.5 ms

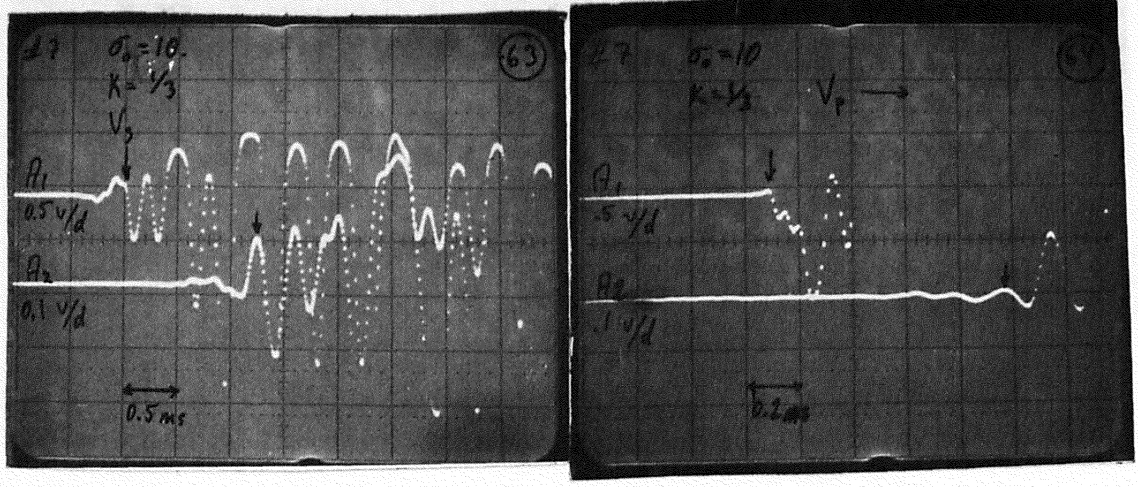
0.5 ms
0.2 ms

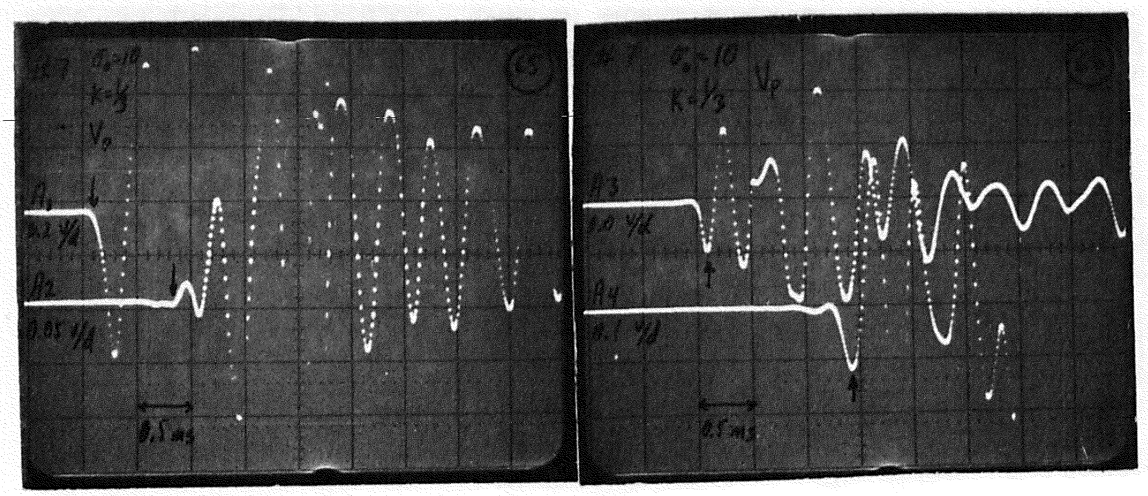
0.5 ms
0.5 ms

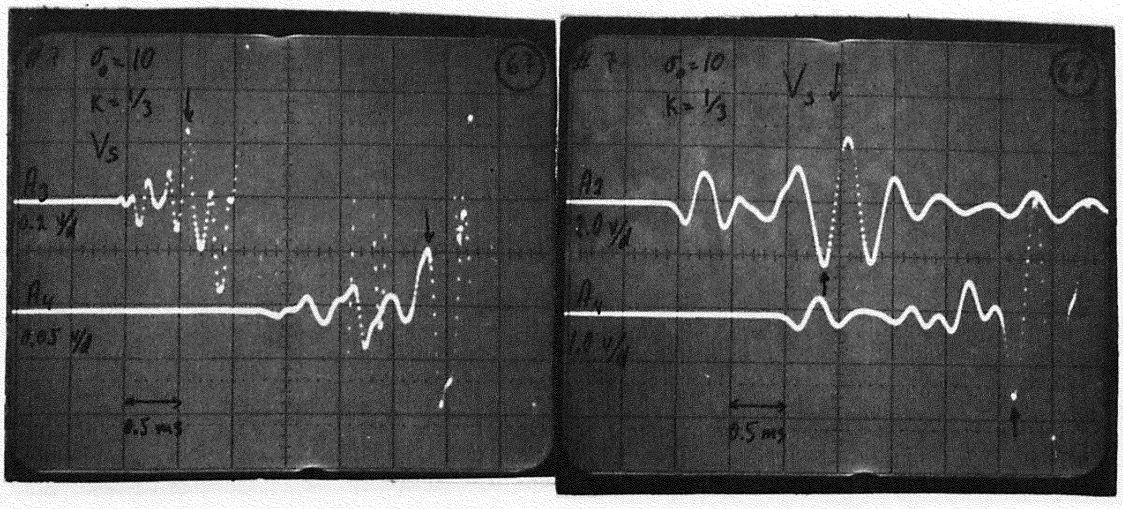
#7 $\sigma_0 = 10$ K = 1/3 V_S 67
A_2 0.2 V/d
A_4 0.05 V/d
0.5 ms
#7 $\sigma_0 = 10$ K = 1/3 V_S 68
A_2 2.0 V/d
A_4 1.0 V/d
0.5 ms

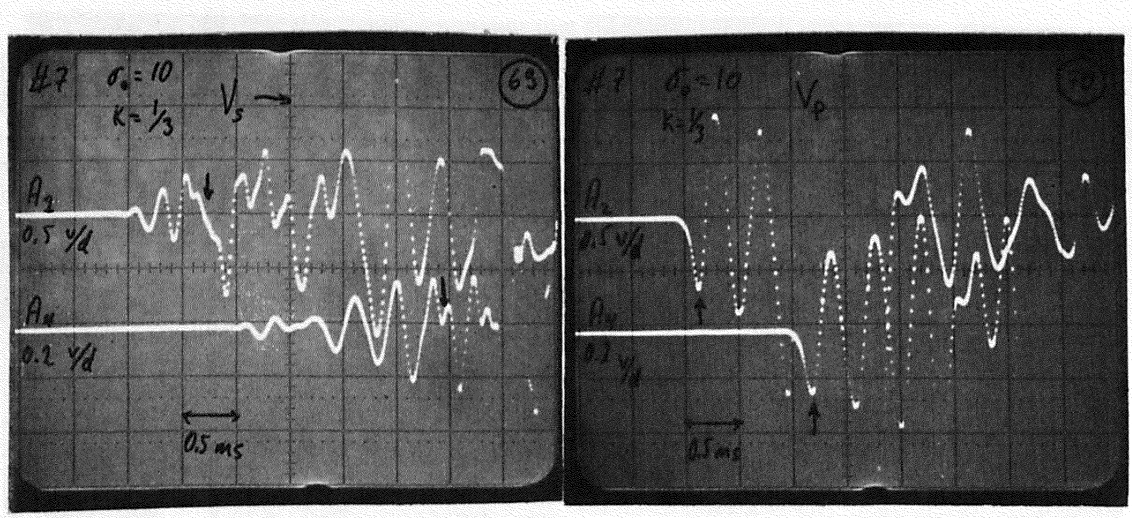
#7 $\sigma_0 = 10$ K = 1/3 V_S 69
A_2 0.5 V/d
A_4 0.2 V/d
0.5 ms
#7 $\sigma_0 = 10$ K = 1/3 V_P 70
A_2 0.5 V/d
A_4 0.2 V/d
0.5 ms

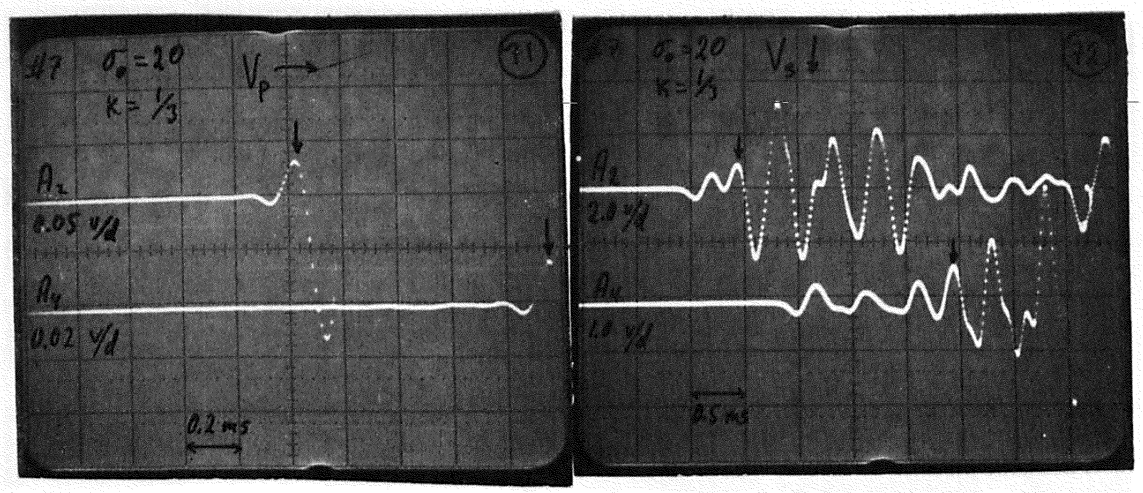
#7 $\sigma_0 = 20$ K = 1/3 V_P 71
A_2 0.05 V/d
A_4 0.02 V/d
0.2 ms
#7 $\sigma_0 = 20$ K = 1/3 V_S 72
A_2 2.0 V/d
A_4 1.0 V/d
0.5 ms

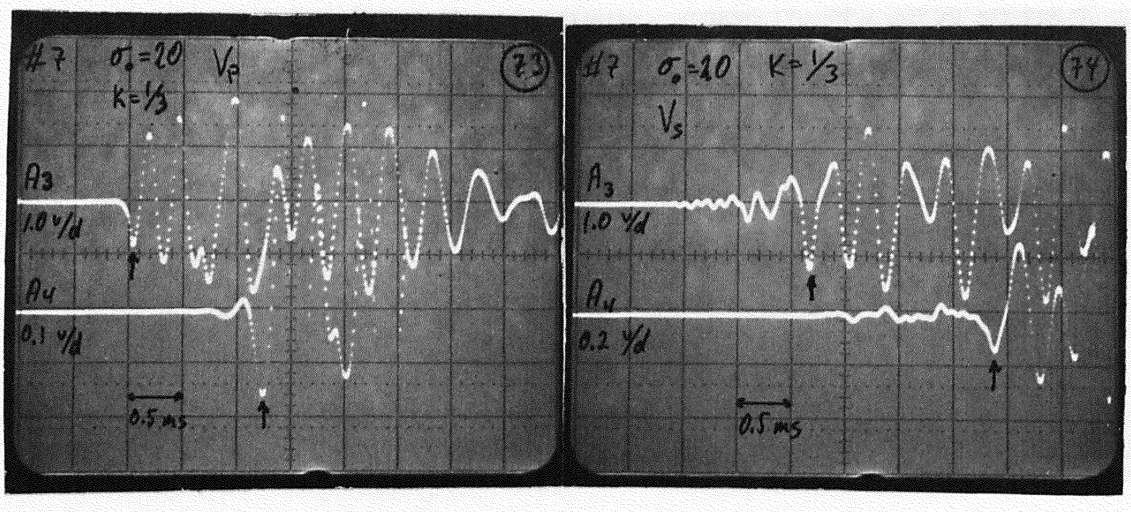
#7 σ₀=20 K=1/3 Vp 73
A3 1.0 v/d
A4 0.1 v/d
0.5 ms
#7 σ₀=20 K=1/3 Vs 74
A3 1.0 v/d
A4 0.2 v/d
0.5 ms

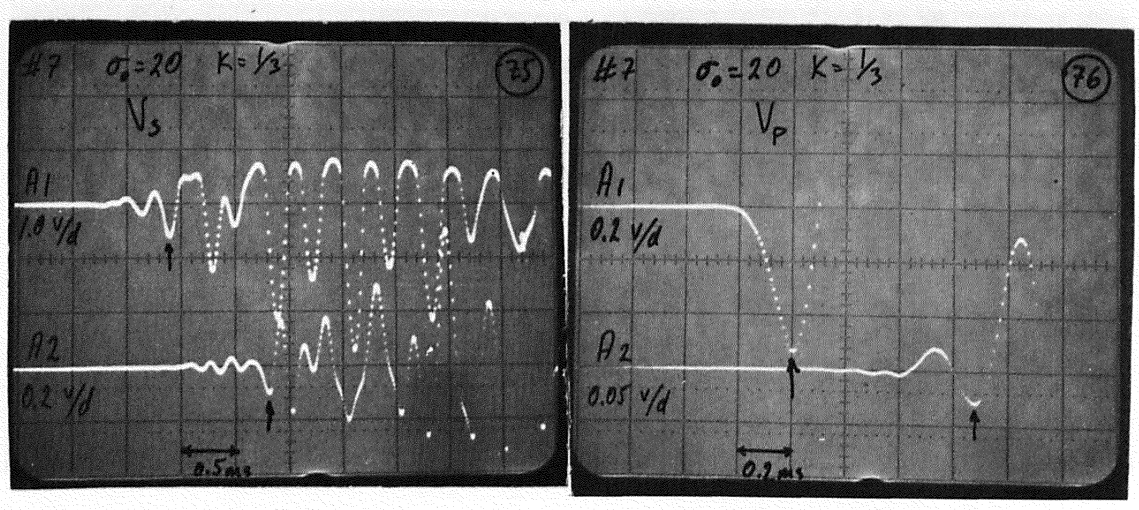
#7 σ₀=20 K=1/3 Vs 75
A1 1.0 v/d
A2 0.2 v/d
0.5 ms
#7 σ₀=20 K=1/3 Vp 76
A1 0.2 v/d
A2 0.05 v/d
0.2 ms

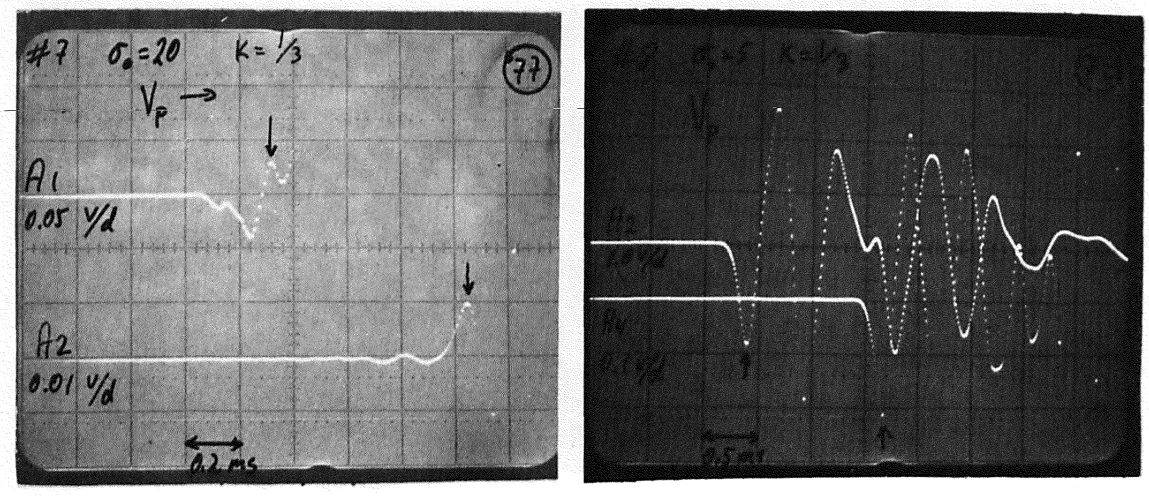
#7 σ₀=20 K=1/3 Vp 77
A1 0.05 v/d
A2 0.01 v/d
0.2 ms
A2 1.0 v/d
A4 0.1 v/d
0.5 ms

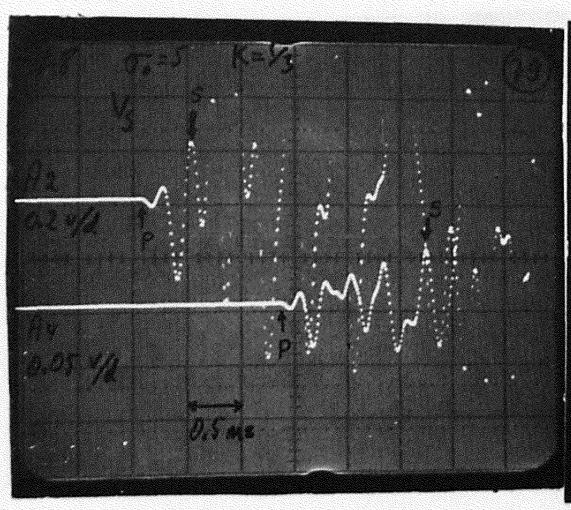
$\sigma_0 = 5$ K = 1/3
V_S
S
P
A2
0.2 v/d
A4
0.05 v/d
0.5 ms

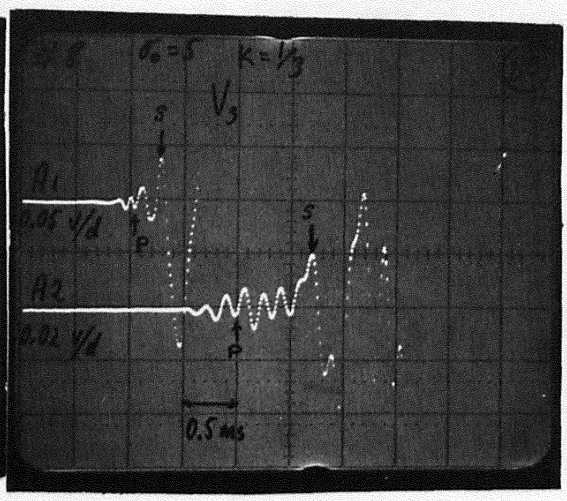
$\sigma_0 = 5$ K = 1/3
V_S
S
P
A1
0.05 v/d
A2
0.02 v/d
0.5 ms

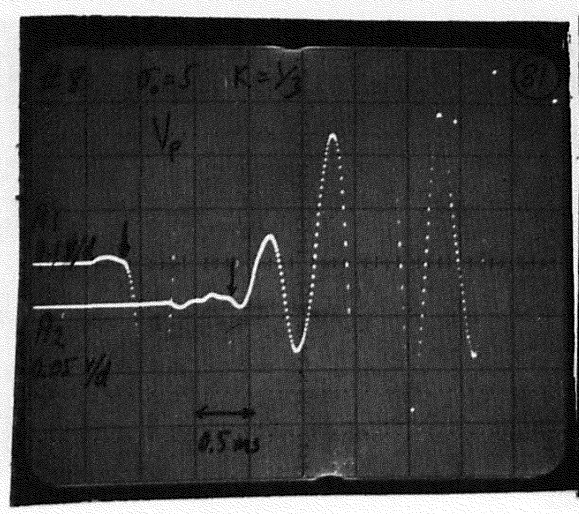
$\sigma_0 = 5$ K = 1/3
V_P
A1
0.1 v/d
A2
0.05 v/d
0.5 ms

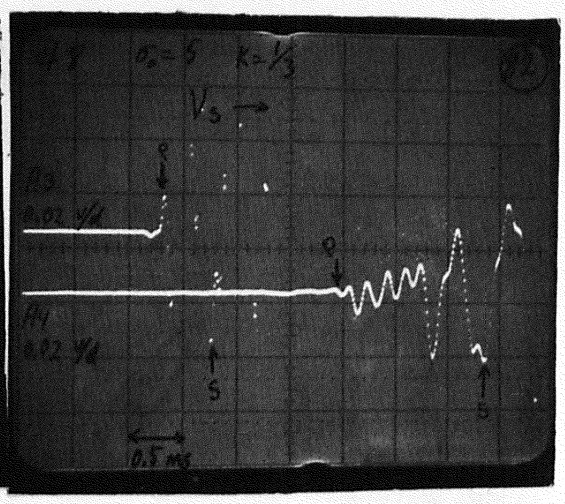
$\sigma_0 = 5$ K = 1/3
V_S
P
S
A3
0.02 v/d
A4
0.02 v/d
0.5 ms

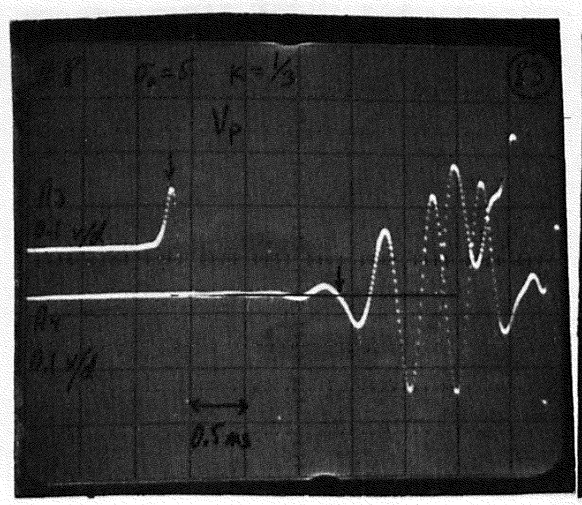
$\sigma_0 = 5$ K = 1/3
V_P
A3
0.1 v/d
A4
0.1 v/d
0.5 ms

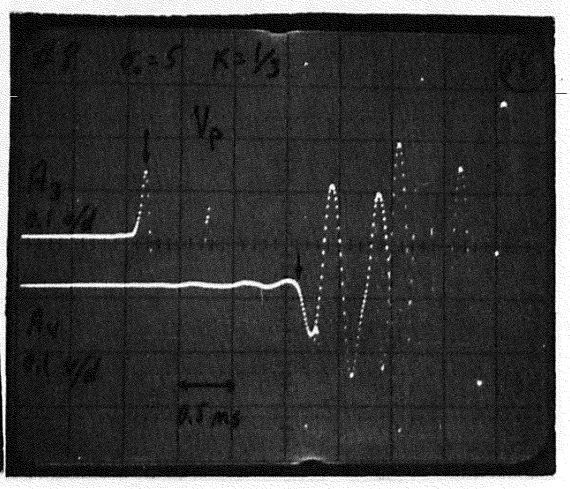
$\sigma_0 = 5$ K = 1/3
V_P
A3
0.1 v/d
A4
0.1 v/d
0.5 ms

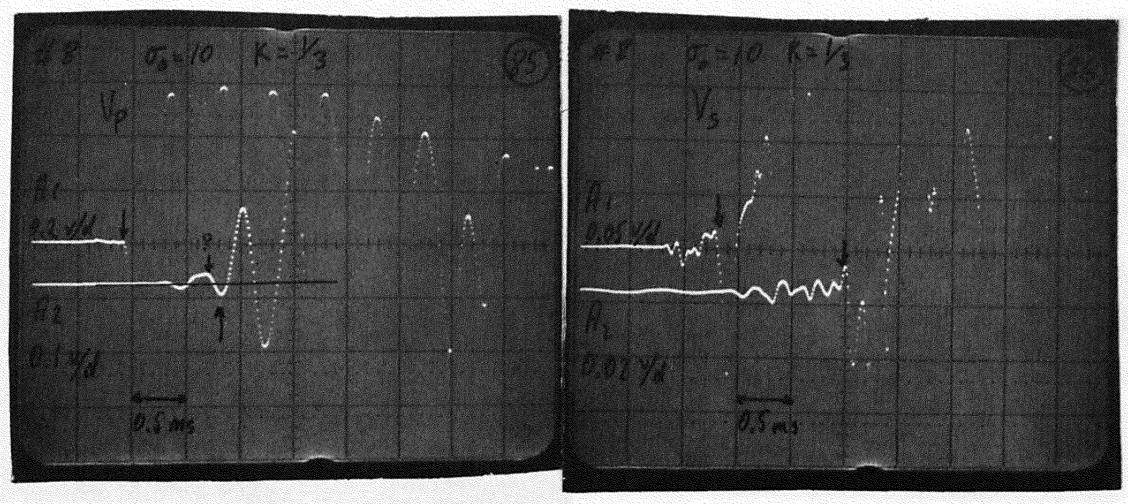
$\sigma_0=10$ K=1/3
V_p
A_1 0.2 v/d
A_2 0.1 v/d
0.5 ms
$\sigma_0=10$ K=1/3
V_s
A_1 0.05 v/d
A_2 0.02 v/d
0.5 ms

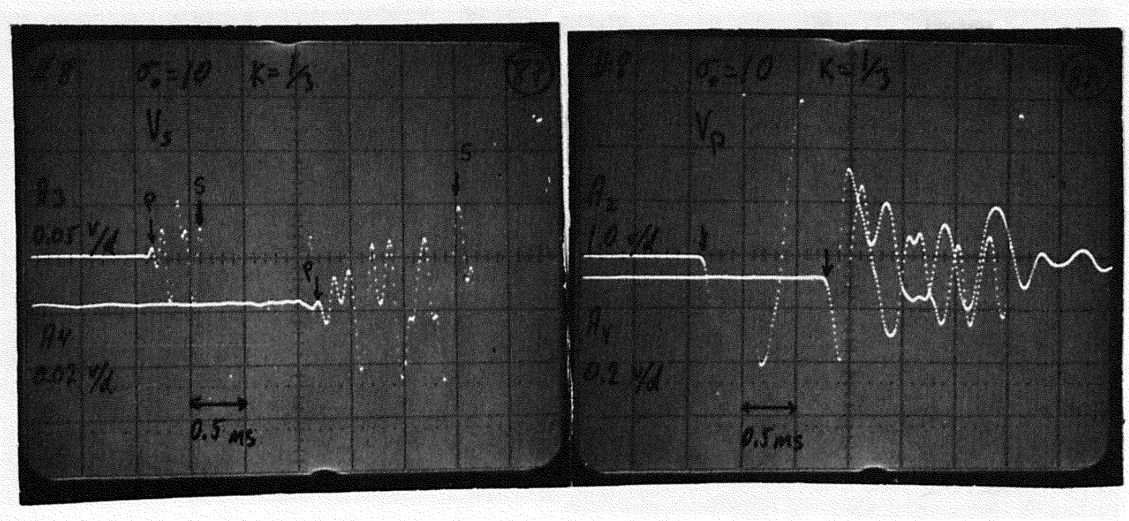
$\sigma_0=10$ K=1/3
V_s
A_2 0.05 v/d
A_4 0.02 v/d
0.5 ms
$\sigma_0=10$ K=1/3
V_p
A_2 1.0 v/d
A_4 0.2 v/d
0.5 ms

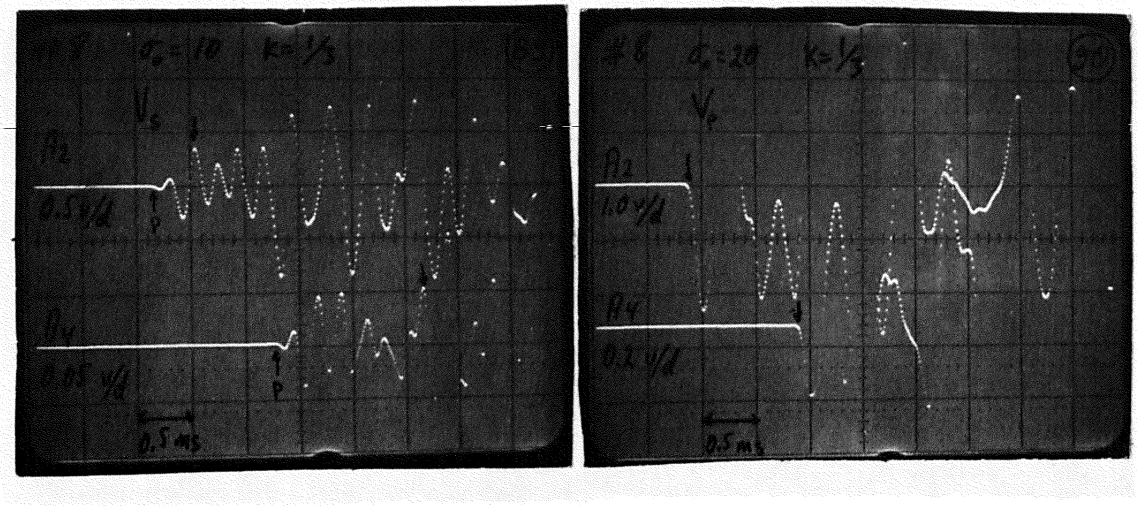
$\sigma_0=10$ K=1/3
V_s
A_2 0.5 v/d
A_4 0.05 v/d
0.5 ms
$\sigma_0=20$ K=1/3
V_p
A_2 1.0 v/d
A_4 0.2 v/d
0.5 ms

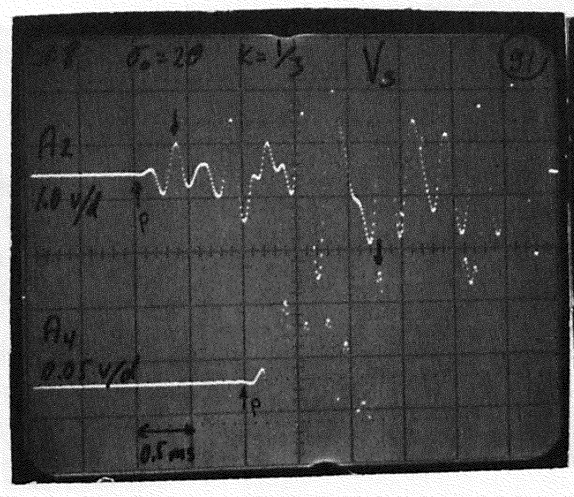
#8 σ_c=20 K=1/3 V_c (91)
A2
1.0 v/d
P
A4
0.05 v/d
P
0.5 ms

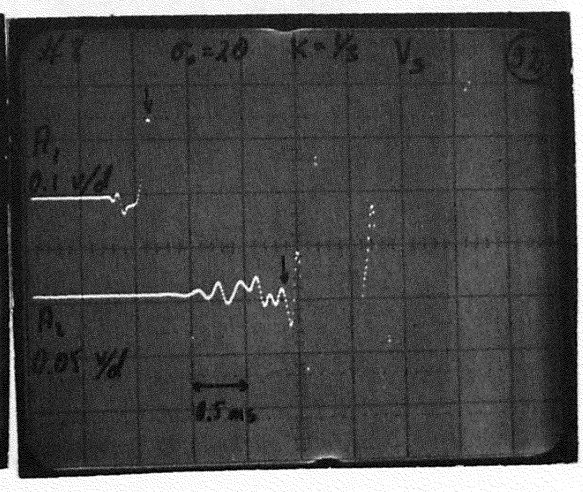
#8 σ_c=20 K=1/3 V_s (92)
A1
0.1 v/d
A2
0.05 v/d
0.5 ms

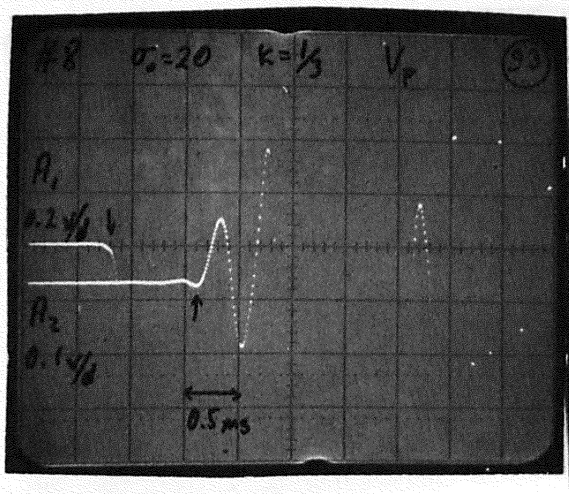
#8 σ_c=20 K=1/3 V_p (93)
A1
0.2 v/d
A2
0.1 v/d
0.5 ms

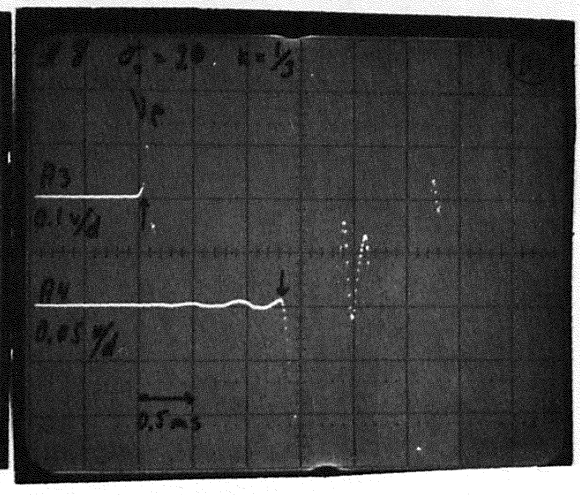
#8 σ_c=20 K=1/3
V_p
A3
0.1 v/d
A4
0.05 v/d
0.5 ms

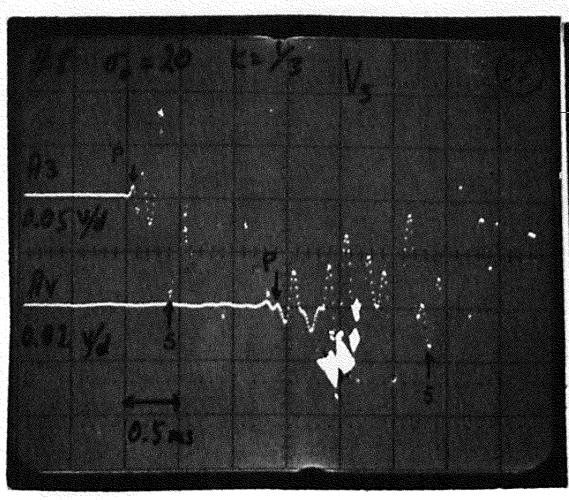
#5 σ_c=20 K=1/3 V_s (94)
A3
0.05 v/d
P
A4
0.02 v/d
P
S
S
0.5 ms

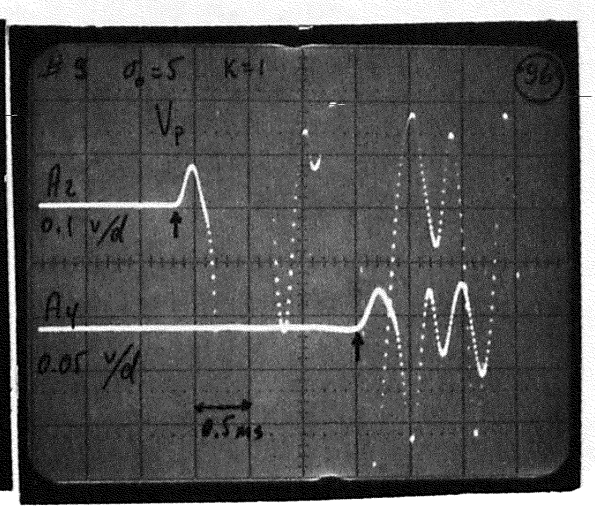
#5 σ_c=5 K=1 (96)
V_p
A2
0.1 v/d
A4
0.05 v/d
0.5 ms

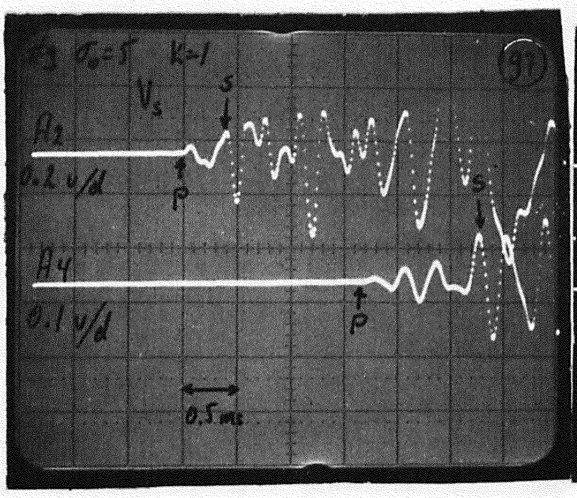
#3 σ_0=5 K=1
V_s
S
A_2
0.2 v/d
P
A_4
0.1 v/d
P
S
0.5 ms

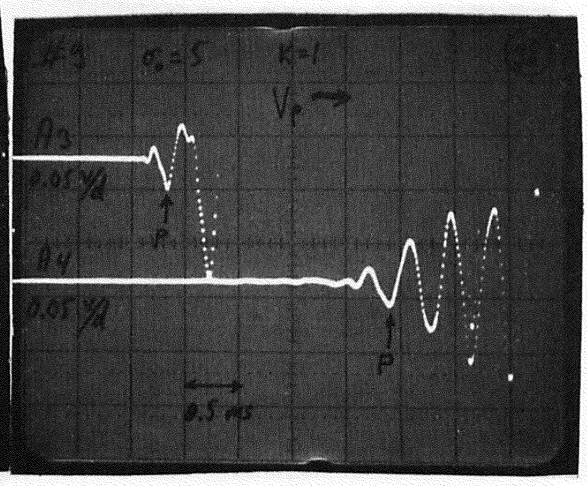
#3 σ_0=5 K=1
V_p
A_3
0.05 v/d
P
A_4
0.05 v/d
P
0.5 ms

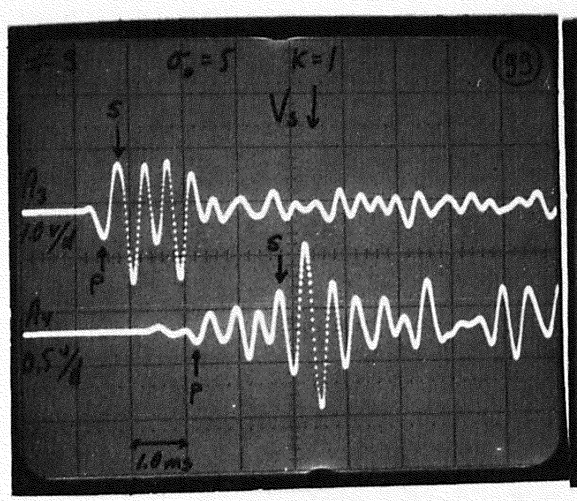
#3 σ_0=5 K=1
V_s
S
A_3
1.0 v/d
P
S
A_4
0.5 v/d
P
1.0 ms

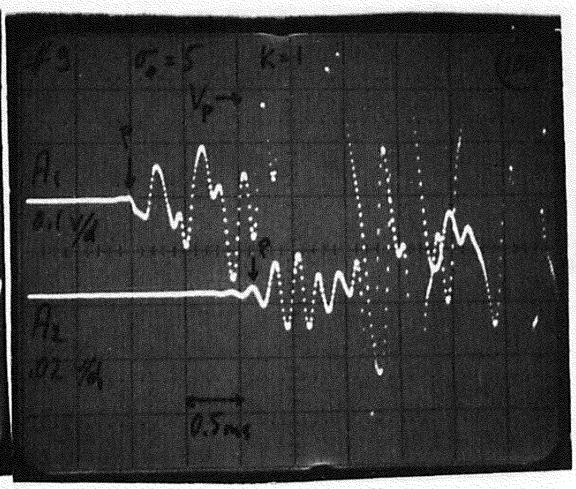
#3 σ_0=5 K=1
V_p
P
A_1
0.1 v/d
P
A_2
0.2 v/d
0.5 ms

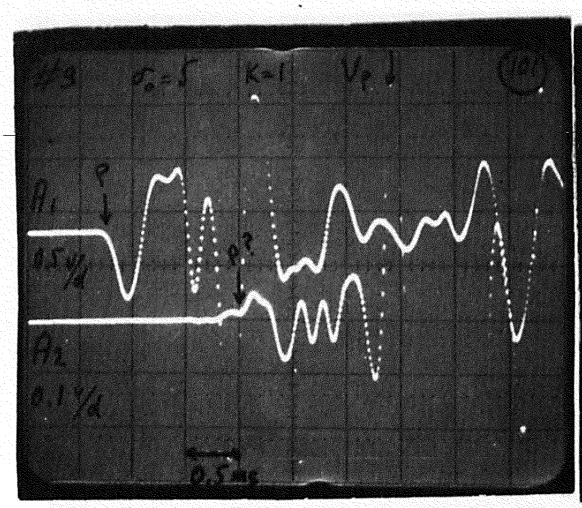
#3 σ_0=5 K=1 V_p
P
A_1
0.5 v/d
P?
A_2
0.1 v/d
0.5 ms

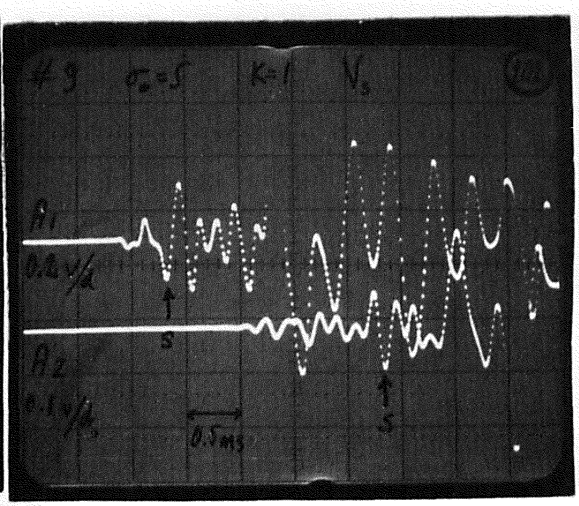
#3 σ_0=5 K=1 V_s
A_1
0.2 v/d
S
A_2
0.1 v/d
S
0.5 ms

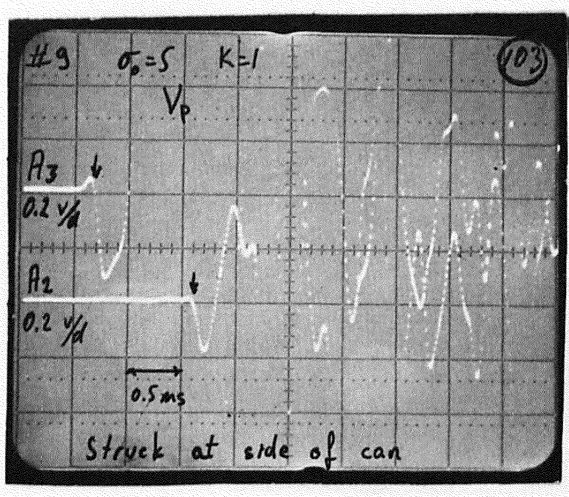
#9 σ_0=5 K=1
(103)
V_P
A_3
0.2 v/d
A_2
0.2 v/d
0.5 ms
Struck at side of can

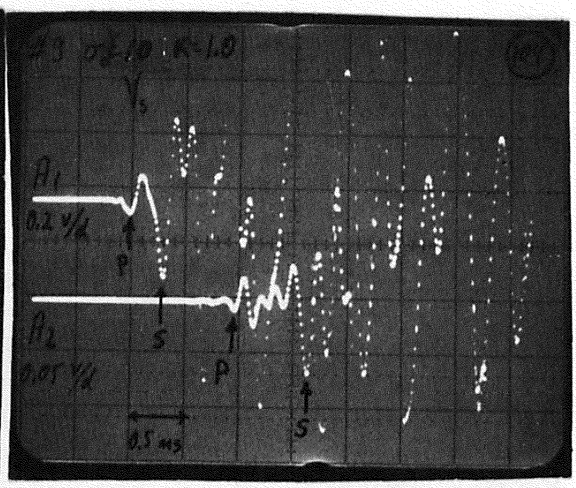
V_S
A_1
0.2 v/d
P
S
P
A_2
0.05 v/d
S
0.5 ms

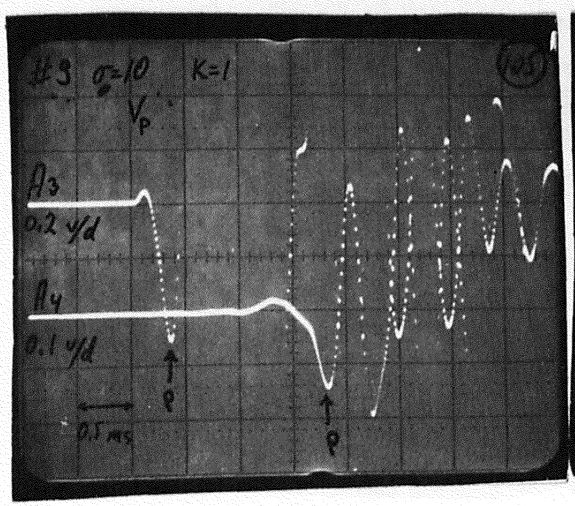
#3 σ_0=10 K=1
(105)
V_P
A_3
0.2 v/d
A_4
0.1 v/d
P
0.5 ms
P

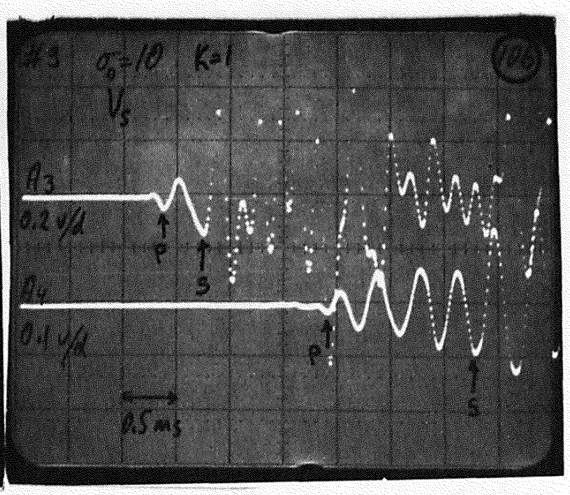
#3 σ_0=10 K=1
(106)
V_S
A_3
0.2 v/d
P
S
A_4
0.1 v/d
P
0.5 ms
S

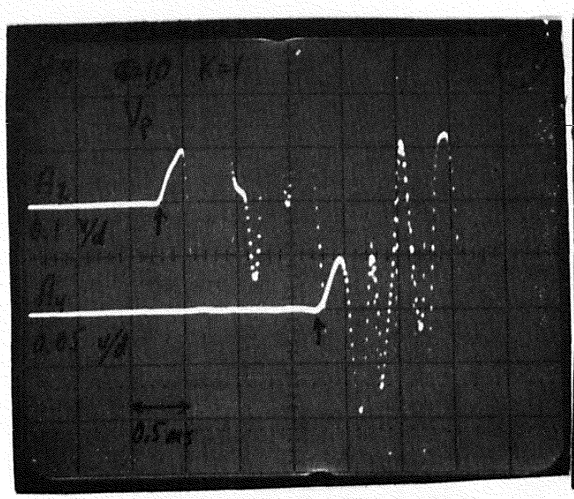
V_P
0.5 ms

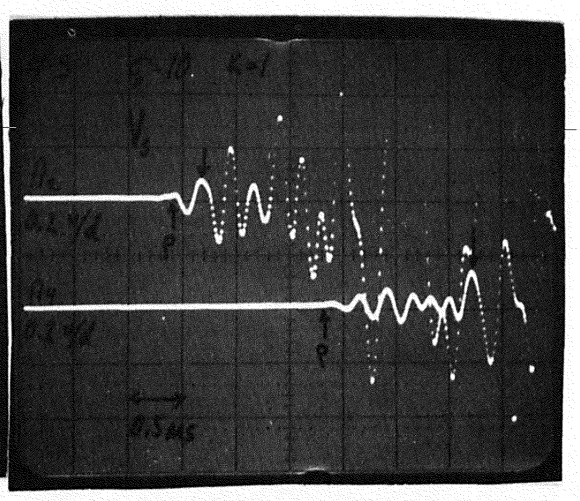
V_S
P
P
0.5 ms

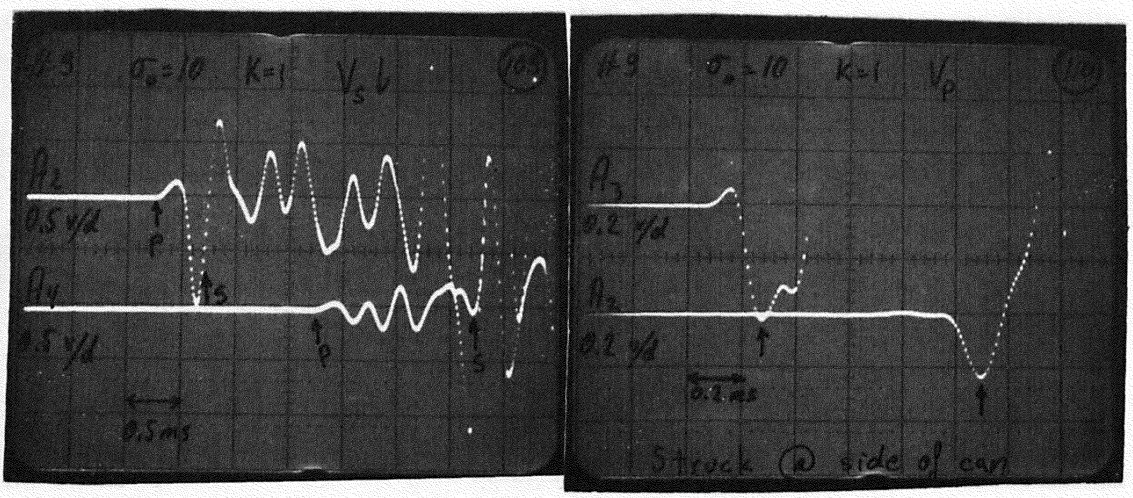
#9 σ_o=10 K=1 V_s ↓
A_2
0.5 v/d
P
S
A_4
0.5 v/d
P
S
0.5ms
#9 σ_o=10 K=1 V_p
A_3
0.2 v/d
A_2
0.2 v/d
0.2 ms
Struck ② side of car

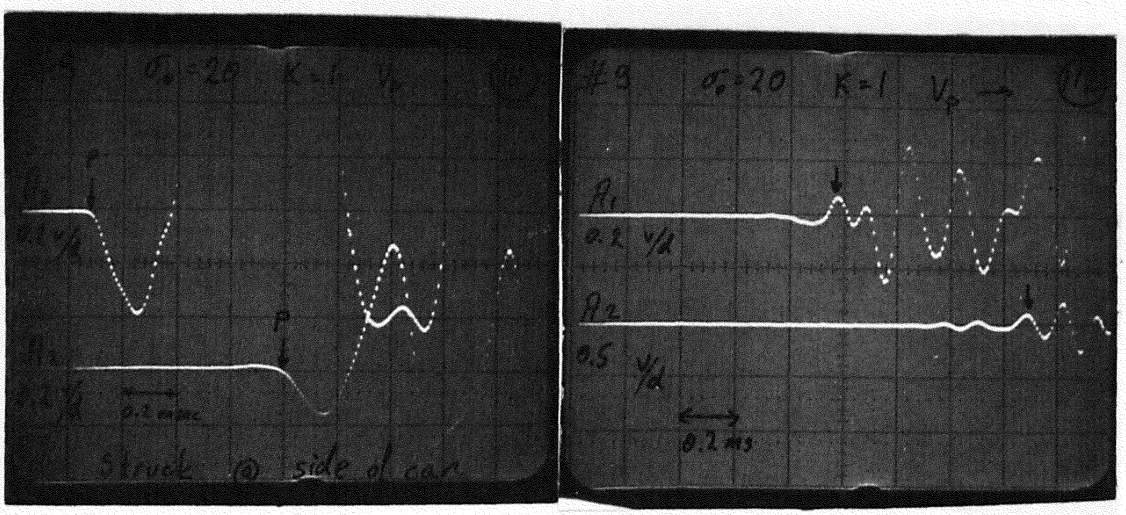
σ_o=20 K=1 V_p
P
P
0.2 msec
Struck ② side of car
#9 σ_o=20 K=1 V_p →
A_1
0.2 v/d
A_2
0.5 v/d
0.2 ms

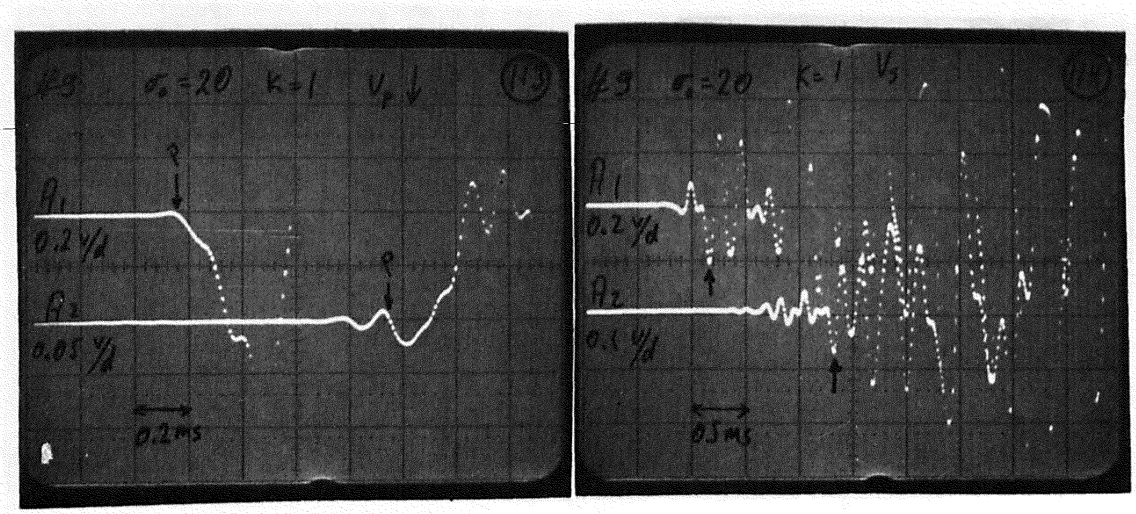
#9 σ_o=20 K=1 V_p ↓
P
P
A_1
0.2 v/d
A_2
0.05 v/d
0.2ms
#9 σ_o=20 K=1 V_s
A_1
0.2 v/d
A_2
0.1 v/d
0.5ms

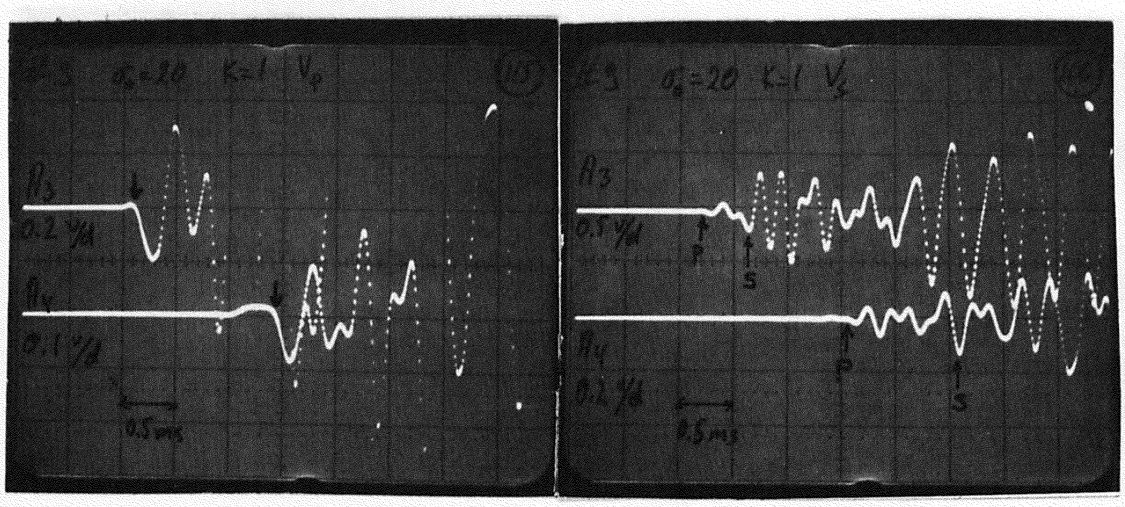
σ_0=20 K=1 V_P
A_3 0.2 v/d
A_4 0.1 v/d
0.5 ms
σ_0=20 K=1 V_S
A_3 0.5 v/d
A_4 0.2 v/d
P
S
0.5 ms

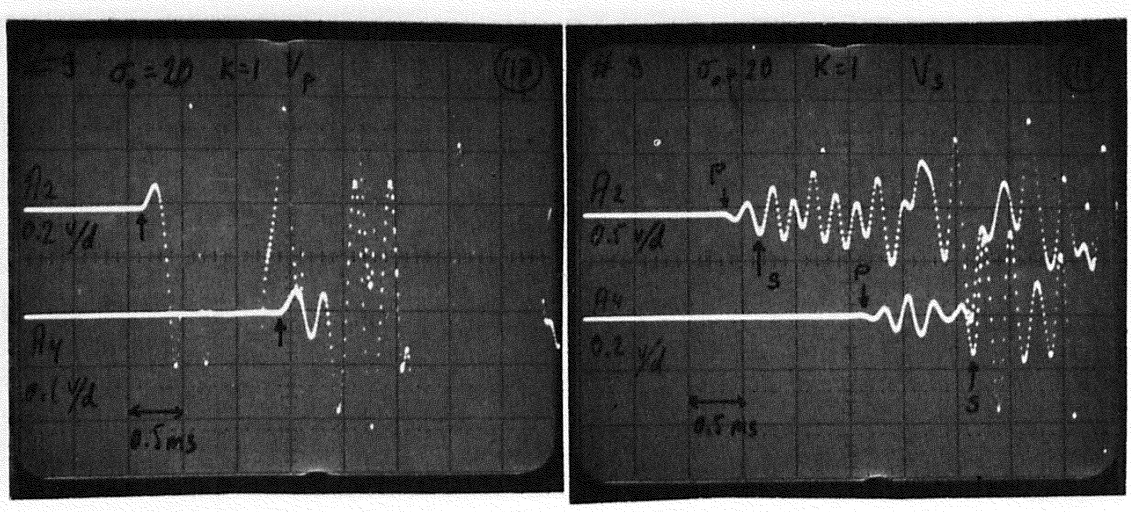
σ_0=20 K=1 V_P
A_2 0.2 v/d
A_4 0.1 v/d
0.5 ms
σ_0=20 K=1 V_S
A_2 0.5 v/d
A_4 0.2 v/d
P
S
0.5 ms

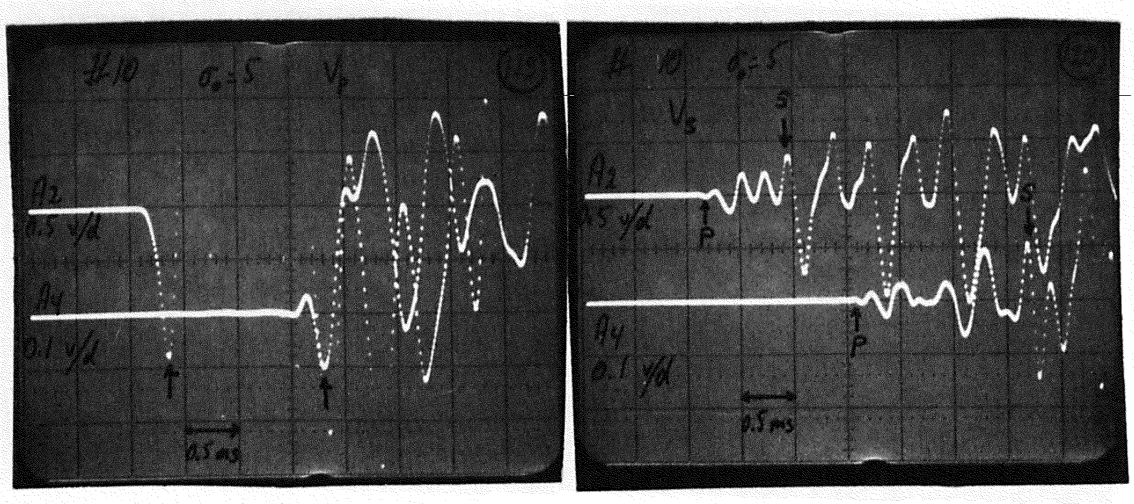
K=10 σ_0=5 V_P
A_2 0.5 v/d
A_4 0.1 v/d
0.5 ms
K=10 σ_0=5 V_S
A_2 0.5 v/d
A_4 0.1 v/d
P
S
0.5 ms

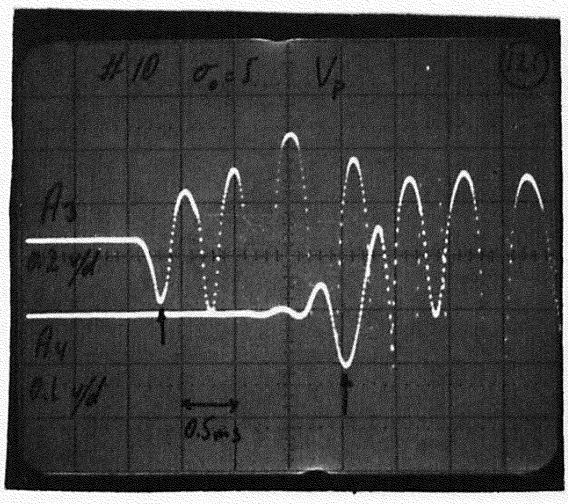
#10 σ_0=5 V_P
121
A3
0.2 v/d
A4
0.1 v/d
0.5 ms

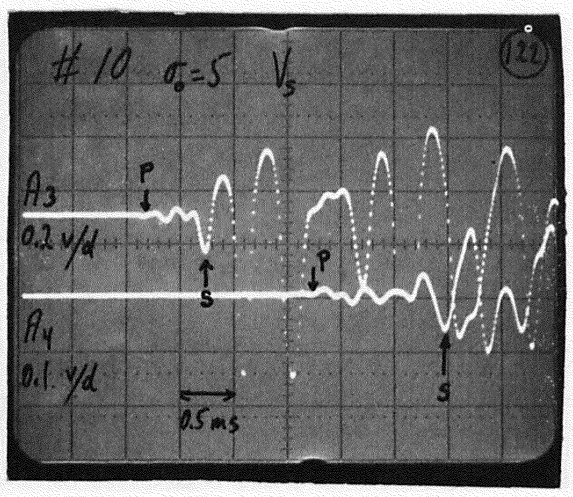
#10 σ_0=5 V_S
122
P
S
P
S
A3
0.2 v/d
A4
0.1 v/d
0.5 ms

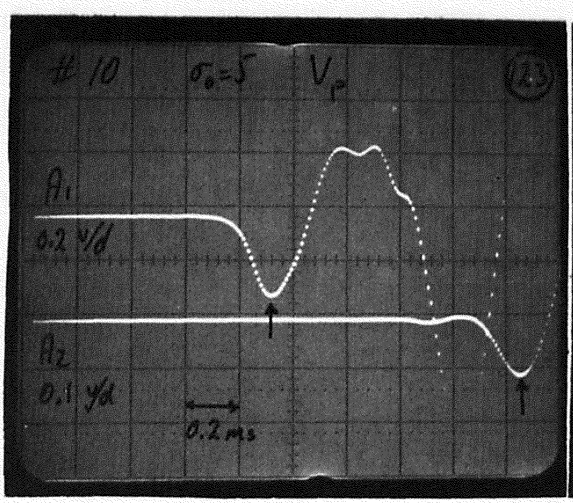
#10 σ_0=5 V_P
123
A1
0.2 v/d
A2
0.1 v/d
0.2 ms

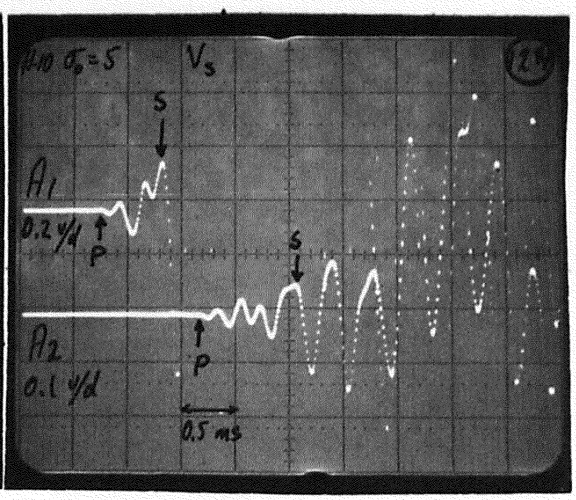
#10 σ_0=5 V_S
124
S
S
P
P
A1
0.2 v/d
A2
0.1 v/d
0.5 ms

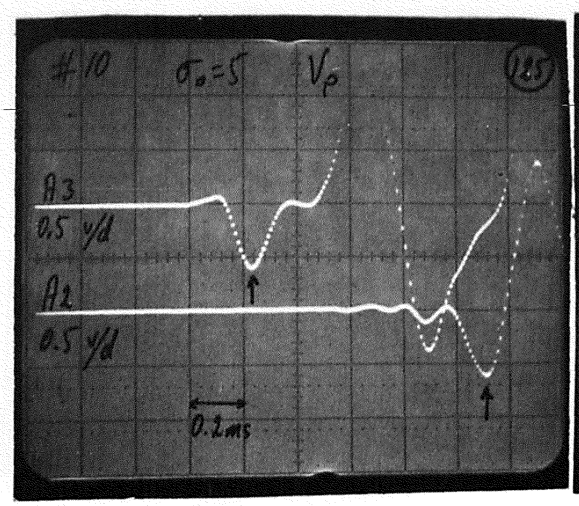
#10 σ_0=5 V_P
125
A3
0.5 v/d
A2
0.5 v/d
0.2 ms

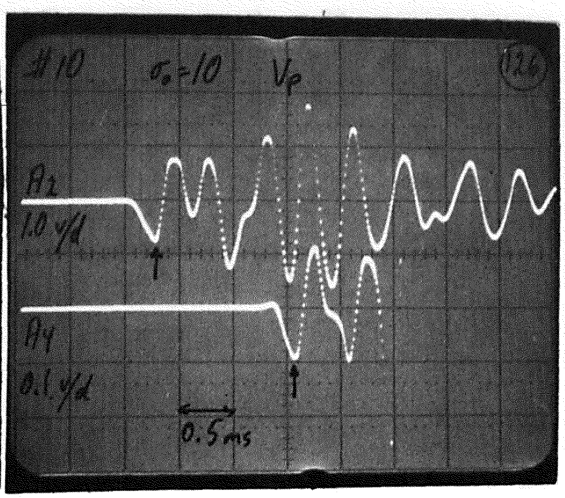
#10 σ_0=10 V_P
126
A2
1.0 v/d
A4
0.1 v/d
0.5 ms

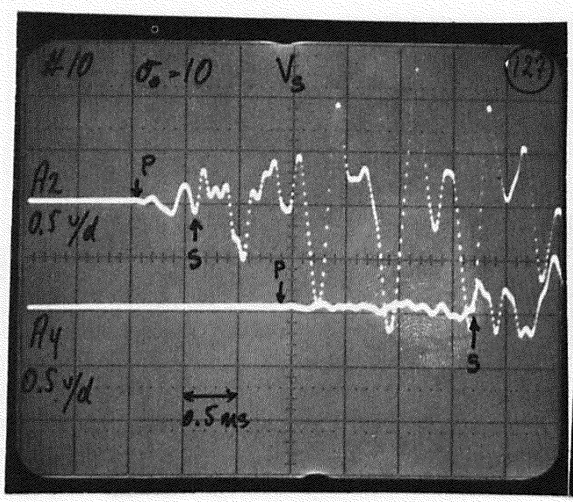
#10 σ_0=10 V_S (127)
A_2 0.5 v/d
P
S
P
S
A_4 0.5 v/d
0.5 ms

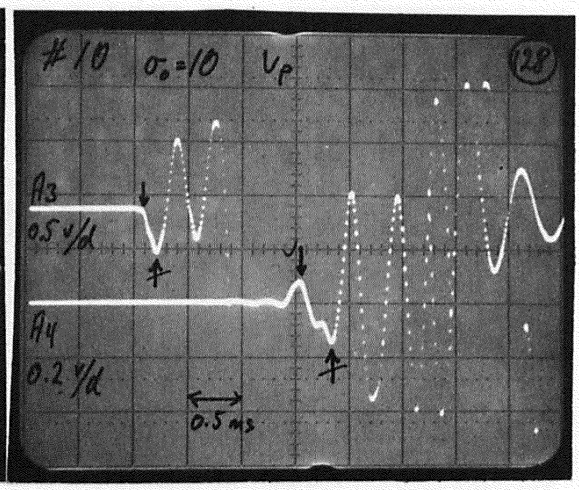
#10 σ_0=10 V_P (128)
A_3 0.5 v/d
A_4 0.2 v/d
0.5 ms

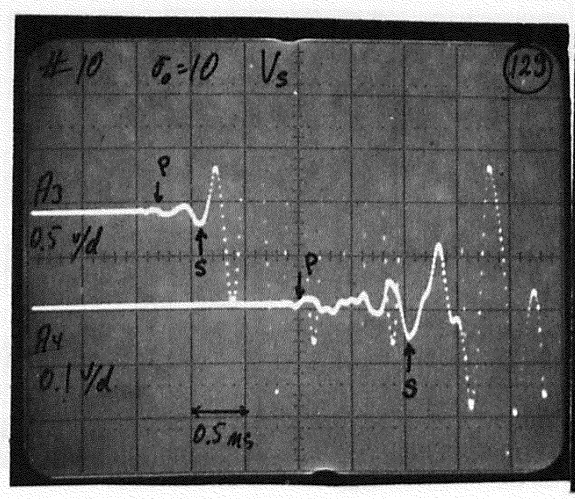
#10 σ_0=10 V_S (129)
A_3 0.5 v/d
P
S
P
S
A_4 0.1 v/d
0.5 ms

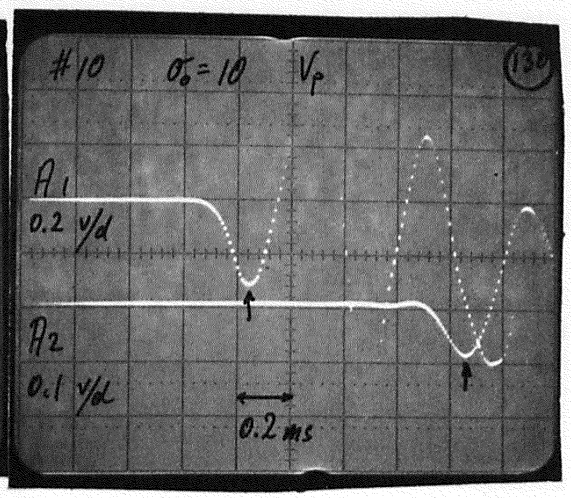
#10 σ_0=10 V_P (130)
A_1 0.2 v/d
A_2 0.1 v/d
0.2 ms

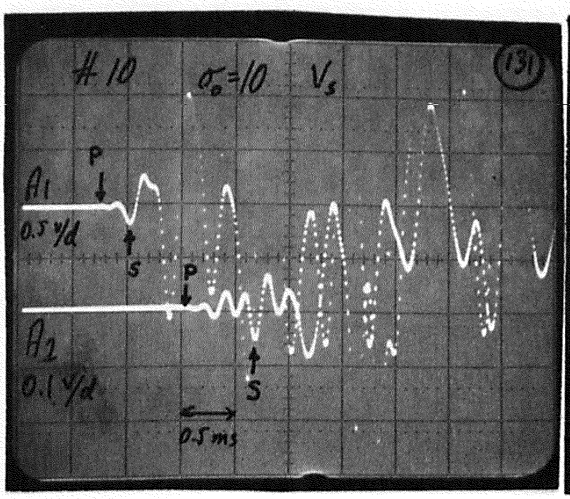
#10 σ_0=10 V_S (131)
A_1 0.5 v/d
P
S
P
S
A_2 0.1 v/d
0.5 ms

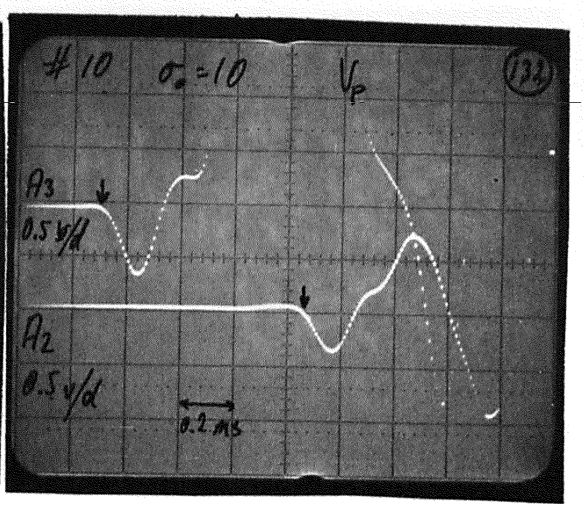
#10 σ_0=10 V_P (132)
A_3 0.5 v/d
A_2 0.5 v/d
0.2 ms

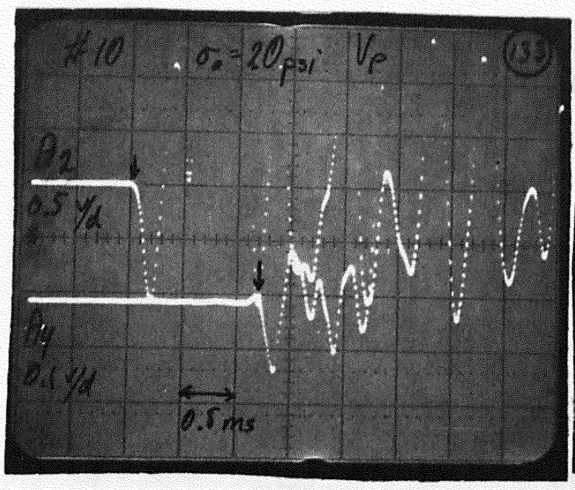
#10 σ_o=20 psi V_p (133)
A2
0.5 v/d
A4
0.5 v/d
0.5 ms

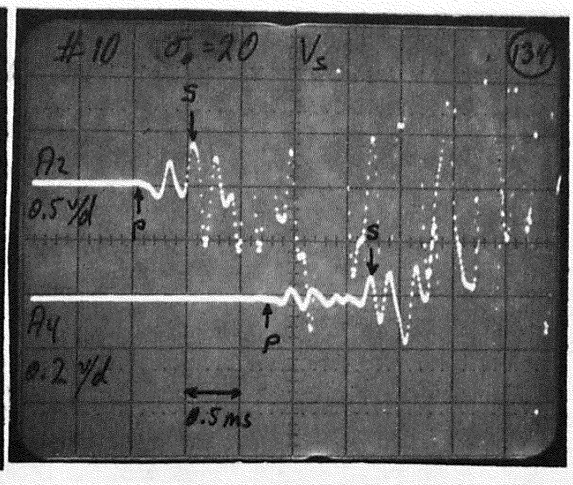
#10 σ_o=20 V_s (134)
S
A2
0.5 v/d
P
S
P
A4
0.2 v/d
0.5 ms

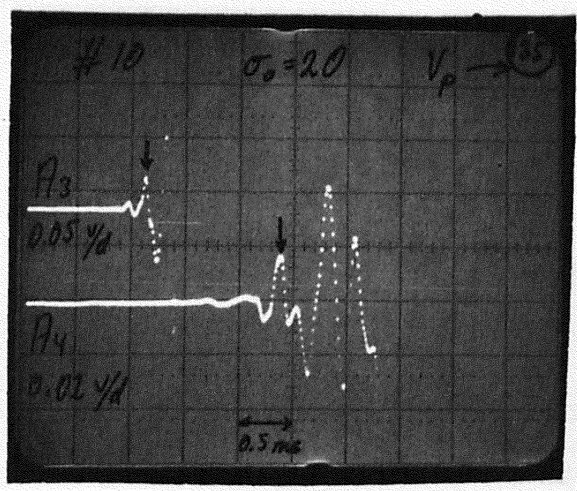
#10 σ_o=20 V_p (135)
A3
0.05 v/d
A4
0.02 v/d
0.5 ms

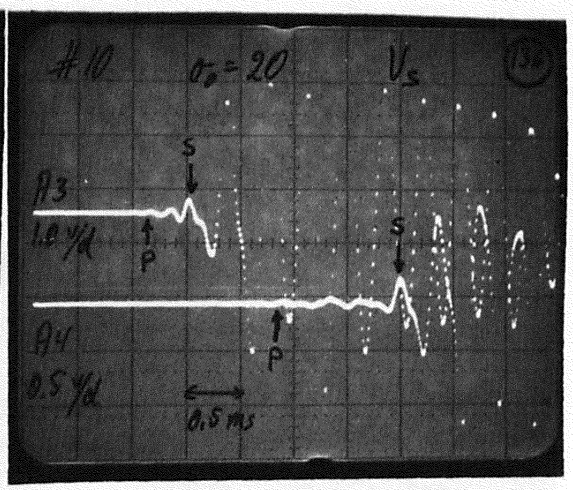
#10 σ_o=20 V_s (136)
S
A3
1.0 v/d
P
S
P
A4
0.5 v/d
0.5 ms

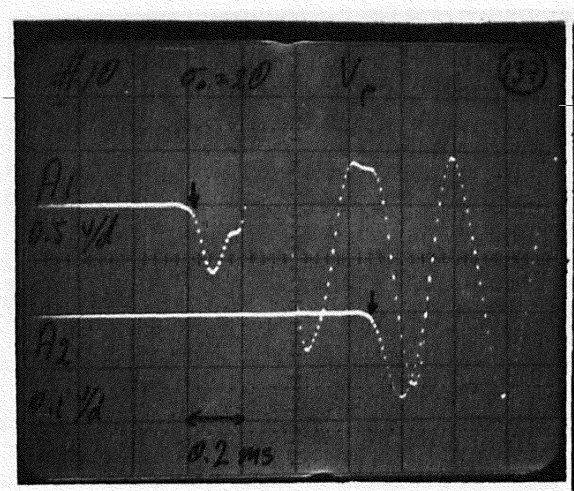
#10 σ_o=20 V_p (137)
A1
0.5 v/d
A2
0.1 v/d
0.2 ms

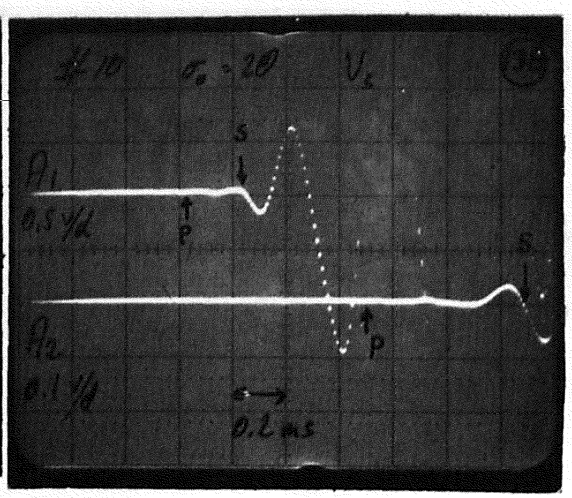
#10 σ_o=20 V_s (138)
S
A1
0.5 v/d
P
S
P
A2
0.1 v/d
0.2 ms

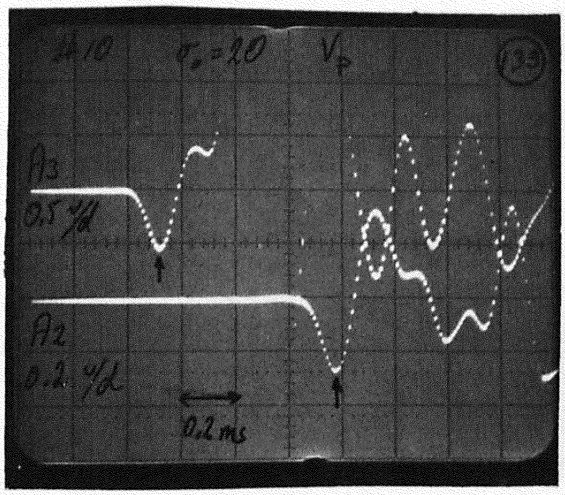
#10 $\sigma_0 = 2.0$ V_p (139)
A3
0.5 v/d
A2
0.2 v/d
0.2 ms

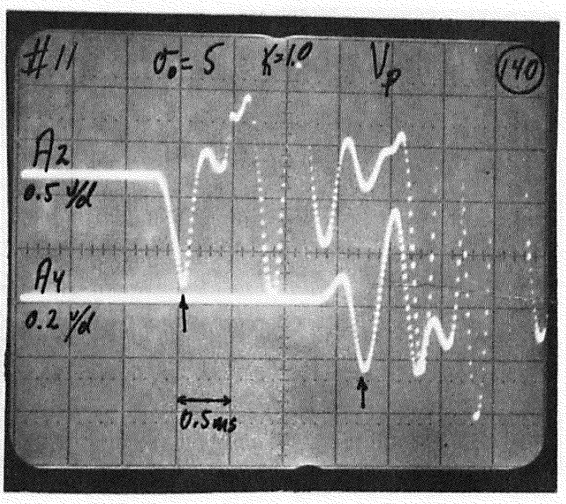
#11 $\sigma_0 = 5$ K=1.0 V_p (140)
A2
0.5 v/d
A4
0.2 v/d
0.5 ms

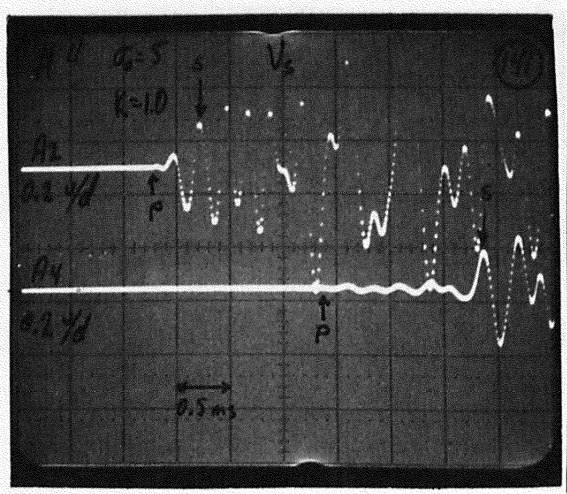
#11 $\sigma_0 = 5$ K=1.0 V_s (141)
S
A2
0.2 v/d
P
A4
0.2 v/d
P
0.5 ms

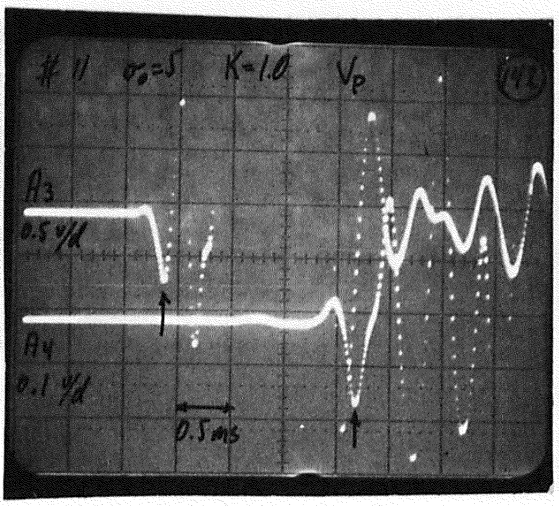
#11 $\sigma_0 = 5$ K=1.0 V_p (142)
A3
0.5 v/d
A4
0.1 v/d
0.5 ms

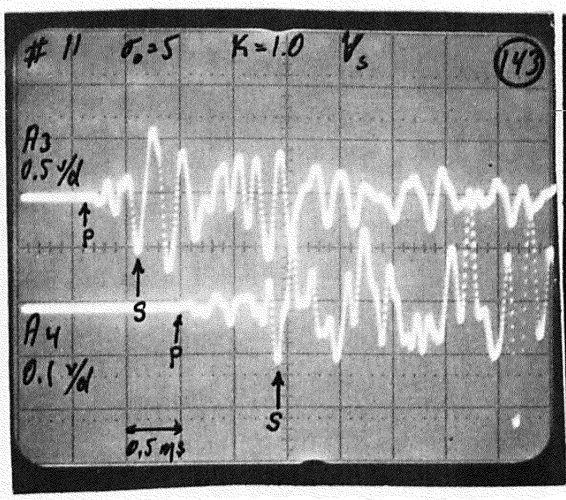
#11 $\sigma_0 = 5$ K=1.0 V_s (143)
A3
0.5 v/d
P
S
A4
0.1 v/d
P
S
0.5 ms

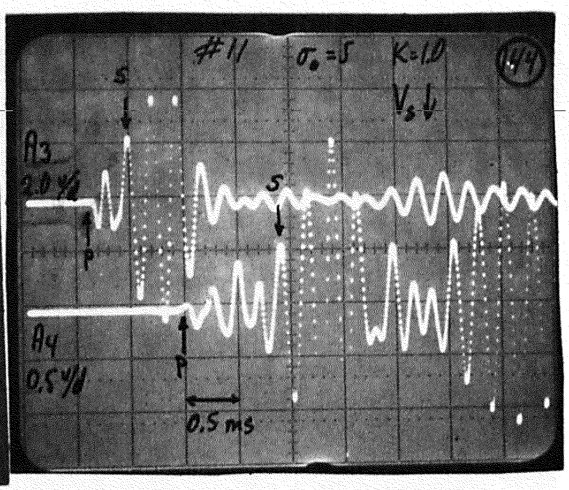
#11 $\sigma_0 = 5$ K=1.0 (144)
V_s
S
A3
2.0 v/d
P
S
A4
0.5 v/d
P
0.5 ms

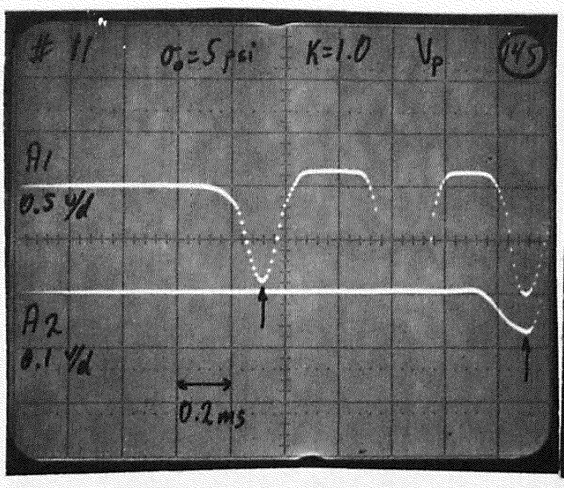
#11 σ_o=5 psi K=1.0 V_p (145)
A1
0.5 V/d
A2
0.1 V/d
0.2 ms

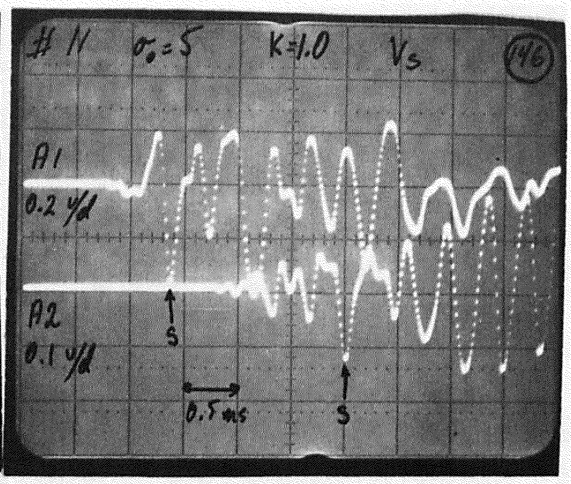
#11 σ_o=5 K=1.0 V_s (146)
A1
0.2 V/d
A2
0.1 V/d
S
S
0.5 ms

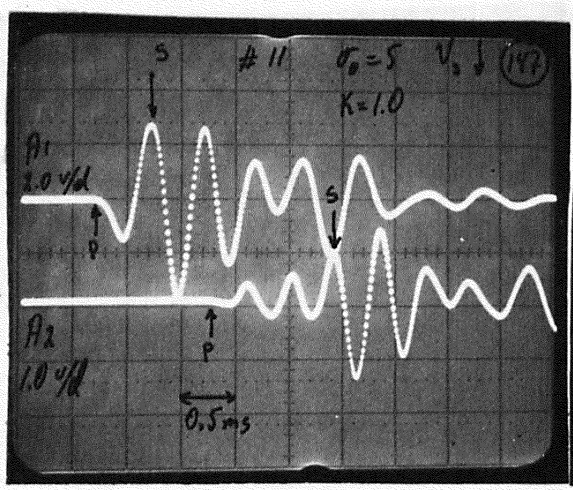
S
#11 σ_o=5 V_s (147)
K=1.0
A1
2.0 V/d
P
S
A2
1.0 V/d
P
0.5 ms

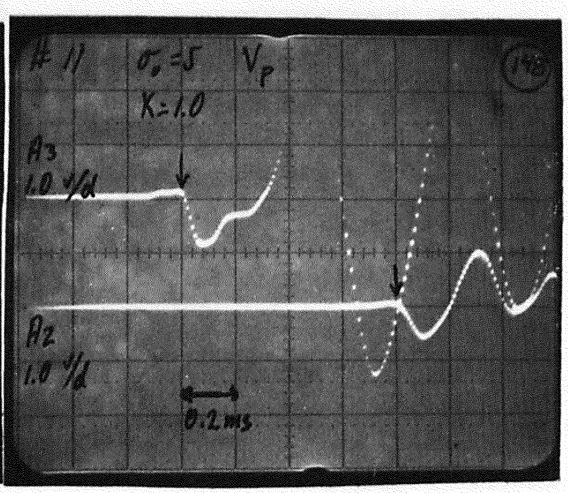
#11 σ_o=5 V_p (148)
K=1.0
A3
1.0 V/d
A2
1.0 V/d
0.2 ms

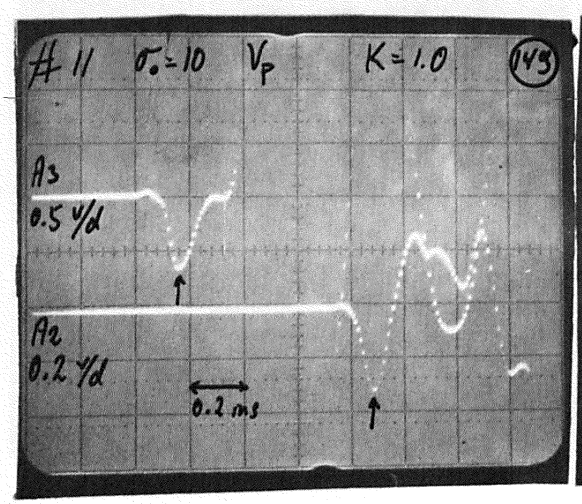
#11 σ_o=10 V_p K=1.0 (149)
A3
0.5 V/d
A2
0.2 V/d
0.2 ms

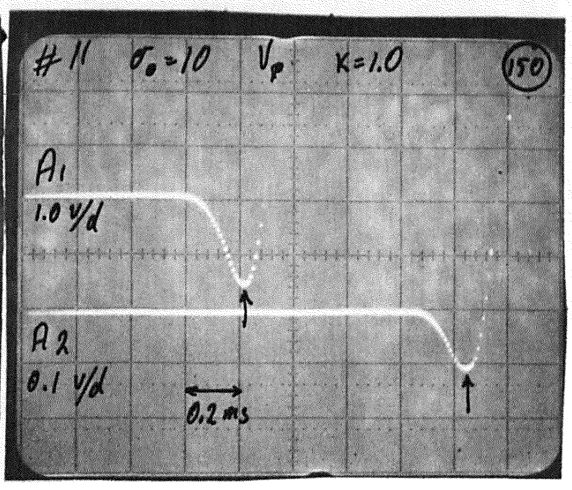
#11 σ_o=10 V_p K=1.0 (150)
A1
1.0 V/d
A2
0.1 V/d
0.2 ms

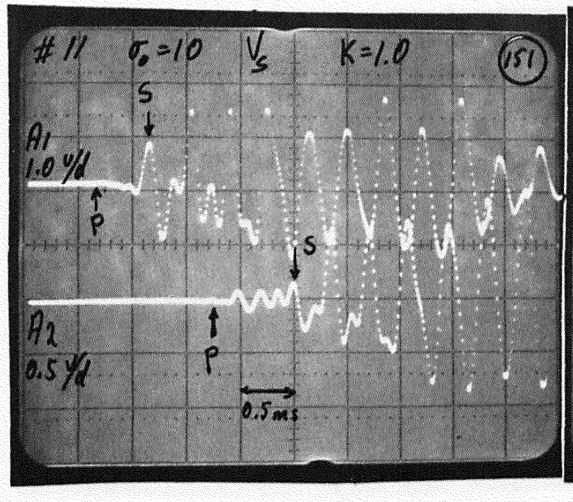
#11 σ₀=10 Vs K=1.0 151
S
A1
1.0 v/d
P
S
A2
0.5 v/d
P
0.5ms

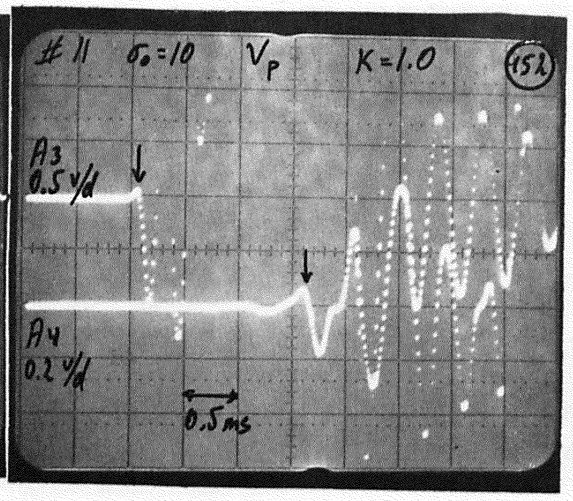
#11 σ₀=10 Vp K=1.0 152
A3
0.5 v/d
A4
0.2 v/d
0.5ms

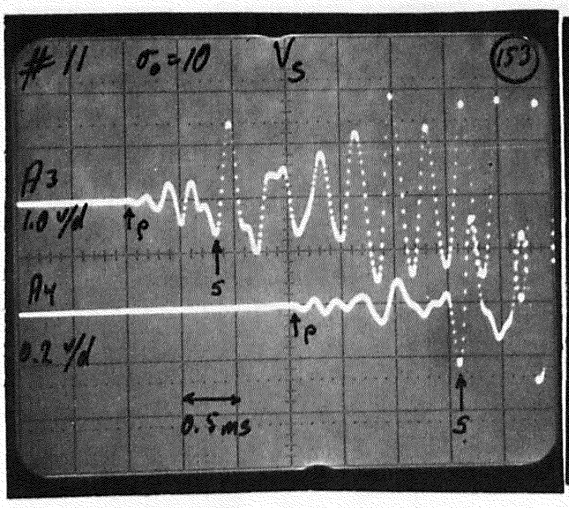
#11 σ₀=10 Vs 153
A3
1.0 v/d
P
S
A4
0.2 v/d
P
0.5ms
S

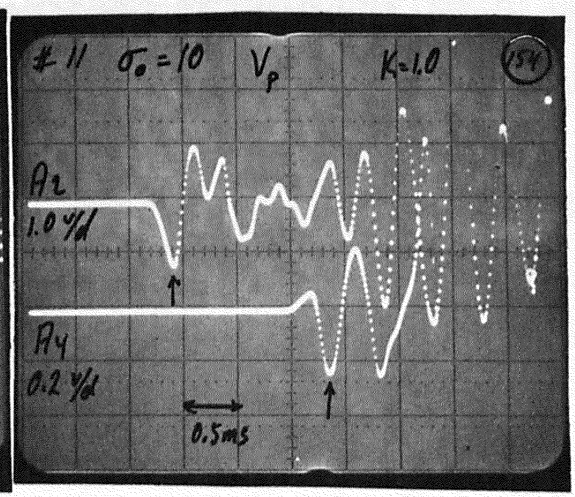
#11 σ₀=10 Vp K=1.0 154
A2
1.0 v/d
A4
0.2 v/d
0.5ms

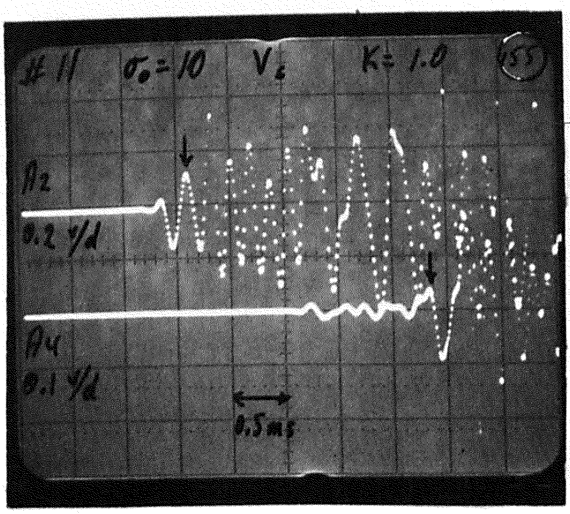
#11 σ₀=10 Vs K=1.0 155
A2
0.2 v/d
A4
0.1 v/d
0.5ms

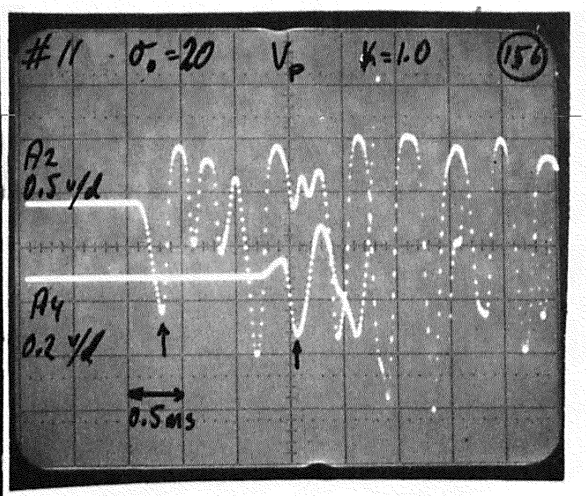
#11 σ₀=20 Vp K=1.0 156
A2
0.5 v/d
A4
0.2 v/d
0.5ms

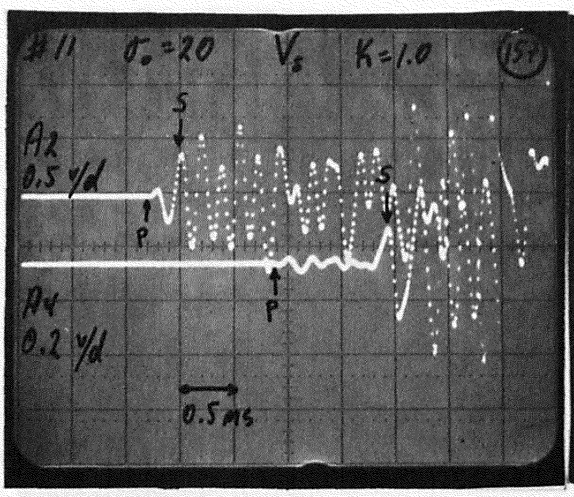
#11 σ₀=20 Vs K=1.0 (154)
A2
0.5 v/d
A4
0.2 v/d
S
P
P
S
0.5 ms

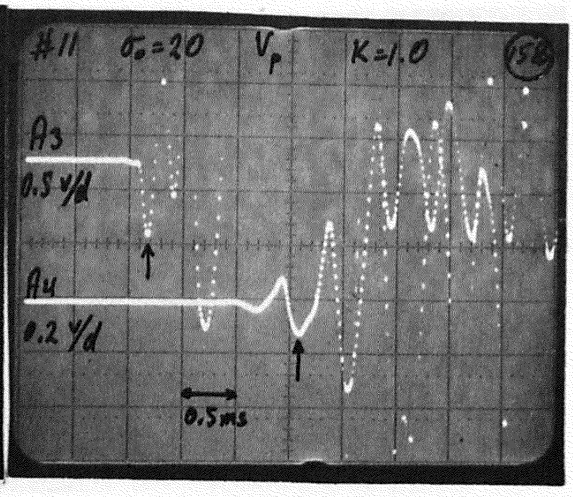
#11 σ₀=20 Vp K=1.0 (156)
A3
0.5 v/d
A4
0.2 v/d
0.5 ms

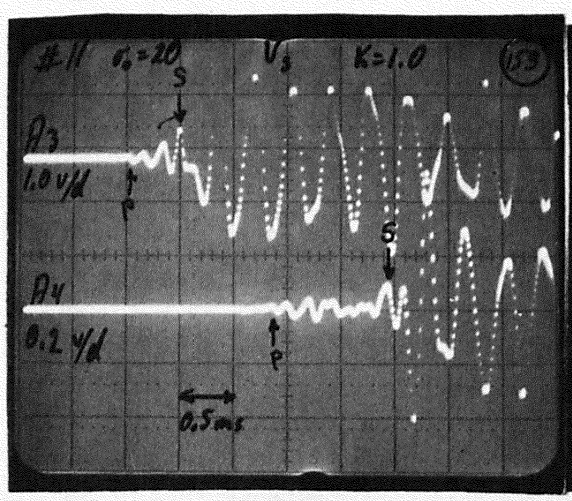
#11 σ₀=20 Vs K=1.0 (153)
A3
1.0 v/d
A4
0.2 v/d
S
P
P
S
0.5 ms

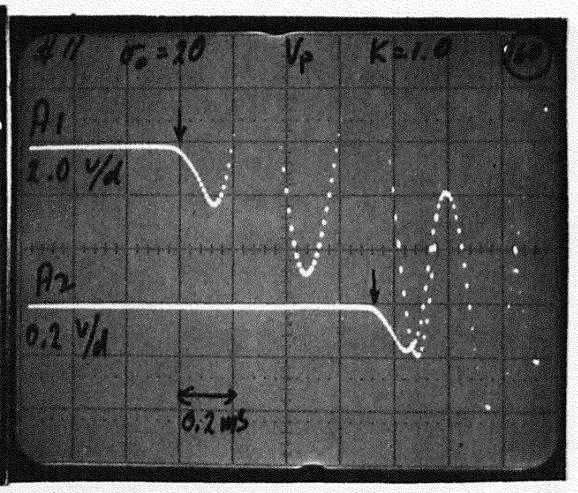
#11 σ₀=20 Vp K=1.0 (160)
A1
2.0 v/d
A2
0.2 v/d
0.2 ms

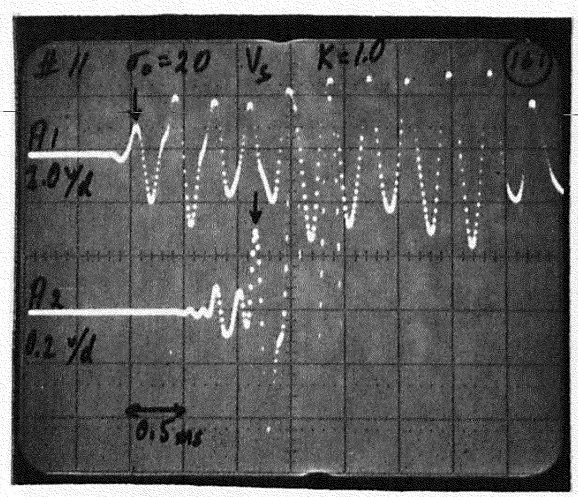
#11 σ₀=20 Vs K=1.0 (161)
A1
2.0 v/d
A2
0.2 v/d
0.5 ms

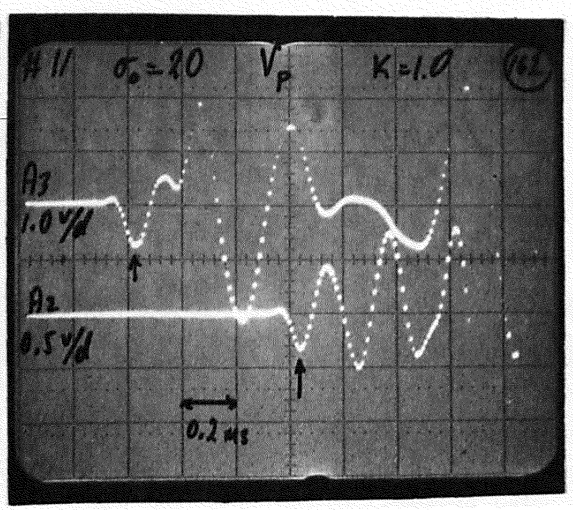
#11 σ₀=20 Vp K=1.0 (162)
A3
1.0 v/d
A2
0.5 v/d
0.2 ms

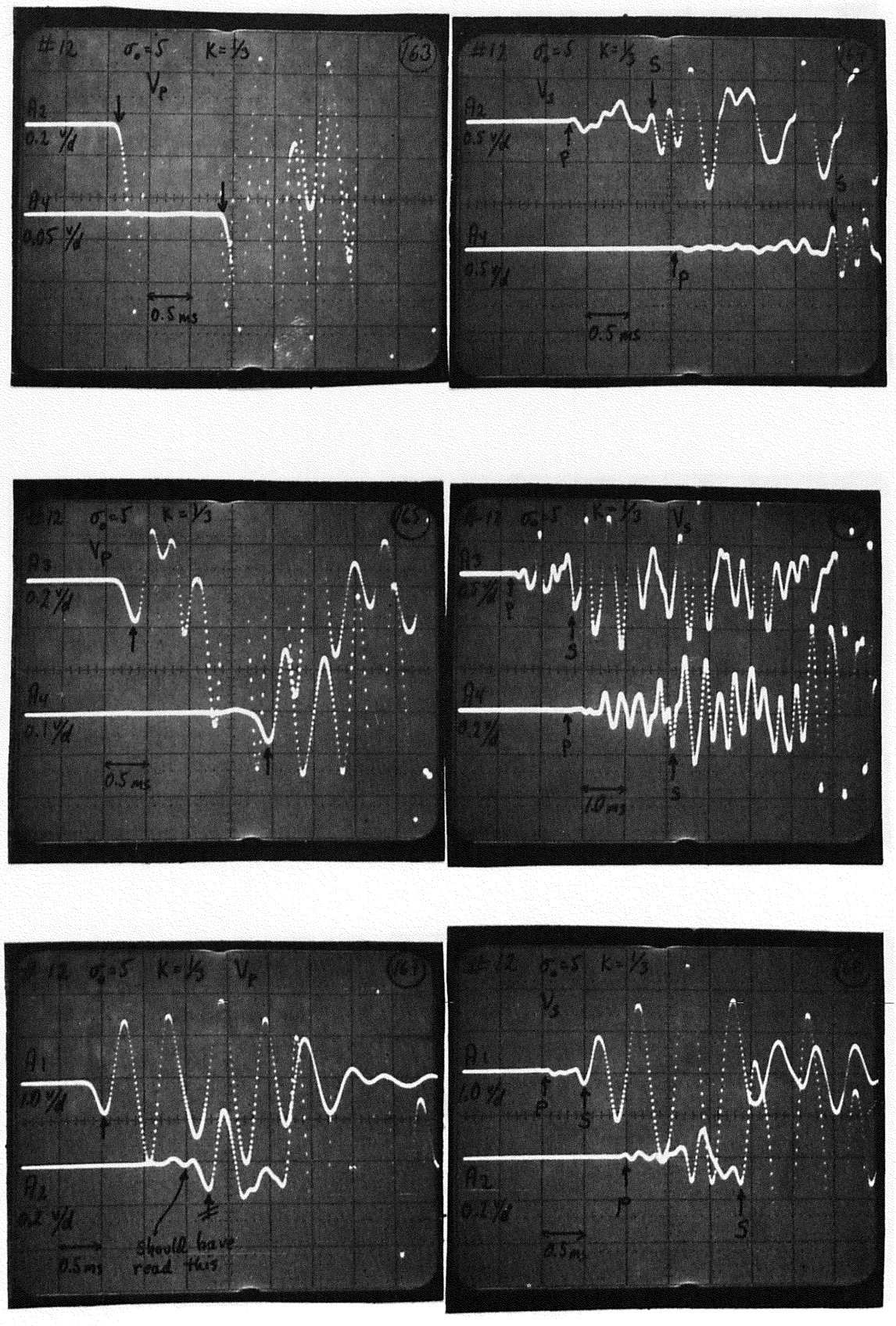
#12 σ_a=.5 K=1/3 (163)
V_P
A2 0.2 V/d
A4 0.05 V/d
0.5 ms
#12 σ_a=.5 K=1/3 S
V_S
A2 0.5 V/d
P
S
A4 0.5 V/d
P
0.5 ms
#12 σ_a=.5 K=1/3 (165)
V_P
A3 0.2 V/d
A4 0.1 V/d
0.5 ms
V_S
A3 0.5 V/d
P
S
A4 0.2 V/d
P
S
1.0 ms
#12 σ_a=.5 K=1/3 V_P (161)
A1 1.0 V/d
A2 0.2 V/d
Should have read this
0.5 ms
#12 σ_a=.5 K=1/3
V_S
A1 1.0 V/d
P
S
A2 0.2 V/d
P
S
0.5 ms

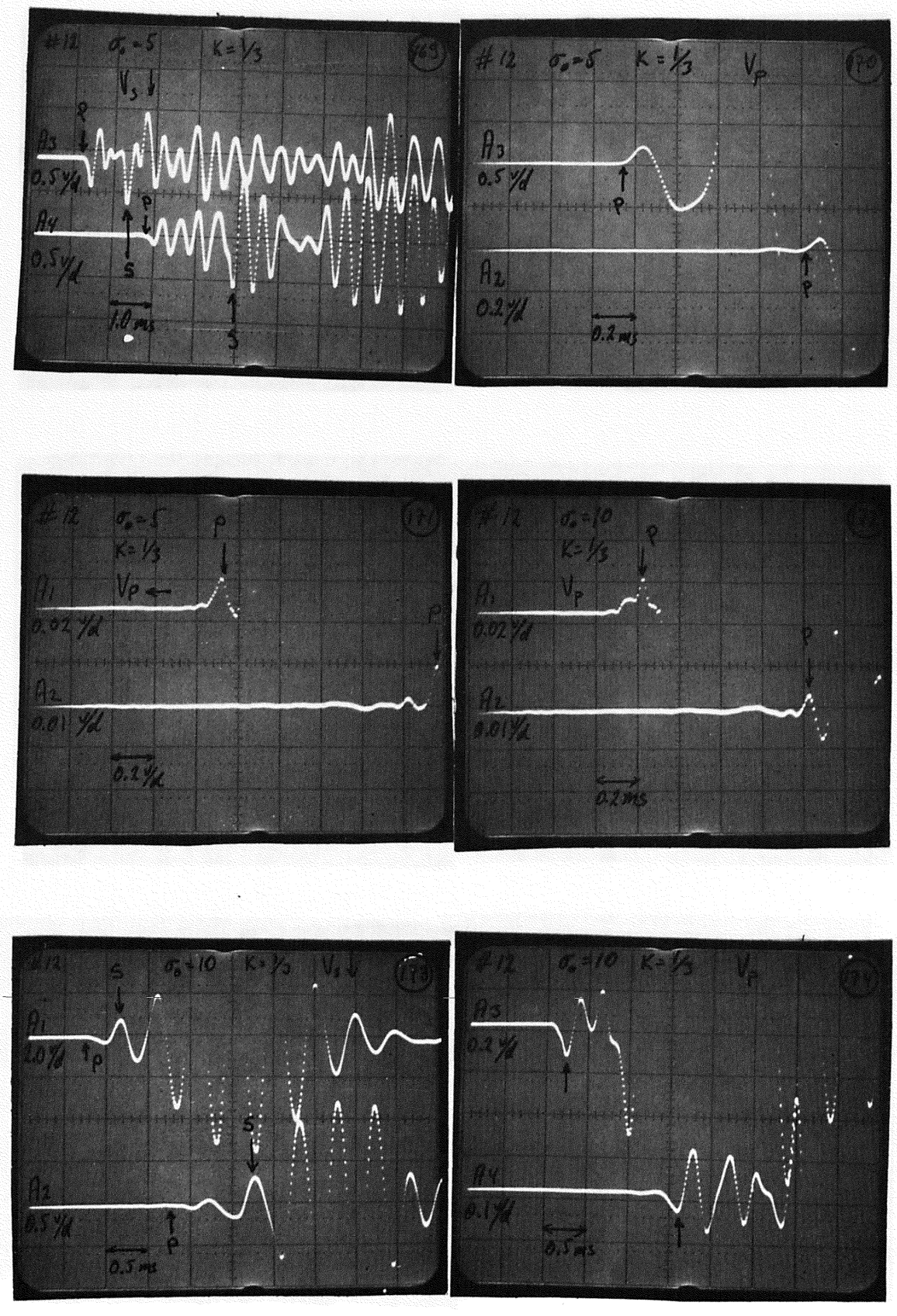
#12 σ_0=5 K=1/3
V_s
P
S
A3
0.5 V/d
A4
0.5 V/d
1.0 ms
#12 σ_0=5 K=1/3 V_p
A3
0.5 V/d
A2
0.2 V/d
0.2 ms
#12 σ_0=5
K=1/3
V_p
A1
0.02 V/d
A2
0.01 V/d
0.2 V/d
#12 σ_0=10
K=1/3
V_p
A1
0.02 V/d
A2
0.01 V/d
0.2 ms
#12 σ_0=10 K=1/3 V_s
A1
2.0 V/d
A2
0.5 V/d
0.5 ms
#12 σ_0=10 K=1/3 V_p
A3
0.2 V/d
A4
0.1 V/d
0.5 ms

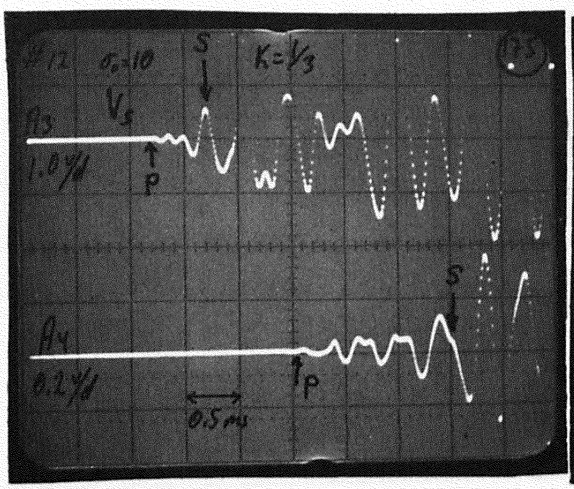
E12 σ_0=10 S K=1/3 (173)
A_3 V_s
1.0 %/d
P
S
A_4
0.2 %/d
T_p
0.5 ms

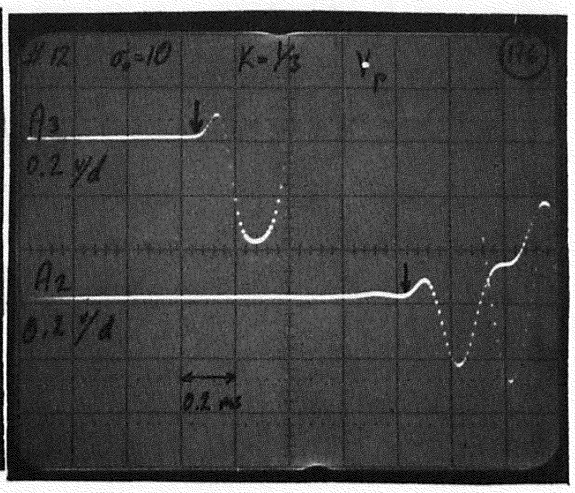
E12 σ_0=10 K=1/3 V_p (176)
A_3
0.2 %/d
A_2
0.2 %/d
0.2 ms

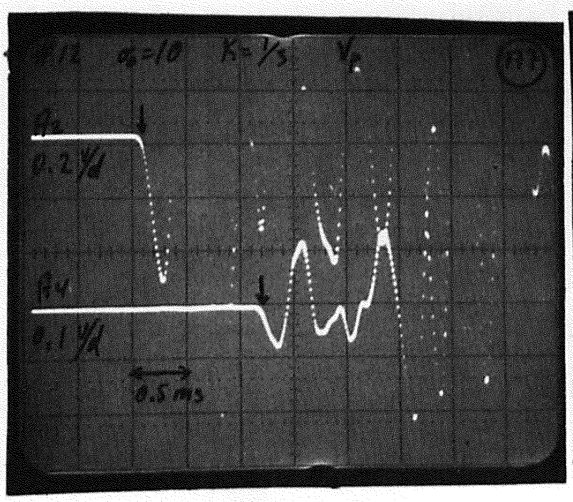
E12 σ_0=10 K=1/3 V_p (181)
A_2
0.2 %/d
A_4
0.1 %/d
0.5 ms

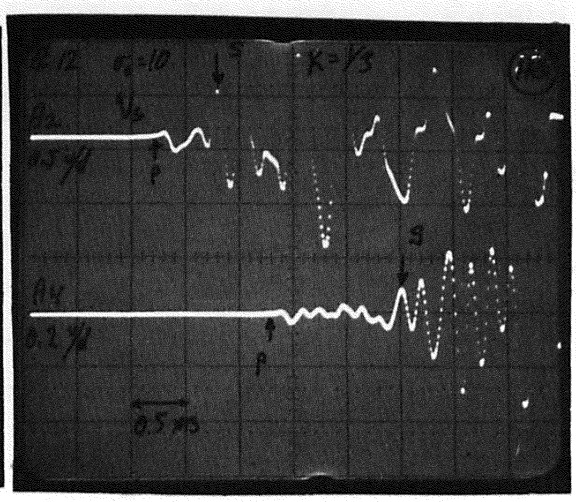
E12 σ_0=10 S K=1/3
V_s
P
S
A_4
0.2 %/d
0.5 ms

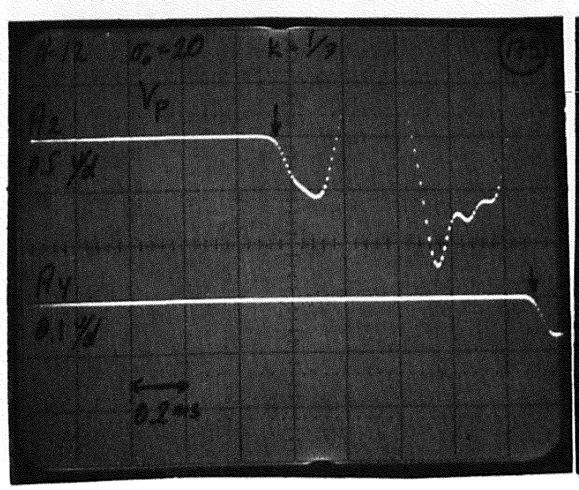
E12 σ_0=20 K=1/3 (174)
V_p
A_2
0.5 %/d
A_4
0.1 %/d
0.2 ms

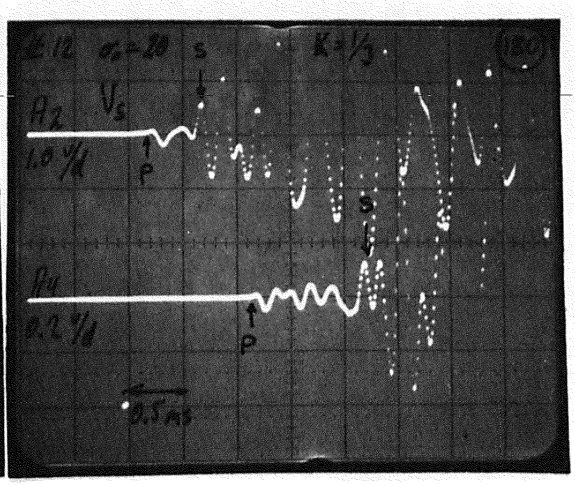
E12 σ_0=20 S K=1/3 (180)
A_2 V_s
1.0 %/d
P
S
A_4
0.2 %/d
P
0.5 ms

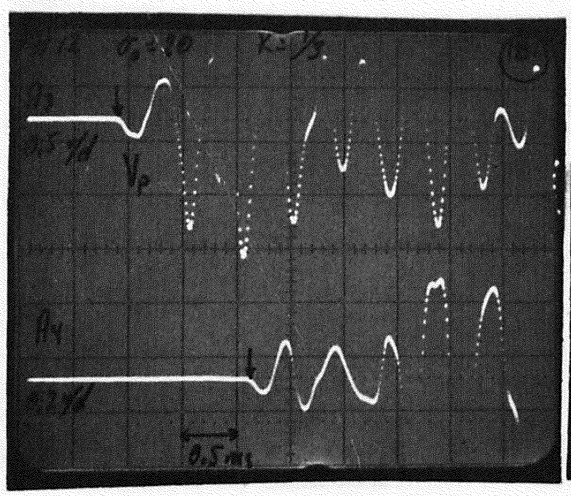
σ_0=20
K=1/3
V_P
A3
0.5 V/d
A4
0.2 V/d
0.5 ms

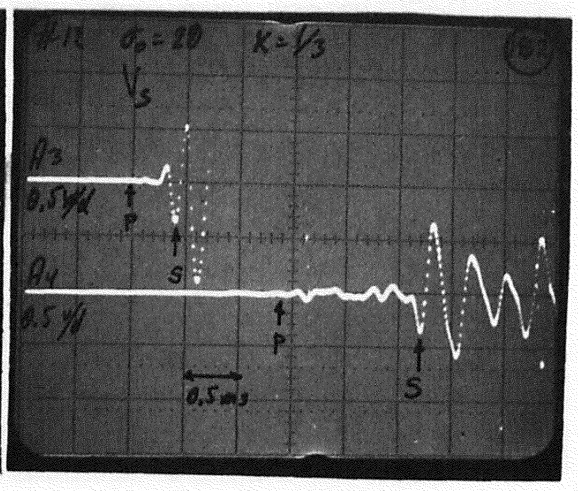
σ_0=20
K=1/3
V_S
A3
0.5 V/d
A4
0.5 V/d
P
S
0.5 ms

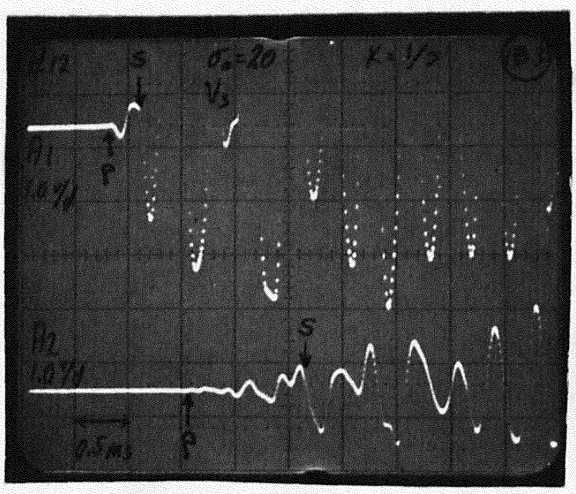
σ_0=20
K=1/3
V_S
A1
1.0 V/d
A2
1.0 V/d
0.5 ms

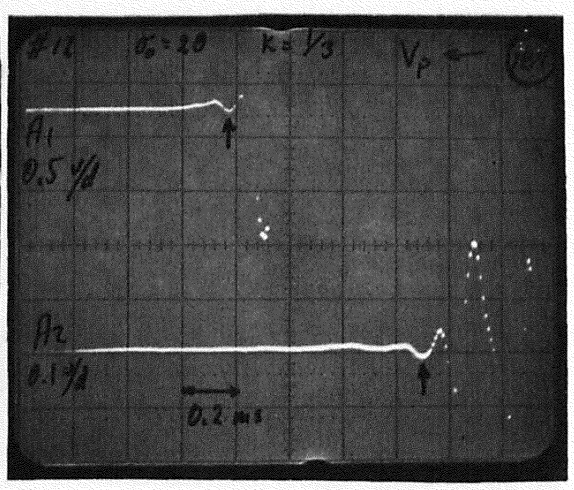
σ_0=20
K=1/3
V_P
A1
0.5 V/d
A2
0.1 V/d
0.2 ms

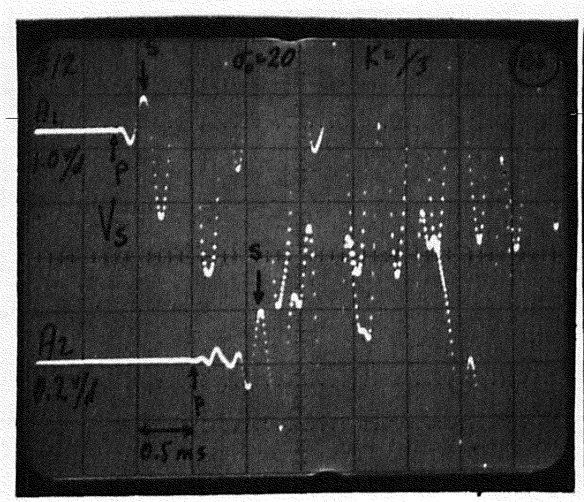
σ_0=20
K=1/3
V_S
A1
1.0 V/d
A2
0.2 V/d
0.5 ms

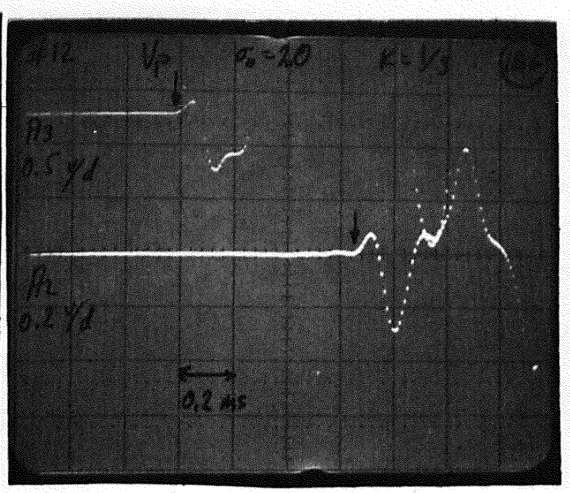
V_P
σ_0=20
K=1/3
A3
0.5 V/d
A2
0.2 V/d
0.2 ms

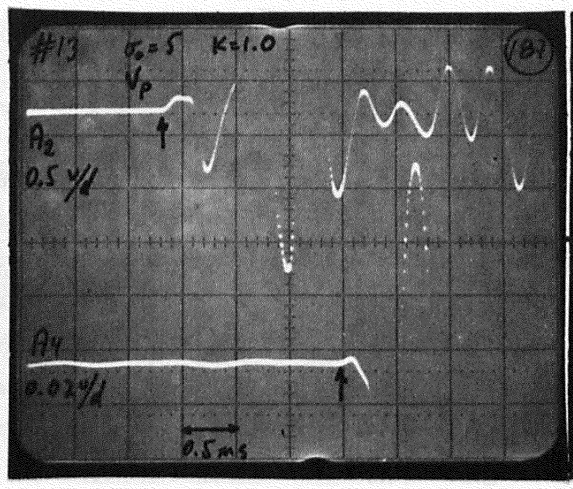
#13 σ_o=5 K=1.0 (182)
V_P
A2
0.5 v/d
A4
0.02 v/d
0.5 ms

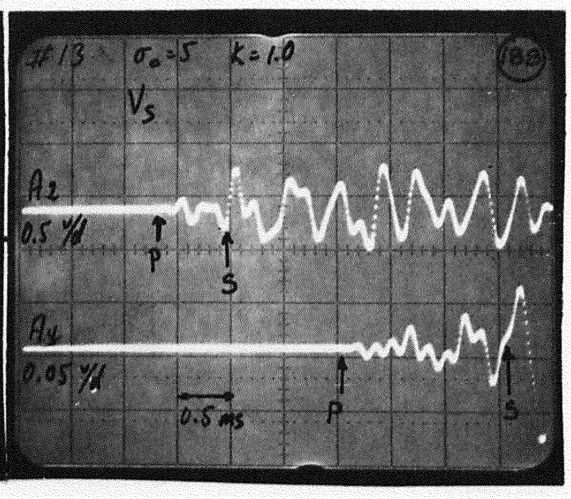
#13 σ_o=5 K=1.0 (183)
V_S
A2
0.5 v/d
P
S
A4
0.05 v/d
0.5 ms
P
S

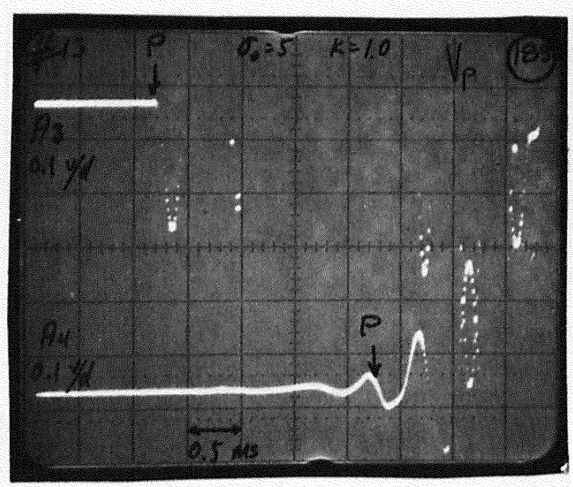
#13 P σ_o=5 K=1.0 V_P (185)
A3
0.1 v/d
A4
0.1 v/d
P
0.5 ms

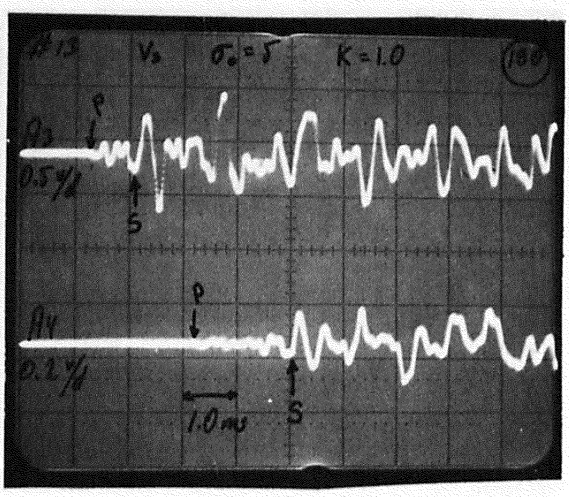
#13 V_S σ_o=5 K=1.0 (184)
P
A3
0.5 v/d
S
P
A4
0.2 v/d
1.0 ms
S

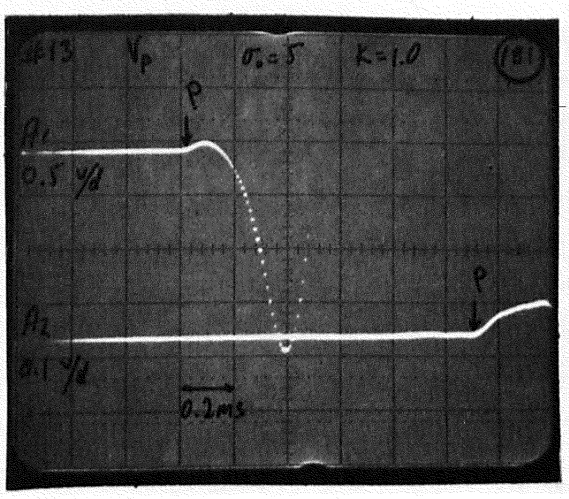
#13 V_P σ_o=5 K=1.0 (181)
P
A1
0.5 v/d
P
A2
0.1 v/d
0.2 ms

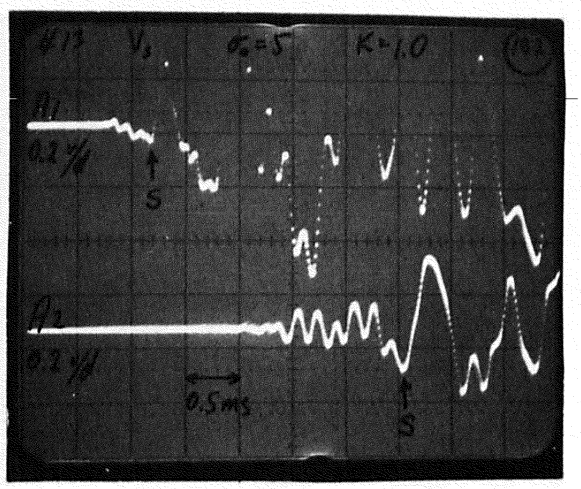
#13 V_S σ_o=5 K=1.0 (183)
A1
0.2 v/d
S
A2
0.2 v/d
0.5 ms
S

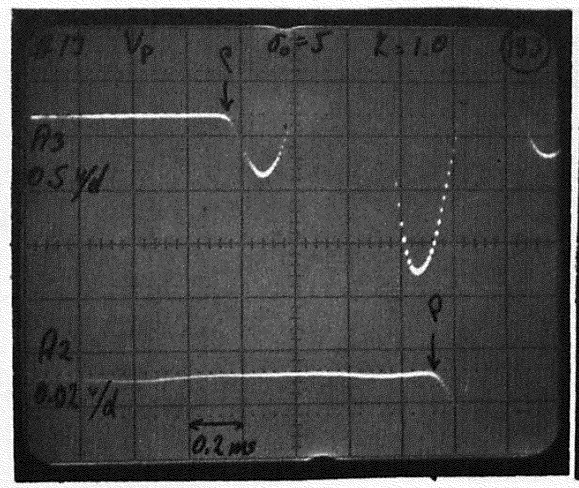
#13 V_P σ_0=5 K=1.0 (134)
P
A3
0.5 %/d
A2
0.02 %/d
P
0.2 ms

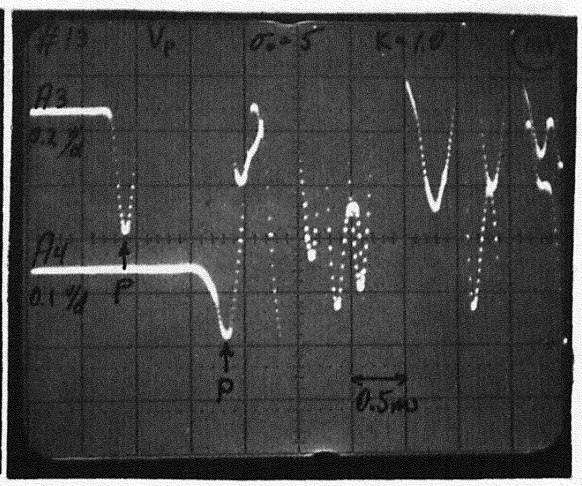
#13 V_P σ_0=5 K=1.0
A3
0.2 %/d
A4
0.1 %/d
P
P
0.5 ms

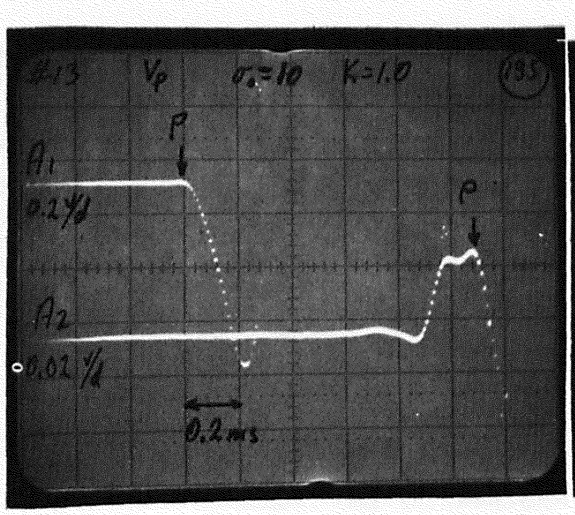
#13 V_P σ_0=10 K=1.0 (135)
P
A1
0.2 %/d
P
A2
0.02 %/d
0.2 ms

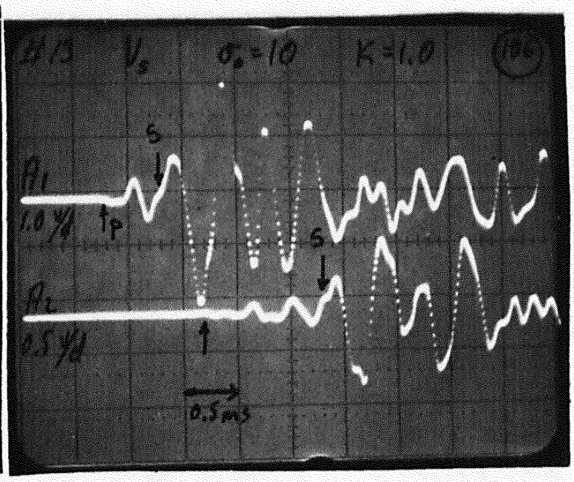
#13 V_S σ_0=10 K=1.0 (136)
S
A1
1.0 %/d
P
S
A2
0.5 %/d
0.5 ms

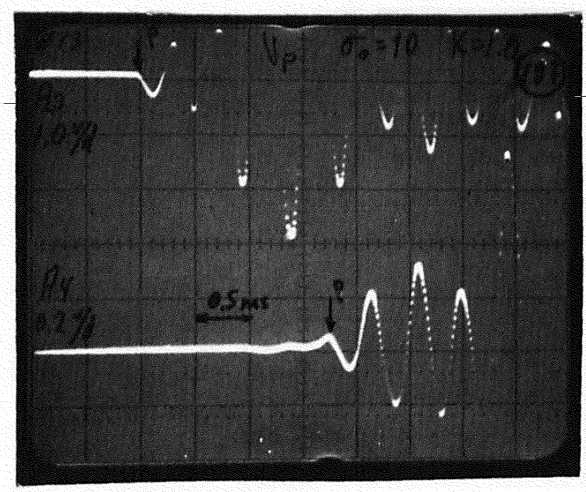
#13 V_P σ_0=10 K=1.0 (137)
A3
1.0 %/d
A4
0.2 %/d
0.5 ms
P

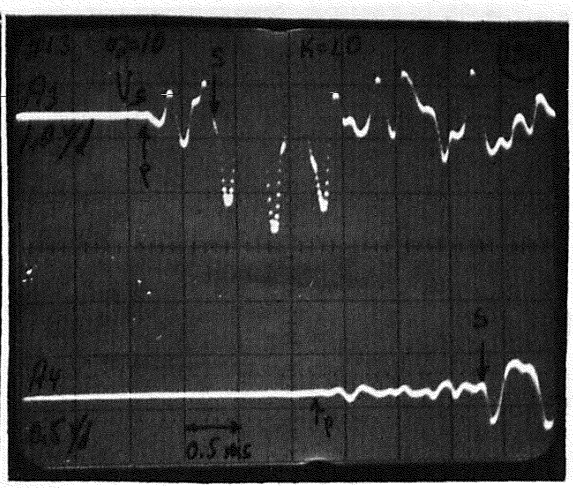
#13 σ_0=10 K=1.0
V_S
S
A3
1.0 %/d
P
A4
S
0.5 %/d
P
0.5 ms

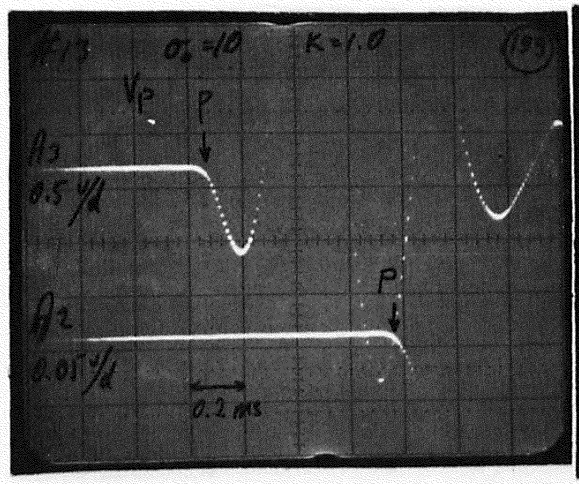
σ_0=10
K=1.0
V_P
P
P
A_3
0.5 V/d
A_2
0.05 V/d
0.2 ms

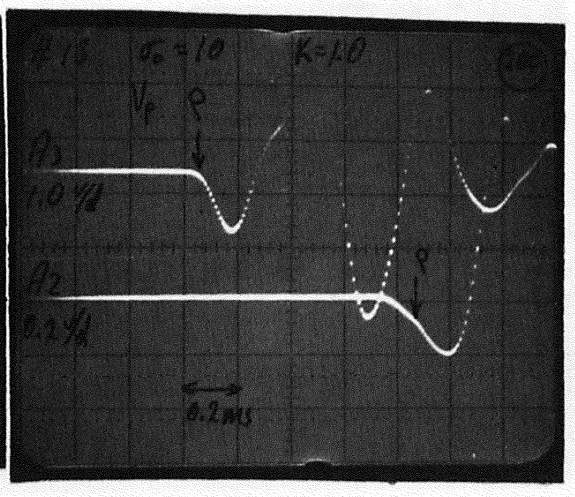
σ_0=10
K=1.0
V_P
P
P
A_3
1.0 V/d
A_2
0.2 V/d
0.2 ms

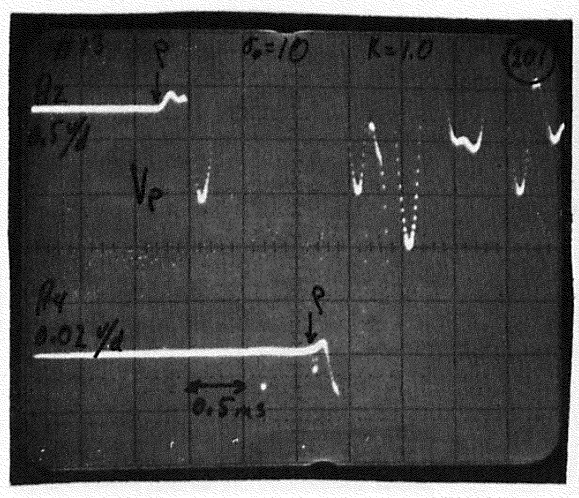
P
σ_0=10
K=1.0
A_2
0.5 V/d
V_P
P
A_4
0.02 V/d
0.5 ms

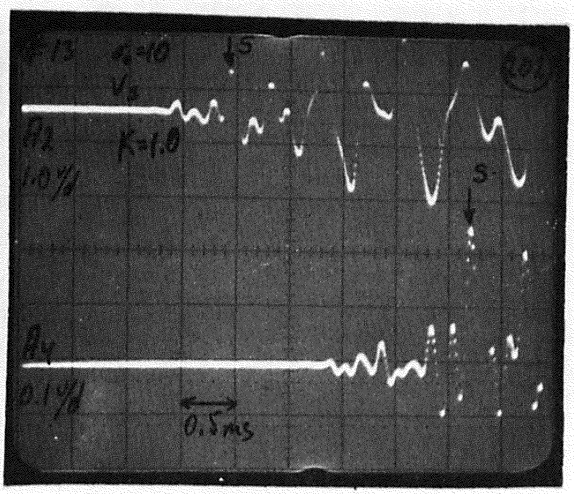
σ_0=10
S
V_S
A_2
K=1.0
1.0 V/d
S
A_4
0.1 V/d
0.5 ms

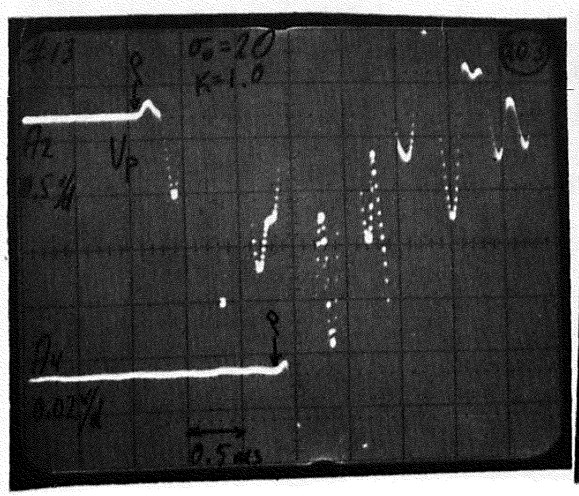
P
σ_0=20
K=1.0
A_2
V_P
0.5 V/d
P
A_4
0.02 V/d
0.5 ms

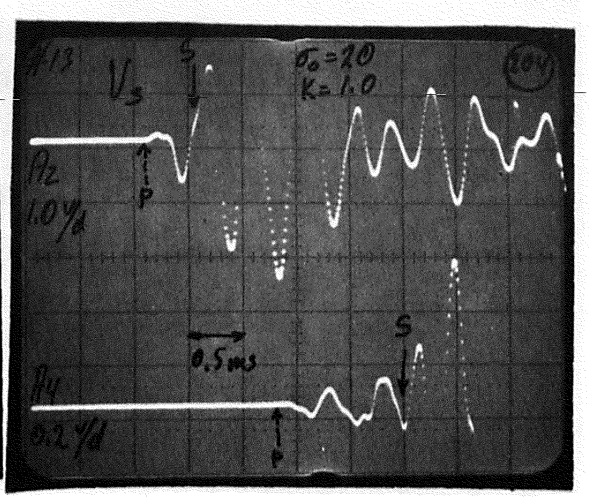
S
σ_0=20
K=1.0
V_S
P
A_2
1.0 V/d
0.5 ms
S
A_4
0.2 V/d
P

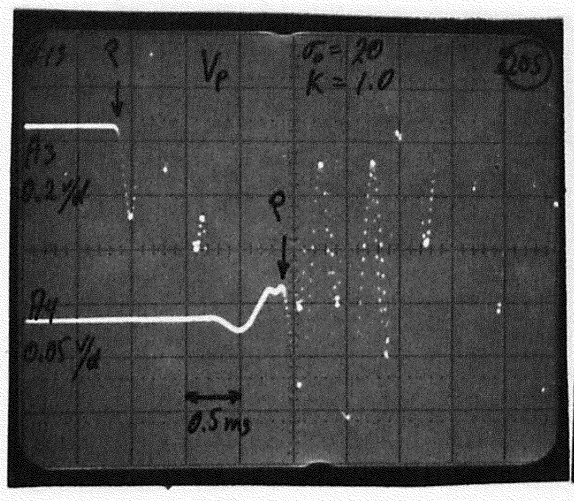
#13
P
V_P
$\sigma_0 = 20$
K = 1.0
205
A3
0.2 V/d
P
A4
0.05 V/d
0.5 ms

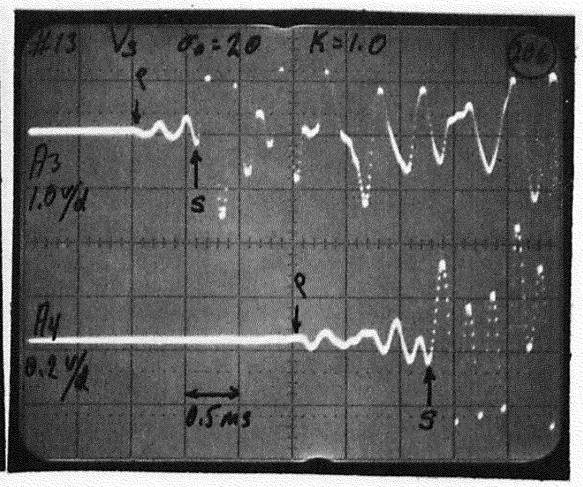
#13
V_S
$\sigma_0 = 20$
K = 1.0
206
P
A3
1.0 V/d
S
P
A4
0.2 V/d
0.5 ms
S

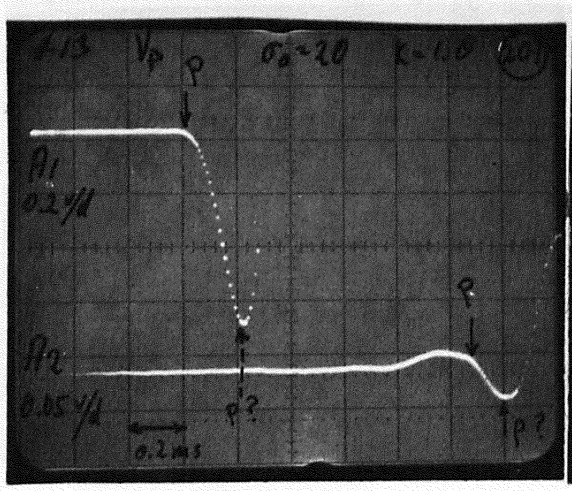
#13
V_P
P
$\sigma_0 = 20$
K = 1.0
207
A1
0.2 V/d
P
A2
0.05 V/d
P?
0.2 ms
P?

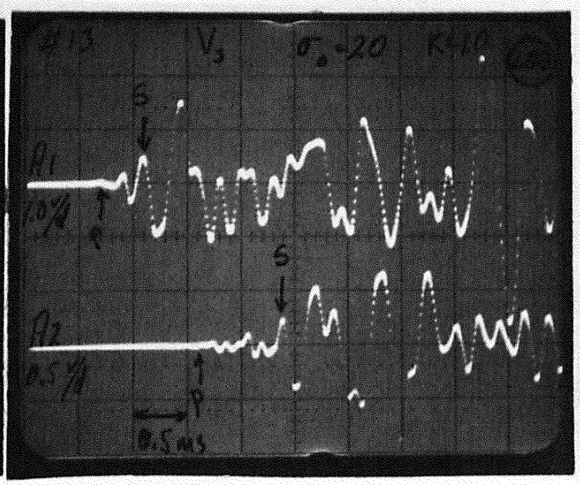
#13
V_S
$\sigma_0 = 20$
K = 1.0
208
S
A1
1.0 V/d
P
S
A2
0.5 V/d
P
0.5 ms

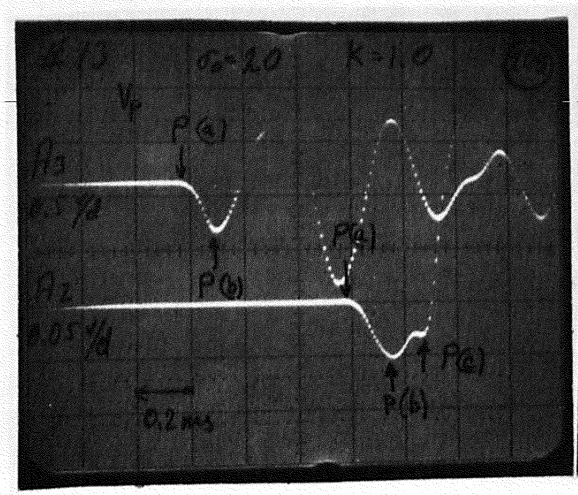
#13
$\sigma_0 = 20$
K = 1.0
209
V_P
P(a)
A3
0.5 V/d
P(b)
P(a)
A2
0.05 V/d
P(c)
P(b)
0.2 ms

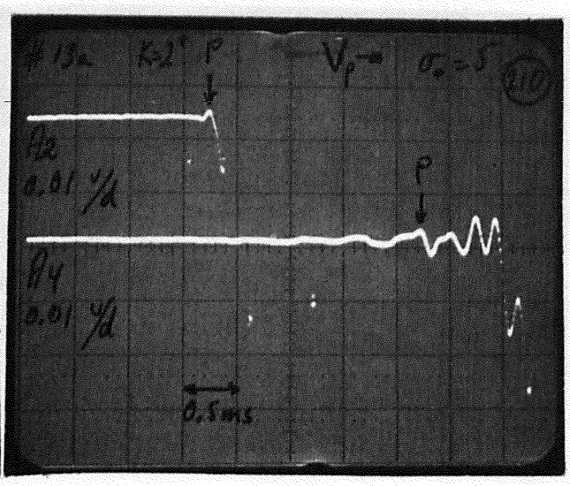
#13a
K=2
P
V_P
$\sigma_0 = 5$
210
A2
0.01 V/d
P
A4
0.01 V/d
0.5 ms

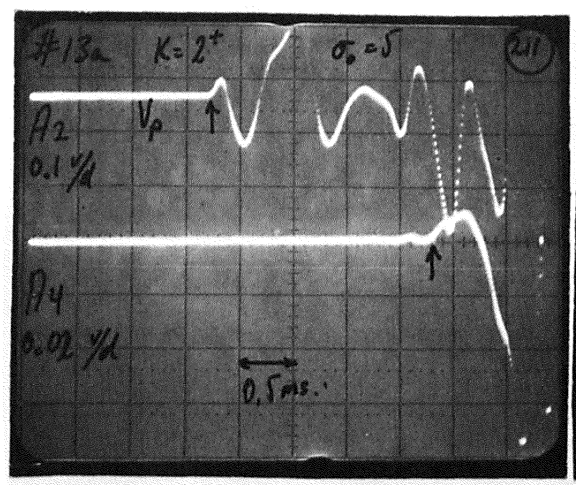
#13a
K=2+
σ=5
A2
0.1 %/d
Vp
A4
0.02 %/d
0.5 ms.

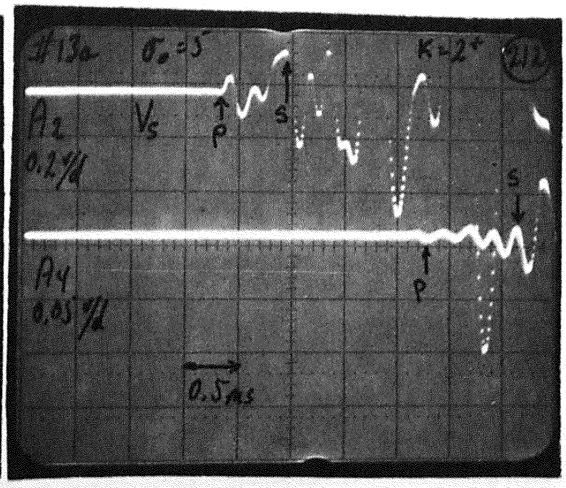
#13a
σ=5
K=2+
A2
0.2 %/d
Vs
P
S
A4
0.05 %/d
0.5 ms

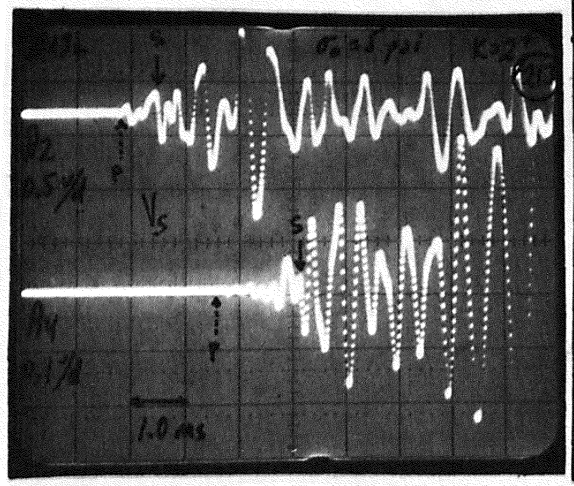
S
P
Vs
A2
0.5 %/d
A4
0.1 %/d
1.0 ms

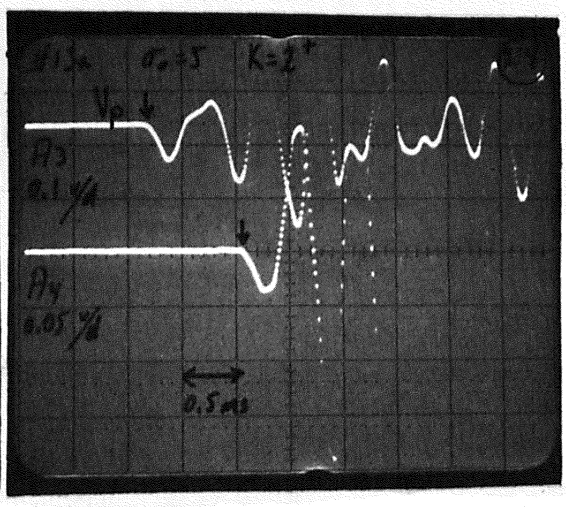
#13a
σ=5
K=2+
Vp
A3
0.1 %/d
A4
0.05 %/d
0.5 ms

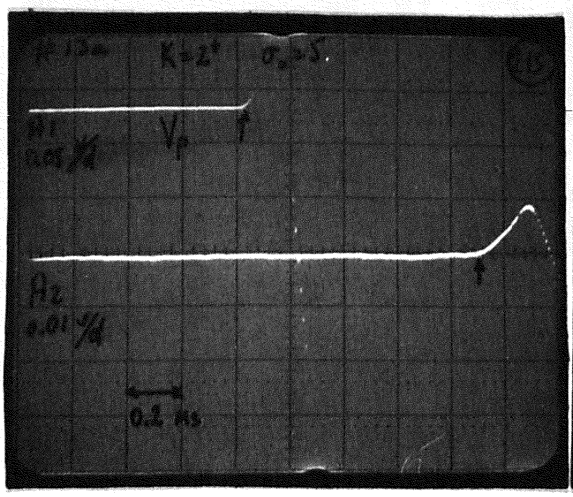
K=2+
σ=5
Vp
A2
0.01 %/d
0.2 ms

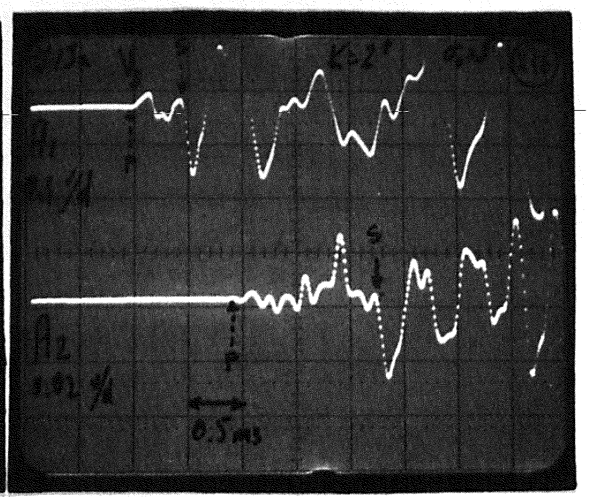
K=2+
S
P
A2
0.02 %/d
0.5 ms

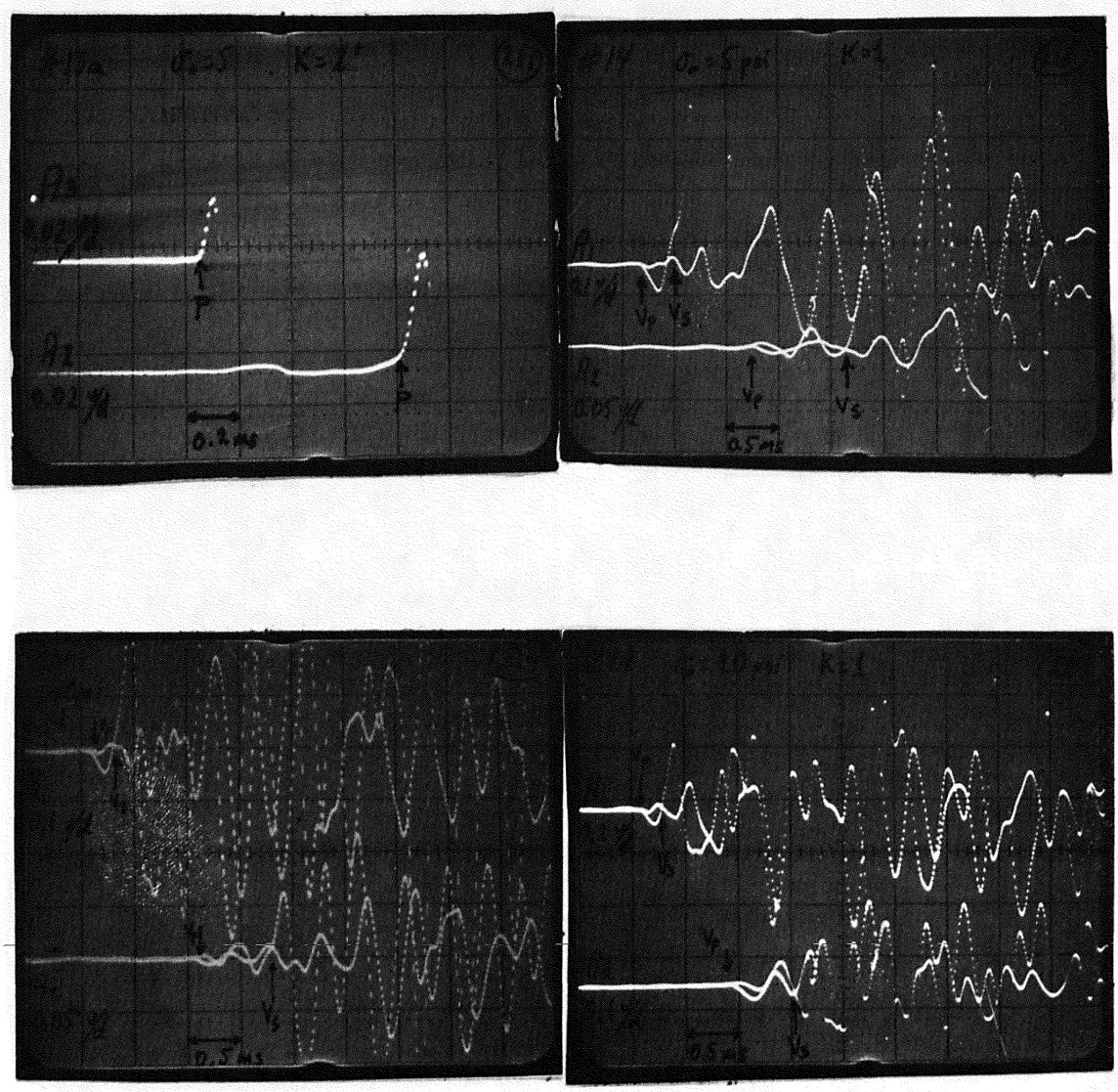
P
P
0.2 ms
Vp
Vs
Vp
Vs
0.5 ms
Vs
0.5 ms
Vs
0.5 ms

APPENDIX B

TABLES OF CORRECTED V_p AND V_s FROM EACH TEST IN ORDER OF TEST NUMBER

TEST NO. 3 K = 1.0

	σ_o' = 5.0 psi			σ_o' = 10.0 psi			σ_o' = 20.0 psi		
	γ_d = 93.3 pcf			γ_d = 93.6 pcf			γ_d = 94.5 pcf		
wave ∠ with horiz.	correct factor	corr. V_p V_s	photo No.	correct factor	corr. V_p V_s	foto No.	correct factor	corr. V_p V_s	foto No.
θ = 90°	.992 .992	1137 473?	—	.986 .988	1223 891	2 5	.979 .982	1396 950	— 9
64°	.991 .986	1104 493?	—	.989 .985	1426 840	1 4	.981 .971	1533 950	— 8
45°	.988 —	1051 —	— —	.983 .983	1188 928	— 3	.964 .976	1351 1077	6 7
0°									

Notes: a) Used Fig. 5 accelerometer pattern
b) Sand wet after test due to membrane leakage. Unit wts. estimated from prev. tests, prob. high.

TEST NO. 4 K = 1/3

	σ_o' = 5.0 psi			σ_o' = 10.0 psi			σ_o' = 20.0 psi		
	γ_d = 92.8 pcf			γ_d = 92.8 pcf			γ_d = 93.0 pcf		
wave ∠ with horiz.	correct factor	corr. V_p V_s	foto No.	correct factor	corr. V_p V_s	foto No.	correct factor	corr. V_p V_s	foto No.
θ = 90°	.984	1403 —	12 —	.980 .980	1615 884	13 22	.971 .971	1753 985	18 26
64°	.987 .988	1315 971	11 20	.984 .985	1507 886	15 23	.978 .978	1683 981	17 25
45°	.995 .993	1256 903	10 19	.993 .992	1506 997	14 21	.987 .987	1593 997	16 24
0°									

Notes: a) Used Fig. 5 accelerometer pattern.

TEST NO. 6 K = 1.0

	σ_o' = 5.0 psi			σ_o' = 10.0 psi			σ_o' = 20.0 psi		
	γ_d = 103.2 pcf			γ_d = 103.4 pcf			γ_d = 103.5 pcf		
wave ∠ with horiz.	correct factor	corr. V_p V_s	photo No.	correct factor	corr. V_p V_s	foto No.	correct factor	corr. V_p V_s	foto No.
θ = 90°	.994	1313	39	.991	1512	41	.990	1748	49
	.994	853	40	.992	960	48	.990	1119	56-55
60°	.993	1366	37	.992	1550	43	.990	1772	51
	.992	895	38	.990	1057	44	.988	1162	52
30°	1.021	1370	35	1.000	1547	45	.992	1796	53
	1.022	856	36	1.005	1101	46-47	.997	1279	54
0°									

Notes: a) First test with Fig. 6 accelerometer pattern.

TEST NO. 7 K = 1/3

	σ_o' = 5.0 psi			σ_o' = 10.0 psi			σ_o' = 20.0 psi		
	γ_d = 102.3 pcf			γ_d = 102.3 pcf			γ_d = 102.5 pcf		
wave ∠ with horiz.	correct factor	corr. V_p V_s	foto No.	correct factor	corr. V_p V_s	foto No.	correct factor	corr. V_p V_s	foto No.
θ = 90°	.993	1730	58	.992	1860	70	.987	2068	71
	.994	851	57	.993	859	68-69	.989	981	72
60°	.996	1567	60	.995	1700	66	0.992	1895	73
	1.000	1008	59	1.000	1008	67	.994	1317	74
30°	1.039	1562	61	1.023	1516	64-65	1.003	1923	76-77
	1.020	825	62	1.018	1063	63	1.008	1448	75
0°									

Notes: a) First test to use Fig. 4 mechanical impact system.
b) First test where we used both impact modes (dropping or swinging ball) to estimate 1st arrivals in ?? cases.

TEST NO. 8 K = 1/3

wave ∠ with horiz.	σ_o' = 5.0 psi, γ_d = 91.6 pcf			σ_o' = 10.0 psi, γ_d = 91.8 pcf			σ_o' = 20.0 psi, γ_d = 92.1 pcf		
	correct factor	corr. V_p V_s	photo No.	correct factor	corr. V_p V_s	foto No.	correct factor	corr. V_p V_s	foto No.
θ = 90°	.986	1493	78	.981	1672	88	.974	1908	90
	.985	871	79	.980	920	89	.974	1012	91
60°	.994	1442	83	.989	1547	84	.984	1732	94
	1.004	877	82	.997	929	87	.990	968	95
30°	1.056	1371	81	1.033	1442	85	1.018	1684	93
	1.045	968	80	1.023	1103	86	1.022	1079	92
0°									

Notes: a) Minor membrane leakage found after test. Wt. dry sand corrected by estimating wt. water (30 lb).
b) H. Margas did 1st arrival interpretations.

TEST NO. 9 K = 1.0

wave ∠ with horiz.	σ_o' = 5.0 psi, γ_d = 92.2 pcf			σ_o' = 10.0 psi, γ_d = 92.5 pcf			σ_o' = 20.0 psi, γ_d = 92.8 pcf		
	correct factor	corr. V_p V_s	foto No.	correct factor	corr. V_p V_s	foto No.	correct factor	corr. V_p V_s	foto No.
θ = 90°	1.007	1146	96	1.001	1314	107	.996	1514	117
	1.004	825	97	1.000	789	108-109	.996	985	118
60°	1.005	1035	98	.999	1560	105	.996	1689	115
	1.010	766	99	1.003	909	106	.994	1177	116
30°	1.043	1210	100	1.016	1363	104	1.000	1627	113
	1.039	674	101	1.013	1002	104	1.001	1140	114
0°	1.017	1260	103	1.003	1375	110	.995	1568	111

Notes: a) First test to obtain V_p at θ = 0° by striking side of tank with ball.

TEST NO. 10 K = 1/3

	σ_o' = 5.0 psi			σ_o' = 10.0 psi			σ_o' = 20.0 psi		
	γ_d = 103.0 pcf			γ_d = 103.2 pcf			γ_d = 103.3 pcf		
wave ⊥ with horiz.	correct factor	corr. V_p V_s	photo No.	correct factor	corr. V_p V_s	foto No.	correct factor	corr. V_p V_s	foto No.
θ = 90°	.982	1324 ?	119	.989	1438 ?	126	.986	1639 ?	133
	.982	871 ?	120	.989	754 ?	127	.987	1126 ?	134
60°	.993	1309 ?	121	.990	1402 ?	128	.988	1813 ?	135
	.993	998 ?	122	.990	1137 ?	129	.987	1151 ?	136
30°	1.024	1460	123	1.004	1650	130	.996	1926	137
	1.026	1079	124	1.007	1122	131	.997	1246	138
0°	1.017	1299	125	1.006	1497	132	1.000	1745	139

Notes: a) V data involving A4 (θ = 90°, 60°) suspect because does not fit previous data patterns. Later careful removal of A4 found no obvious reason for problem.
b) Velocity interpretations checked by Dr. Woods.

TEST NO. 11 K = 1.0

	σ_o' = 5.0 psi			σ_o' = 10.0 psi			σ_o' = 20.0 psi		
	γ_d = 101.6 pcf			γ_d = 101.8 pcf			γ_d = 101.9 pcf		
wave ⊥ with horiz.	correct factor	corr. V_p V_s	foto No.	correct factor	corr. V_p V_s	foto No.	correct factor	corr. V_p V_s	foto No.
θ = 90°	1.013	1163	140	1.008	1374	154	1.004	1607	156
	1.010	750	141	1.006	863	155	1.003	1023	157
60°	1.010	1276	142	1.006	1452	152	1.003	1606	158
	1.013	843	143-144	1.012	1018	153	1.007	1174	159
30°	1.043	1414	145	1.026	1614	150	1.015	1803	160
	1.044	832	146-147	1.023	936	151	1.011	1182	161
0°	1.017	1429	148	1.005	1589	149	.998	1843	162

Notes: a) Velocity interpretations checked by Dr. Woods.

TEST NO. 12 K = 1/3

wave ∠ with horiz.	σ_o' = 5.0 psi, γ_d = 102.5 pcf: correct factor	corr. V_p V_s	foto No.	σ_o' = 10.0 psi, γ_d = 102.6 pcf: correct factor	corr. V_p V_s	foto No.	σ_o' = 20.0 psi, γ_d = 102.8 pcf: correct factor	corr. V_p V_s	foto No.
θ = 90°	.998	1541	163	.995	1749	177	.989	2012	179
	.998	883	164	.995	1132	178	.989	1281	180
60°	.999	1389	165	.996	1670	174	.993	1881	181
	1.002	883	169	.999	987	175	.995	988	182
30°	1.033	1293	171	1.013	1640	172	1.003	1831	184
	1.033	730	168	1.015	814	173	1.004	1200	183
0°	1.017	1291	170	1.006	1468	176	.999	1702	186

Notes: a) Velocity interpretations checked by Dr. Woods.

TEST NO. 13 K = 1.0

wave ∠ with horiz.	σ_o' = 5.0 psi, γ_d = 92.7 pcf: correct factor	corr. V_p V_s	foto No.	σ_o' = 10.0 psi, γ_d = 92.9 pcf: correct factor	corr. V_p V_s	foto No.	σ_o' = 20.0 psi, γ_d = 93.2 pcf: correct factor	corr. V_p V_s	foto No.
θ = 90°	1.000	1176	187	.996	1353	201	.992	1575	203
	.999	753	188	.996	868	202	.992	1012	204
60°	.999	1141	189	.995	1289	197	.992	1508	205
	1.000	787	190	.996	907	198	.991	1041	206
30°	1.030	1226	191	1.009	1217	195	.993	1270	207
	1.030	578	192	1.008	872	196	.995	999	208
0°	1.013	1377	193 194	1.002	1505	199 200	.995	1665	209

Notes: a) Dr. Woods attended test and made most velocity interpretations.

b) Followed several days later with test 13a, using σ_o' = 5.0 psi, but with K = 2.2. See section 5.2.

TEST NO. 14 K = 1.0

wave with horiz.	σ_o' = 5.0 psi, γ_d = pcf: correct factor	corr. V_p	corr. V_s	photo No.	σ_o' = 10.0 psi, γ_d = pcf: correct factor	corr. V_p	corr. V_s	foto No.	σ_o' = 20.0 psi, γ_d = pcf: correct factor	corr. V_p	corr. V_s	foto No.
θ = 90°												
60°												
30°	1.018 1.019	1300	822	218	.998 1.001	1288	904	219	989 991	1592	1014	220
0°												

APPENDIX C

NOTATION

A_{pp}	Peak to peak maximum vibration amplitude
a_{max}	Maximum acceleration in simple harmonic motion
B	Dynamic bulk modulus or modulus of volume compressibility
B_0	B when $\theta = 0°$
B_{90}	B when $\theta = 90°$
f	Frequency, Hz
G_{max}	Maximum shear modulus
g	Gravitational constant = 32.2 ft/sec^2
K	Principal stress ratio = σ_3/σ_1
S_y	Standard error (see Equation 3)
T_s	Period of the shear wave
V_p	Velocity of the compression or push wave
V_s	Velocity of the shear wave
V_θ	Velocity of push or shear wave when traveling in θ direction
V_0	V_θ when $\theta = 0°$
V_{90}	V_θ when $\theta = 90°$
γ	Shear strain
γ_d	Dry unit weight
θ	Angle between direction of wave travel and plane on which σ_1 acts
ρ	Mass density = γ_d/g
σ_o	Octahedral normal stress = $(\sigma_1 + \sigma_2 + \sigma_3)/3$
σ_1	Major principal normal stress
σ_2	Intermediate principal normal stress, = σ_3 this research
σ_3	Minor principal normal stress

NOTE: All primed qualities used for stresses are understood to be effective stresses.